GLUT1 STRUCTURE FUNCTION; CONTEXT,

LIGAND COOPERATIVITY, AND MUTAGENESIS

STUDIES

A Dissertation Presented by

Trista K Robichaud

Submitted to the Faculty of the University of Massachussetts Graduate School of

Biomedical Sciences, Worcester

In partial fulfillment of the requirements for the degree of

Doctor of Philosophy

Department of Biochemistry and Molecular Pharmacology

GLUT1 STRUCTURE-FUNCTION: CONTEXT, LIGAND BINDING AND MUTAGENESIS STUDIES

A Dissertation Presented

By
Trista K. Robichaud

The signatures of the Dissertation Defense Committee signifies completion and approval as to style and content of the Dissertation

---

Anthony Carruthers, Thesis Advisor

Kendall Knight, Member of Committee

Haley Melikian, Member of Committee

Ann Rittenhouse, Member of Committee

Christopher Cheeseman, External Member of Committee

The signature of the Chair of the Committee signifies that the written dissertation meets the requirements of the Dissertation Committee

---

Mary Munson, Chair of Committee

The signature of the Dean of the Graduate School of Biomedical Sciences signifies that the student has met all graduation requirements of the school.

Anthony Carruthers, Ph D.,

Dean of the Graduate School of Biomedical Sciences

Program in Biochemistry & Molecular Pharmacology

July 29, 2008

ACKNOWLEDGEMENTS & DEDICATIONS

For Tony, without whom kinetic mathemagic would hold little appeal. Thank you.

For my lab mates and lab neighbors past and present, including but not limited to Laura Andersh, David Blodgett, Erin Cloherty, Anthony Cura, Julie Kelly DeZutter, Otto Gildemeister, Jeffry Leitch, Kara Levine, Pusha Karim, Tabitha Kramarz, and Moses Prabu, whose patience, conversations, and inspiration were invaluable. Thank you.

For all my teachers, especially my committee members: Mary Munson, Ann Rittenhouse, Haley Melikian, Kendall Knight, and Christopher Cheeseman. You've given me the torch of knowledge, and I intend to pass it on. I hope I can emulate your successes. Thank you.

For my fellow students and friends, thank you, especially to Mary Porter Goff, Melonnie Furgason, and Jennifer Songer. Without your patience, perspective, motivation, and therapeutic advice, I would be lost. Thank you.

For my Mom, Dad, Jordan, Dustin, and my in-laws Dan and Jan Robichaud. You are wonderful, understanding, and supportive. Thank you.

Most importantly, for my husband, Daniel R Robichaud II. We dreamed this dream together. I am deeply proud to share this achievement with you. Thank you.

TABLE OF CONTENTS

TABLE OF FIGURES

ABSTRACT

Carrier mediated nutrient import is vital for cell and tissue homeostasis. Structural insights of carrier mediated transport, particularly the human glucose transporter GLUT1, are essential for understanding the mechanisms of human metabolic disease, and provide model systems for cellular processes as a whole.

GLUT1 function and expression is characterized by a complexity unexplained by the current hypotheses for carrier-mediated sugar transport (*9*). It is possible that the operational properties of GLUT1 are determined by host cell environment. A glucose transport-null strain of *Saccharomyces cerevisiae* (RE700A) was transfected with the p426 GPD yeast expression vector containing DNA encoding the wild-type human glucose transport protein (GLUT1) to characterize its functional properties. Identical protein sequences generated different kinetic parameters when expressed in RE700A yeast, erythrocytes, and HEK293 cells. These findings support the hypothesis that red cell sugar transport complexity is host cell-specific.

Cytochalasin B (CB) and forskolin (FSK) inhibit GLUT1-mediated sugar transport in red cells by binding at or close to the GLUT1 sugar export site. Paradoxically, very low concentrations of these inhibitors produce a modest stimulation of sugar transport *(16)* This result is consistent with the hypothesis that the glucose transporter contains multiple, interacting, intracellular binding sites for e1 ligands CB and FSK. The present study tests this hypothesis directly and, by screening a library of cytochalasin and forskolin analogs, asks what structural features of exit site ligands

determine binding site affinity and cooperativity. Our findings are explained by a carrier that presents at least two interacting endofacial binding sites for CB or FSK. We discuss this result within the context of GLUT1 quaternary structure and evaluate the major determinants of ligand binding affinity and cooperativity.

Cytochalasin B (CB) inhibits GLUT1 substrate transport at or near the endofacial sugar binding site. N-bromosuccinamide analysis combined with ^{3}H-CB photolabeling implicates the region between Trp388 and Trp412 in ligand binding. Although its structure has been modeled(5), the specific residues comprising the sugar binding site are unknown. A series of alanine point mutants were made, and mutant protein 2-deoxy glucose transport was tested in the presence of increasing [CB]. Arg126Ala and Cys421Ala GLUT1 mutations altered CB affinity but were determined not to be in the e1 site. The Arg400Ala mutation decreased binding affinity for CB, and may comprise part of the e1 binding site. Because point mutations were individually insufficient to abrogate CB binding, Trp388 to Trp412 chimeras were made. GLUT1/GLUT4$_{388-412}$/GLUT1 and GLUT1/GLUT5$_{388-412}$/GLUT1 chimeras showed moderately less sensitivity to CB inhibition of transport; these amino acids likely comprise regions determinant of CB binding affinity. Furthermore GLUT1/GLUT5$_{388-412}$/GLUT1 shows enhancement of 2-DG uptake at 50nM CB, but an overall dose response indistinguishable from WT GLUT1. A multisite fit of the data suggested GLUT1/GLUT5$_{388-412}$/GLUT1 chimera possesses strong first site affinity for CB but slight negative second-site cooperativity. We conclude that point mutants were insufficient to abrogate CB binding and that the Trp388 to Trp412 sequence is necessary for CB binding affinity but is not the sole

determinant of inhibition of 2 deoxyglucose uptake by CB. We discuss these results with

their implications for structure-function sequence localization of the CB binding site, and

by extension, the e1 sugar binding site.

INTRODUCTION

Glucose Transport Studies

Glucose is the preferred energy substrate for cellular metabolism; cellular demand and glucose availability are of utmost importance to both unicellular and multicellular organisms. Surrounded by an impermeant lipid bilayer, cells acquire glucose and other nutrients by utilizing integral membrane proteins, making nutrient channels and carriers fundamental to life. The work described here discusses the human erythrocyte sugar transporter GLUT1, the first characterized sugar porter(*18*). GLUT1 is expressed in all tissue types, is thought to be responsible for basal glucose homeostasis, and is the primary vehicle for transport of sugar from blood into brain as well as across other blood and tissue barriers. Defects in GLUT1 or its regulation may result in epileptic-like seizures (*19*), growth defects, or embryonic inviability. Furthermore, GLUT1 is a valuable model system for structural analysis of integral membrane proteins as well as nutrient transport. Structural understanding of glucose transport will further our knowledge of carrier mediated glucose homeostasis within cells and tissues, and may lead to treatment of chronic metabolic disease.

Protein Mediated Nutrient Uptake

Cells are surrounded by an amphipathic lipid bilayer known as the plasma

Figure 1.1 Crystal Structures of Membrane Transport Proteins.

 A. A top-down view of aquaporin, with the membrane side view of the monomer. (*10*)

B. Top and side view of KvaP, a mammalian potassium channel. (*14*)

C. An ABC transporter (normal to the plane of the bilayer), the crystallized catalytic

intermediate of the maltose transport protein complex. (*15*)

D. Cytoplasmic and side view of GlpT, a Major Facilitator Superfamily bacterial sugar

transporter. (*17*) Structures are shown in ribbon formats.

Fig 1.1

A

B

C

Periplasm

MalF (P2)

MBP

MalF
MalG
Maltose

MalK
MalK

2 ATP

Cytoplasm
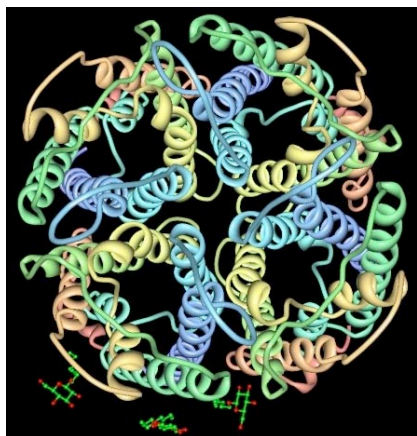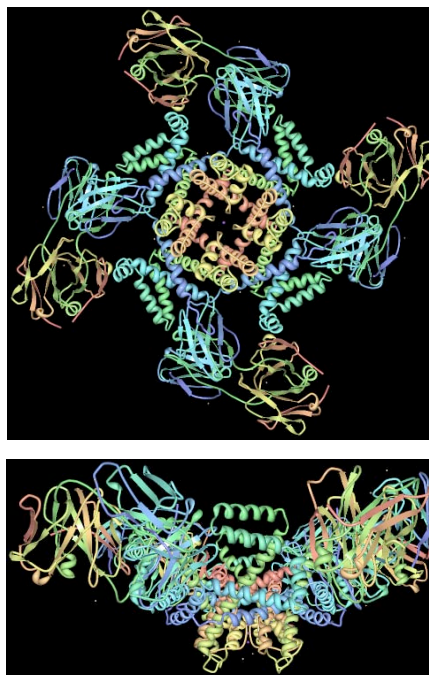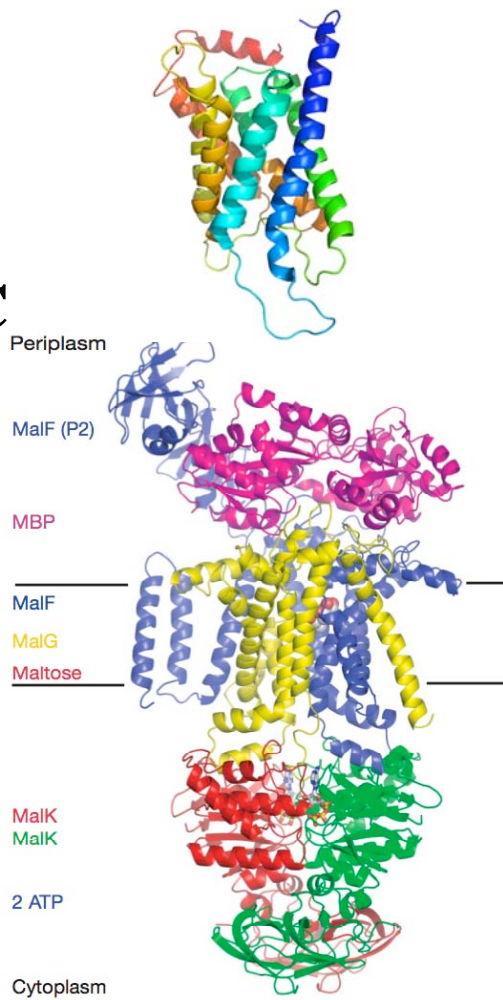
D
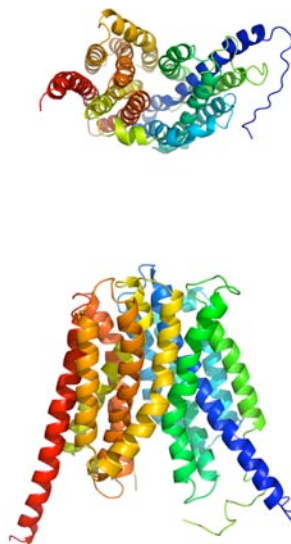
membrane, whose primary function is to maintain cellular homeostasis (*20*). Without

protein-mediated nutrient uptake lipid bilayers are impermeant to large, polar, or charged

molecules including ions, cofactors, and glucose. Water, small hydrophobic molecules,

gases, and lipophillic drugs diffuse freely through the membrane into the cell. Large or

charged molecules may diffuse, but do so slowly. Cells overcome the problem of

excluding important metabolites and ions by utilizing integral membrane proteins which

include channels and carriers. Protein mediated transport is metabolite specific and is

often fine-tuned by regulation of transporter expression or activity to meet cellular

demands.

Channel proteins are membrane resident and stabilize a pore normal to the lipid

bilayer, which provides simultaneous access to both sides of the membrane. Channels

may be highly specific, facilitating movement of one ion, or nonspecific 'porins',

permitting free water and ion access across a lipid bilayer. Channel selectivity is thought

to be governed by pore diameter. The crystallized channel protein Kv1.2, a voltage gated

K^+ channel (Fig 1.1B) (*14*), has a pore diameter of approximately 1.5Å (*21*), while the

aquaporin GlpF has a pore diameter of 3.4x3.8Å at its narrowest (*22*). For Kv1.2, a tight

fit ensures dehydration of the K^+ ion and subsequent transport, keeping out smaller-radius

ions like Na^+ (*14, 21*) Aquaporins like GlpF (Fig 1.1A) are predominantly expressed in

endothelial cell types requiring or mediating high rates of more permissive fluid transport

(*22, 23*). A tetrameric, integral membrane protein, aquaporin functions by permitting

water flow through a pore within each subunit lined with hydrophilic amino acids,

permitting single-file flux to the opposite side. Net water flow always proceeds in the

direction of $[water]_{high}$ to $[water]_{low}$.

Unlike porins, channels typically isomerize between closed, open, and desensitized states. Channels transition between states in response to protein-protein interactions, voltage across the lipid bilayer, changes in temperature, or ligand binding (*24*).

Three classes of carrier proteins facilitate bidirectional transport of small molecules across membranes: "Primary Active" carriers, facilitative carriers, and secondary active carriers. "Primary Active" carriers, also known as active transporters or pumps, (see the maltose transporter, Fig 1.1C) mediate transport against an electrochemical gradient by coupling substrate transport to ATP hydrolysis (*20*). Secondary active carriers are symporters or antiporters because net uphill transport of substrate is coupled to and driven by the co-transport or antiport of a second species – typically a cation such as Na^+ or H^+ – down its electrochemical gradient (Fig 1.2)(*20*). Facilitative carriers like GLUT1 catalyze both unidirectional substrate uptake and export. Since the direction of net substrate transport always proceeds down the electrochemical gradient, most often without primary active carriers transmembrane electrochemical gradients are not established. These gradients allow channels, secondary active carriers, and facilitative carriers to do useful work.

Pathophysiology of Transport Proteins

When fundamental channel and carrier processes are perturbed, the resulting disease states are chronic and debilitating. Almost 20% of sequenced human genome

Figure 1.2 Types of Secondary Active Carriers.

In all cases, facilitated carrier mediated transport utilizes existing substrate concentration gradients. Uniporters transport a single solute (gray circles) down its concentration gradient. Symporters utilize a common solute (yellow squares) to drive the uptake of a rarer substrate (blue triangles) against its concentration gradient. Antiporters use the high concentration of a common cellular substrate to facilitate the uptake of a low concentration solute against its concentration gradient.

Fig 1.2
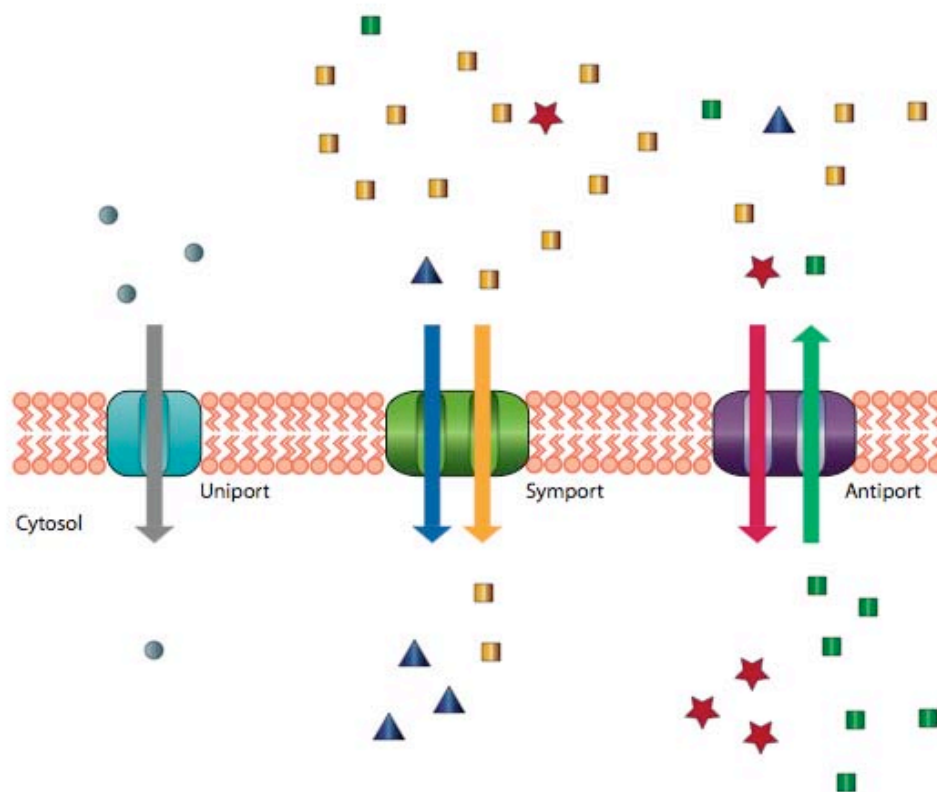
proteins are integral membrane proteins; of these, 90% are considered viable therapeutic

drug targets for human disease (*25*). Moreover, the Transport Classification Database at

UCSD listed over thirty-seven human diseases affiliated with mutant channels or carriers

(*26*). Most of these debilitating diseases are genetic, and extant therapies only treat

symptoms. Understanding how to ameliorate mutant function reveals important insights

into the role of that protein within the body, and facilitates development of novel

treatments to increase patient quality of life. The following perturbations of integral-

membrane protein mediated cellular functions will be discussed in more detail: faulty

chloride channels and cystic fibrosis, the role of sugar porters and multidrug resistance

transporters in cancer and cancer therapies, diabetes states, both adult-onset and juvenile,

and lastly, GLUT1 Deficiency Syndrome and the effects of insufficient glucose transport

on cerebral function and development.

ANION TRANSPORT AND CYSTIC FIBROSIS

One of the most common inherited childhood diseases, cystic fibrosis is caused by

a mutation in a protein known as the cystic fibrosis transmembrane conductance regulator

(CTFR), a chloride ion channel. These channels are commonly found in tissues that

produce sweat, mucus, and other secretions. Anion transport aids in regulating the

osmotic balance across membranes of secretory tissues. Without chloride secretion,

water cannot flow to thin the mucus in the lung and other tissues, resulting in damage and

breathing difficulties (*27*). While afflicted children have a life expectancy of forty years

with surgical lung replacement, structural understanding of CTFR may lead to small

molecule activators of the channel to ameliorate deficient function. Mutations in CTFR

are often retained within intracellular vesicles in a manner similar to wild type GLUT4 sequestration. Understanding the recruitment of GLUT4 and its homologous sibling GLUT1 to the cell surface may suggest further therapies for cystic fibrosis.

CANCER, SUGAR PORTERS & MULTIDRUG RESISTANCE TRANSPORTERS

Cancerous cells grow and multiply faster than normal cells, resulting in an acutely increased demand for energy. Warburg first observed in 1956 (*28*) that tumors have high rates of anaerobic glycolysis. The level of glycolysis, typified by the high expression of lactate dehydrogenase, has been used as a benchmark for lymphomas, leukemias, and colon cancer (*29*). A shift to lactate from pyruvate is thought to deprive the mitochondria, reducing the TCA cycle and therefore ATP output. All of these factors intensify the cancer cell's need for glycolysis, and therefore, glucose (*30*).

The increased demand for glucose in cancerous cell lines as well as benign and malignant tumors results in up-regulation of glucose transporter expression, especially GLUT1 (*30*). Tumor analysis has also shown glucose transporters to be up-regulated by hypoxia resulting from poor perfusion (*31*). Similarly, tissue culture attendant hypoxia is thought to be a primary determinant of GLUT1 upregulation in cultured cells (*32*). Some breast cancers also increase sugar transporter-mediated uptake in response to estrogen treatment, likely as a result of metabolic depletion (*33*). While it is unlikely that increased sugar porter production is a cause or an effect of cancer, the sugar porters themselves remain seductive drug targets to starve tumorigenic masses.

Multidrug Resistance (MDR) transporters are another class of integral membrane proteins that directly affect human anticancer strategies. Efflux pumps such as ABCG2

expressed in the calnilicular membranes of the human liver, microvascular endothelium of the brain, and the apical surface of the small intestine epithelium drain small molecule chemotherapeutic delivery by facilitating rapid drug clearance (*34*). It is unsurprising that human MDR inhibitors are fiercely sought after anticancer agents.

DIABETES

Diabetes is a disease of metabolism in which glucose homeostasis is disrupted; it has also been called the most quietly received epidemic in the US (*35*). The World Health Organization reports that 5% of deaths worldwide are caused by type 2 diabetes; in the absence of medical intervention that number is expected to increase 50% in the next ten years (*36*).

GLUT4, the insulin-sensitive glucose transporter, is a passive yet critical element in this disease. Upon food intake, pancreatic beta cells release the peptide hormone insulin. When insulin interacts with cell surface insulin receptors in muscle and adipose, a signaling cascade is triggered causing the cell surface recruitment of intracellular GLUT4. Consequently, this results in the reduction of blood glucose levels as well as strongly increased cellular sugar transport capacity in skeletal muscle and adipose tissue (*37, 38*). There are several steps in the signaling cascade that may be perturbed and it is the locus of the disruption that determines what type of diabetes clinically presents.

Diabetes may be classified as two types; Type I (Juvenile) Diabetes is usually genetic, involves the autoimmune destruction of insulin secreting beta cells, and begins at infancy. Type II diabetes, the 'industrialized epidemic' (*35*) may involve genetic predisposition, but is a mature-onset disease state where skeletal muscle, adipose, and

liver tissues become insulin resistant. This leads to systemically increased blood glucose levels resulting in muscle and liver damage, adult blindness, and potential limb atrophy.

Ultimately, the pathophysiology of glucose homeostasis is an exponentially increasing healthcare challenge to the developed world. Understanding glucose transporter structure function may introduce alternative oral strategies for regulation of serum glucose, obviating the need for insulin injections or other therapies for the insulin resistant.

GLUT1 DEFICIENCY SYNDROME

The human glucose transporter 1 (GLUT1) was the first glucose transporter to be cloned, purified, and characterized. (*18, 39, 40*). GLUT1 is ubiquitously expressed and is the most thoroughly characterized human sugar porter. The dense expression of GLUT1 in the brain microvascular endothelial cells results in high capacity glucose transfer from the circulatory system to the brain (*41*). Numerous deleterious point and missense mutations in GLUT1 result in GLUT1 Deficiency Syndrome (GLUT1DS), an inheritable disease characterized by retarded brain development, reduced cranial size, and epileptic-like seizures. Diagnosed early, infants may be placed on a ketogenic diet (80% fat, 20% carbohydrates and protein) to facilitate early cerebral development and control seizures. On the ketogenic diet, the monocarboxylate transporters (MCTs) provides the necessary cellular fuel via the ketone body metabolism pathway in the brain. GLUT1 Ds is typically heterozygous in clinical study, while homozygous mutant GLUT1 is thought to be embryonically lethal (*42-44*).

GLUT1 plays a pivotal role in other neural conditions which interrupt the

microvascular endothelium and perturb the brain's fuel supply. Examples where glucose transport may become rate limiting include ischemia (stroke), Alzheimer's disease, other forms of epilepsy, hypoxia, and brain trauma (*41, 45*). Research into GLUT1 function and regulation offer the potential of developing therapies for these debilitating conditions. Ultimately, an understanding of GLUT1 structure and function may also facilitate engineering small molecule delivery systems for transport into damaged areas of the brain.

Structural Features of Major Facilitator Superfamily Proteins

Over 100 families of nutrient import proteins in microorganisms have been classified, half of which fall into two 'superfamilies' of structurally related transporters. These are the ATP Binding Cassette (ABC) superfamily, and the Major Facilitator Superfamily (MFS). (*46*) ABC transporters are generally hetero-oligomeric in nature, and are considered primary active carriers with transport coupled to ATP hydrolysis. MFS transporters do not require ATP, may function as monomers or homo-oligomers, and may be passive or secondary active carriers.

The first, largest, and most extensively studied subfamily of the MFS is the sugar porters. The typical sugar porter fold includes 12 putative or confirmed transmembrane-spanning alpha helical regions and intracellular N and C termini (Fig 1.3). Sugar porters are typically 400 to 800 amino acids in length, with the smaller peptides generally found in prokaryotes. Under normal conditions, sugar porters function via solute uniport or Na+ or H+-driven symport (Fig 1.2). Given a high concentration of sugar within the cell, however, sugar-sugar antiport is commonly observed (*46*).

MFS Crystal Structures

Three crystal structures of bacterial MFS proteins have been reported; the lactose permease LacY (3.3Å resolution), glycerol-3-phosphate transporter GlpT(3.2Å resolution, Fig 1D), and the oxalate transporter OxlT(6.5Å resolution (*17, 47, 48*)). These structures contain alpha-helical transmembrane (TM) domains arranged in a squared-off pyramid, connected by randomly coiled extramembranous loops. Perhaps the most striking information from these MFS folds is that despite sequence dissimilarity, the helices adopt a near identical packing arrangement. (Fig 1.3A,B) Each structure has been crystallized in the e1 or cytoplasmic-facing configuration. Helices 3, 6, and 9 are the shortest, and along with helix 12 are thought to be involved in structural support within the membrane. The arrangement of the remaining helices suggest that they line a funnel-shaped, 30 Å hydrophilic cavity, with TM's 2,5,8, and 11 on the periphery, and 1,4,7 and 10 in the core. A marked twofold axis of symmetry across the large endofacial loop supports the suggestion of a gene duplication early in the genesis of these proteins. While early studies modeled sugar translocation proceeding as through a water-filled pore or channel (*49*) or by wholesale rotation of the transporter, *Wang, et al* utilized kinetic evidence to support a valve-like rocking switch mechanism of sugar movement with translocation (*50*). This is consistent with both Jardetzky's (*51*) and Singer's (*52*) model of a fixed, two site carrier discussed later in this work.

Glucose Metabolism & the Human Glucose Transporter Family

The biochemical reactions used to obtain cellular energy (ATP) from glucose are

Figure 1.3 Helix interactions in a MFS transporter.

A. GLUT1 sequence mapped onto a GlpT three dimensional scaffold, in the e1 (endofacial) conformation. The structure is shown in ribbon format and is normal to the plane of the bilayer. **B.** GLUT1 helix packing arrangement as observed from the cytosol, with the endofacial sugar vestibule facing the viewer. Helices 3,6,9, and 12 (green) are the shortest and thought to provide structural stability. Helices 1,4,7, and 10 (magenta) are thought to line the e1, sugar binding cavity of the protein. Adapted from (*4, 5*).

Fig 1.3

A

Lipid

Cytoso

C-terminus

B
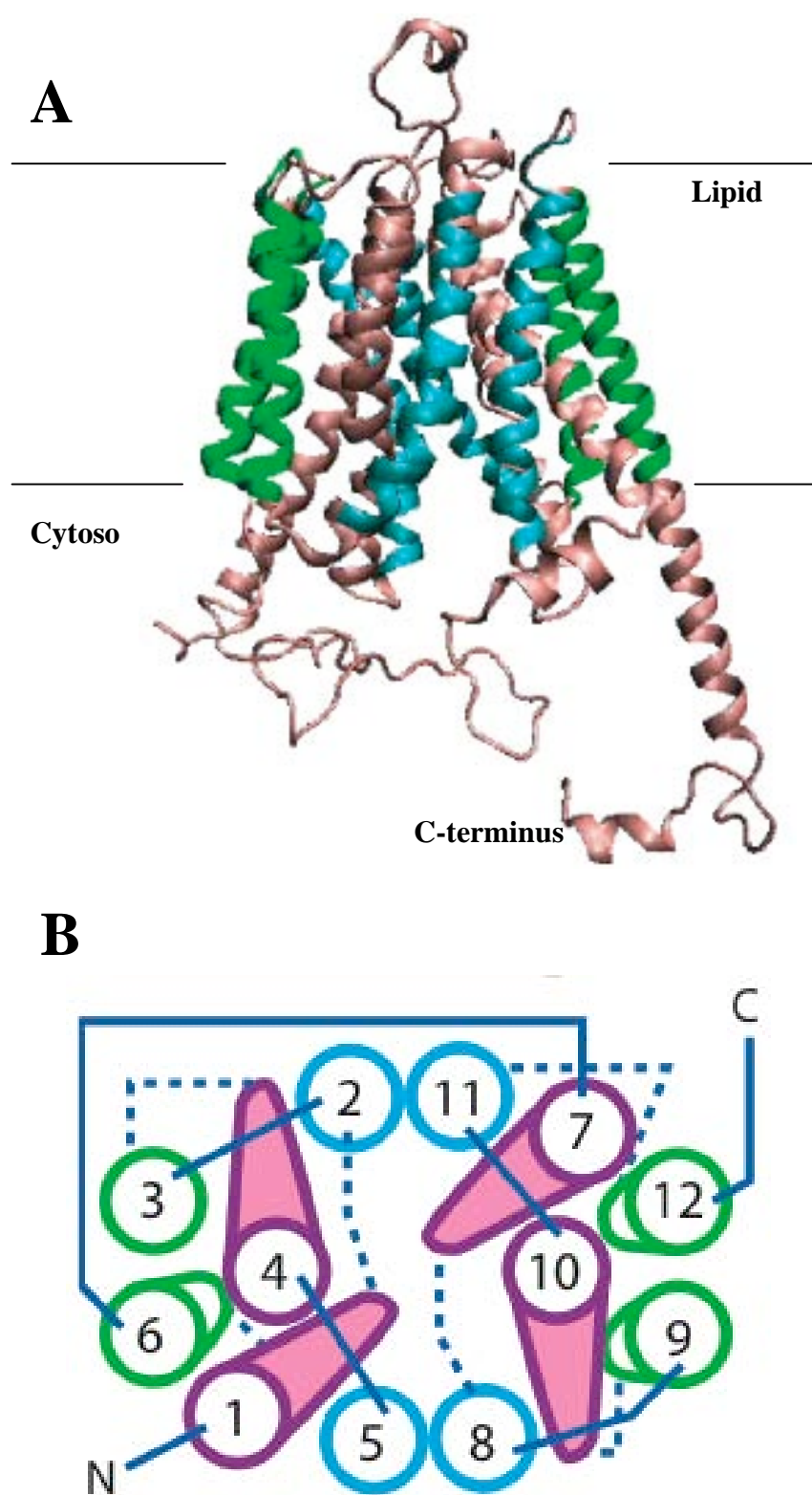
well conserved from bacteria to humans. Glucose metabolism occurs via two pathways -

an anaerobic pathway and an oxidative or aerobic pathway. Anaerobic metabolism is a

cytosolic process which occurs primarily in tissues that need to generate energy quickly,

such as muscles. This process, known as glycolysis, breaks down glucose into smaller

monosaccharides, dihydroxyacetone and glyceraldehyde, generating ATP and pyruvate.

Anaerobic metabolism can meet sudden, stringent demands for energy, but is inefficient

and the thermodynamic payout (in ATP) per glucose is low. However, the buildup of

pyruvate may be funneled into the oxidative Krebs cycle later to replenish ATP as well as

generating amino acids and other cellular building blocks (*53*).

Aerobic or oxidative metabolism involves the Krebs cycle, pentose phosphate

shunt and use of mitochondria (*53*). Compartmentalization and time make possible a

greater amount of energy payout in the form of ATP and NADH per glucose entered into

the system; glycolysis yields two ATP equivalents per glucose, while the mitochondrial

path results in 38 (*41, 53*). Because oxidative metabolism is more 'profitable' in terms of

ATP synthesis, glucose and glucose transport remain vital throughout the human body.

Thirteen human glucose transporters (GLUT1-12, HMIT) have been

characterized, each with their own tissue-specific expression pattern (*38*). When

compared by sequence identity, the glucose transporters fall into three groups. Group 1

contains GLUT1-4, Group 2 contains GLUTs 5, 7, 9, and 11, and Group 3 comprises

GLUTs 6, 8, 10, 12, and the myo-inositol transporter HMIT. (Table 1.1)

Group 1 transporters are similar in that their primary function is high affinity

Table 1.1

GLUT	Group	Gene Name	Substrate[a]	Expression[b]	Oocyte K_m[c]
GLUT1	1	SCL2A1	Glucose	Erythrocytes, Endothelial Barrier Cells, Smooth Muscle, Cardiac Muscle	5mM
GluT2	1	SCL2A2	Glucose, Fructose	Liver, Pancreatic Islets	11mM
GluT3	1	SCL2A3	Glucose	Brain, Neurons	1mM
GluT4	1	SCL2A4	Glucose	Cardiac & Skeletal Muscle, adipocytes	5mM
GluT5	2	SCL2A5	Fructose	Intestine, Testis, Kidney	6mM
GluT7	2	SCL2A7	ND	Intestine	0.3mM
GluT9	2	SCL2A9	Urate, Glucose	Liver, Kidney	0.3mM
GLUT11	2	SCL2A11	Glucose, Fructose	Cardiac & Skeletal Muscle	0.2mM
GluT6	3	SCL2A6	Glucose	Spleen, Leukocytes, Brain	High K_m
GluT8	3	SCL2A8	Glucose, Fructose	Testis, Blastocyst, Brain	2.4mM
GLUT10	3	SCL2A10	Glucose	Liver, Pancreas	0.3mM
GLUT12	3	SCL2A12	Glucose	Placenta, Testis, Breast, possibly Cardiac Muscle	4-5mM
HMIT	3	SCL2A13	Inositol, H+	Brain	0.1mM

Table 1.1 The Human Sugar Porter Family

Sugar porters are arranged according to groups based on sequence similarity, with the porters in Group 1 discovered first(*1-3*). [a] Where two substrates are both transported, the one with higher catalytic activity is listed first. [b] Expression listed in order of most concentration to least concentration within the tissue. [c] The listed K_m is that for oocyte-expressed transporter uptake of D-glucose (*2*).

equilibrative transport of glucose. GLUT1 is preferentially expressed in endothelial barriers such as the blood-brain barrier, as well as the surface of erythrocytes and smooth muscle cells, although it has low, ubiquitous expression in most tissues (*38, 54*).

GLUT2 is primarily expressed in hepatocytes, pancreatic beta cells, and absorptive epithelial cells in the small intestine and kidney, and may transport glucose or fructose (*54, 55*). GLUT3 is the most prevalent sugar transporter in the brain and other nerve tissues, although it has basal expression in kidney, placenta, and liver (*38*). GLUT4 is the 'insulin-sensitive' glucose transporter present in muscle and adipocytes. While GLUTs 1, 2, and 3 may be regulated via altered expression or activity, insulin regulation of GLUT4 results in GLUT4 redistribution between cell surface and intracellular membranes(*54*).

Group 2 transporters (5,7,9,11) are not as well characterized as those in Group 1. GLUT5 is highly expressed at the apical membrane in the small intestine, and is the major vehicle for dietary fructose uptake. It is also expressed in the brain endothelium, as well as in muscle and fat cells (*54*). GLUT7 is expressed in small intestine and possesses high affinity for glucose and fructose in culture, though its physiological substrate is yet unknown (*56*). GLUT9 is a glucose transporter primarily expressed in the kidney and liver; interestingly, mutations in GLUT9 result in defective uric acid metabolism and increased sensitivity to gout (*57-59*). GLUT11 transports glucose and fructose, and is expressed as three functionally similar alternative splicing variants (*60*). Unlike the Group 1 transporters, Group 2 transporters are only weakly inhibited by the classic GLUT1 inhibitor cytochalasin B.

Group 3 (6,8,10,12, HMIT) transporters still possess 12 putative TM regions, but the large extracellular loop is located between TM's 9 and 10 rather than 1 and 2. (*54*) Each isoform has its own tissue specific expression pattern, and all transport glucose except HMIT. GLUT13 or HMIT, the human 1:1 H^+ myo-inositol cotransporter, is the last discovered gene with glucose-transport-like motifs. HMIT is expressed primarily in the brain, with low-level expression in adipocytes and kidney (*54, 61*).

GLUT1 Model Systems

From expression we move on to GLUT1 model systems. In 1952, Widdas first theorized that sugar transport was a saturable, protein-mediated process using sheep blood-placental transport as his model system (*62*). Since then, erythrocytes have provided an ideal model system for the study of GLUT1 kinetic properties: Red cells are readily available by donation, are uniform in size and volume, may be lysed and resealed with desired contents, and GLUT1 is thought to occupy 6% of the cell surface. Membrane-resident erythrocyte GLUT1 may be readily purified for biochemical study. GLUT1 isolated from red cells is more heterogeneously glycosylated than is observed in other tissues. While this impacts biochemical analysis, it is not thought to affect functional behavior. (*63*). Nonetheless, erythrocyte GLUT1 provides a window into the kinetic properties of mammalian sugar flux.

The major disadvantage of erythrocyte GLUT1 is that it is not amenable to mutagenic analysis. While clinical cases of GLUT1 DS have provided some insight, they are resistant to systematic structural exploration. Three model systems have been successfully employed to address this; *Xenopus laevis* oocytes, brewer's yeast, and

mammalian cell lines such as 3T3L1 adipocytes, Chinese Hamster Ovary (CHO) cells, and Human Embryonic Kidney Cells (HEK).

XENOPUS LAEVIS

Mutant GLUT1 has been most commonly expressed via RNA injection in *X. laevis* oocytes (*64*). Oocytes, with their consistent size and volume, provide a convenient vehicle for analysis of kinetic properties of mutant transporters by measuring the transport of radiolabelled sugars. However, oocyte expressed GLUT1 is not uniformly gylcosylated, is not expressed at a sufficiently high density for purification, and it does not self-associate into dimers and tetramers as observed in red cells (*65*). This results in differing kinetic behavior from the human erythrocyte model, notably the lack of reductant sensitivity (*66, 67*). In other words, sugar uptake into control erythrocytes without extracellular reductant (DTT-) is almost twofold greater than erythrocytes treated with DTT (*65*). Oocyte expressed GLUT1 is unaffected by the presence of extracellular reductant (*66, 67*).

SACCHAROMYCES CEREVISIAE

S. cerevisiae possesses a family of HXT membrane transporters with similar topology to GLUT1 (*68-70*). These facilitative transport proteins are thought to be uniformly glycosylated and therefore provide a suitable background for mutant/wild type study. While large stocks of yeast may be grown, the resilience of the yeast cell wall often makes purification of large amounts of protein for biophysical analysis difficult (Levine and Robichaud, unpublished observations). However, the ease of genetic manipulation in *S. cerevisiae's* could facilitate mutagenesis approaches to analysis of the

GLUT1 structure function relationship.

Transient transfection of GLUT1 into Chinese Hamster Ovary (CHO) cells or Human Embryonic Kidney 293T (HEK 293) cells have also proved a convenient vehicle for studying the glucose fluxes of mutant GLUT1. Both cell types have a very low concentration of endogenous glucose transporters, thereby facilitating heterologous overexpression of mutant transporters. HEK 293 cells have the advantage that they retain erythrocyte-like glycosylation patterns on the protein (*66*). Their disadvantages lie in the cost of culture, and a lower protein density as compared to the erythrocyte, rendering mutant protein purification a more expensive and complex operation.

Structural Features of GLUT1

Proteins may be analyzed according to primary, secondary, tertiary, and quaternary structure. *Mueckler et al.* (*40*) cloned the postulated human glucose transporter 1 (GLUT1) sequence from HepG2 hepatoma cells and confirmed that it was identical to the GLUT1 protein seen in erythrocytes. GLUT1 comprises 492 amino acids producing a transporter of molecular weight of 54,117 daltons (*71*). GLUT1 sequence contains a single glycosylation domain at N45 (*40*). Since 60% of GLUT1 amino acids are hydrophobic, it is unsurprising that GLUT1 is an integral membrane protein. (Fig 1.4)

Other primary structural features of GLUT1 support the hypothesis that GLUT1 is an integral membrane protein typical of the Major Facilitator Superfamily (MFS) of nutrient importer proteins. Hydropathy sequence analysis, glycosylation topology, and homology modeling suggest GLUT1 has 12 membrane-spanning alpha helices (*8, 40*).

GLUT1 has cytoplasmic N and C termini and contains a large intracellular loop between transmembrane (TM) domains 6 and 7, typical of MFS protein folds. The pseudo-twofold symmetry is thought to result from an ancient gene duplication event of the first six TMs (*46, 72*). The termini, the large exofacial loop between TM 1 and 2, and the large cytoplasmic loop are thought to form the most flexible extramembranous domains of the protein. *Mueckler et al* inserted consensus glycosylation sequences into GLUT1 loops to confirm membrane topology (*8*). This scanning glycosylation method was paired to assays of GLUT1 deglycosylation which confirmed the location of extracellular loops between TM's 1&2, 3&4, 5&6, 7&8, 9&10, and 11&12.

GLUT1 sequence common to sugar porters includes the endofacial RXGRR loop sequences (between TM2-3 and 7-8) (*73*). GLUT1 also has three sites with sequences homologous to adenylate kinase nucleotide binding domains (*74*), one in the central cytoplasmic loop at residues 225-229, another at residues 332-343 localized in intracellular loop 5, and the third domain comprises a Walker A ATP binding motif at residues 111-117, in the exofacial loop between TMs 3 and 4 (*8, 40*).

GLUT1 secondary structural information is limited, as GLUT1 hydrophobicity and motional freedom of the long loops linking TMs result in a protein that is difficult to crystallize. As yet, no structure has been reported. *Jung et al* show using deuterium-exchange data that 80% of GLUT1 amide protons freely exchange with an aqueous environment, implying significant flexibility (*75*). Some secondary structure has been deduced by biophysical methods. Fourier transform infrared spectroscopy as well
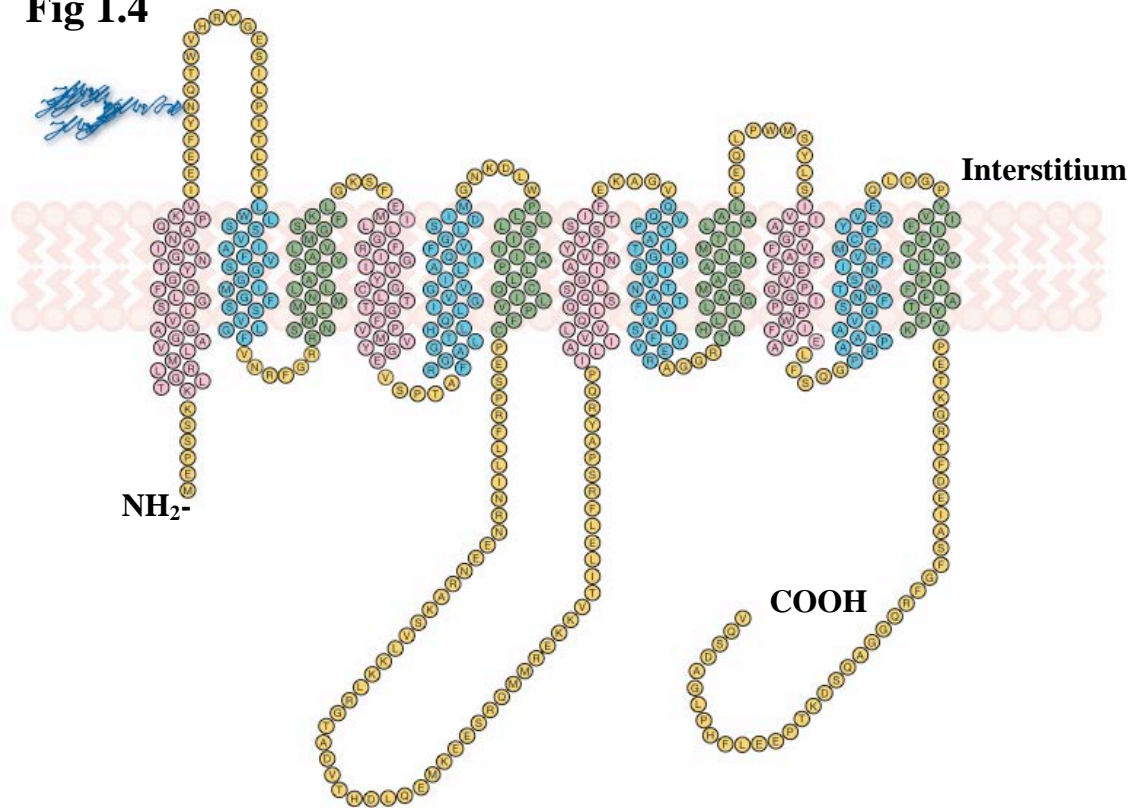
Figure 1.4 Hydropathy Plot of GLUT1 & Primary Sequence.

Lipophillic intermembrane stretches initially postulated through hydrophobic analysis of

amino acid sequence, later confirmed by *Mueckler et al* using inserted glycosylated

reporters (*8*). GLUT1 possesses12 transmembrane domains, an exoplasmic N-linked

glycosylation site, and cytosolic N and C termini as well as a large endofacial loop.

as circular dichroism measurements indicate that the secondary structure of GLUT1 is predominantly alpha-helical in the membrane spanning regions, and that these transmembrane domains are perpendicular to the membrane bilayer (*73, 76, 77*). *Salas-Burgos et al* (*5*) computationally modeled the GLUT1 sequence onto the scaffold of crystallized GlpT and successfully minimized the structure, suggesting the GLUT1 sequence may fit the MFS helical packing model.

More detailed tertiary helical packing information was determined by *Mueckler, et. al.* By combining expression of a cysteineless GLUT1 construct in *X Laevis* oocytes along with site directed mutagenesis, *Mueckler et al* systematically replaced each amino acid in a given TM domain with a cysteine. Then oocytes expressing each mutant were treated with p-chloromercuribenzenesulfonic acid (PCMBS), a sulfhydryl-reactive inhibitor of transport. PCMBS does not penetrate the lipid bilayer well, so transport inhibition is thought to show that the altered amino acid has access to the aqueous environment. Their results confirm that residues in TM's 1, 2, 5, 6, 7, 8, 10, 11, and 12 that demonstrate PCMBS-sensitive inhibition (*73, 78-83*). PCMBS complexation does not affect glucose transport in helices 3 and 4, while 9 remains to be analyzed. Overall, this method is in agreement with the MFS helix packing model (Fig 1.3) with two exceptions – TM 4 has aqueous access, while TM 12 does not (*84*).

GLUT1 quaternary associations in the membrane remain a topic of keen interest. Monomeric GLUT1 may function as a simple uniporter (*85, 86*). Key to the multimeric hypothesis is the hypothesized presence of a intramolecular disulfide between

Cys 347 and 421; in the presence of reductant, red cell GLUT1 ligand binding is consistent with the behavior of a simple uniporter (*65, 87*). Glucose transport, ligand binding, and regulation by intracellular nucleotides also appears dependent on oligomeric state (*65, 87-89*).Furthermore, the crystallized LacY structure suggests that the diameter of a monomeric MFS carrier is approximately 7.5 nm at 10ºC. The hydrodynamically derived diameter of octylglucoside solublized GLUT1 is approximately 15 nm at 10ºC. Rotary-shadowing EM of freeze-fractured erythrocyte membranes showed a protein diameter of ~10 nm, again consistent with a multimeric protein (*11*). These results suggest that GLUT1 forms a multimeric structure in detergent micelles and in lipid bilayers.

The Simple Carrier Model

In 1952, WF Widdas first noted the inability of diffusion to account for sugar transport into sheep placenta. He used a simplified Michaelis-Menton equation to simulate radiolabeled glucose fluxes and as a result of his analysis developed the simple carrier model (*18, 62*). (Fig. 1.5)

In the simple carrier, a monomer isomerizes between two conformations in the membrane. Of these, one state possesses a pocket ready to receive sugar at the cytosolic surface, known as the 'e1' or sugar exit site, and a second state with an interstitial binding pocket at the outside surface of the membrane called the 'e2' or sugar entry site. Glucose import occurs when a sugar binds to e2, promoting a conformational change. This results in translocation of substrate across the plasma membrane, forming the e1 state from which the substrate is released. Translocation-like conformational

changes may occur with or without a sugar present, and at any given time a protein may only display one sugar binding site, either e1 or e2 (*63*).

Functionally, this model may account for the observations suggesting that overall substrate transport in red cells is asymmetric. Assuming the simple carrier is correct, asymmetry is explained in the model by differing rates of empty carrier movement as opposed to substrate loaded translocation. The kinetic experiments to test these phenomena utilize trace quantities of radiolabeled sugar, and are classified according to side of the membrane on which radiolabeled sugars are located as well as overall sugar transport direction (Fig 1.6). Four classic erythrocyte sugar transport kinetic experiments will be discussed here: 1.) Equilibrium exchange, 2.) Zero-Trans Uptake, 3) Infinite-Cis Exit, and 4) Zero-Trans Exit. Equilibrium exchange measurements take place when substrate is present in equal concentrations on both sides of the membrane, and measures the rate of labeled sugar entry or exit. Equilibrium exchange is typically measured utilizing a radiotracer that is neither metabolizable nor retained within the cell, such as 3-O Methyl Glucose. (3MG) (Fig. 1.6) Equilibrium exchange transport at 20ºC (intracellular [D-glucose] = extracellular [D-glucose]) is characterized by a K_m of 17 mM and a V_{max} of 352 mmol L^{-1} min^{-1} (*90*). In contrast, zero-trans uptake occurs when substrate is present only in the interstitum, and is typically measured by a metabolically trapped sugar such as 2-deoxy glucose (2-DG). In erythrocytes at 20ºC, D-Glucose zero-trans uptake has a K_m (1/affinity) of 1.6 mM and a V_{max} (half-maximal rate) of 36 mmol*L*min^{-1} (*90*) Zero-trans efflux measures the outward flow of radiolabeled sugar from preloaded erythrocytes diluted into sugar-free

Figure 1.5   The Simple Carrier Model

   A. Graphical representation of substrate translocation and conformational changes. (*7*)   Sugar import proceeds as follows 1) Substrate binds the e2 or exofacial binding pocket on a GLUT1 monomer. 2) A conformational change takes place in which the substrate is translocated through the membrane. 3) The e1 site forms, and the substrate dissociates from the transporter into the cell.   These conformational changes can take place with or without substrate present.

   B. King-Altman diagram of the simple carrier model of peptide uniport   This model contains all of the listed states in the graphical representation. k1 and k_1 are rates of enzyme translocation with loaded substrate. Empty carrier translocation rates are expressed as k_o and $k_{\_o}$. The affinity constant for substrate binding to E_1 is K1, and the corresponding affinity constant for E_2 is K2. From this model mathematical expressions can be derived to express the overall rate of sugar flux in any direction.

Fig 1.5

A

B
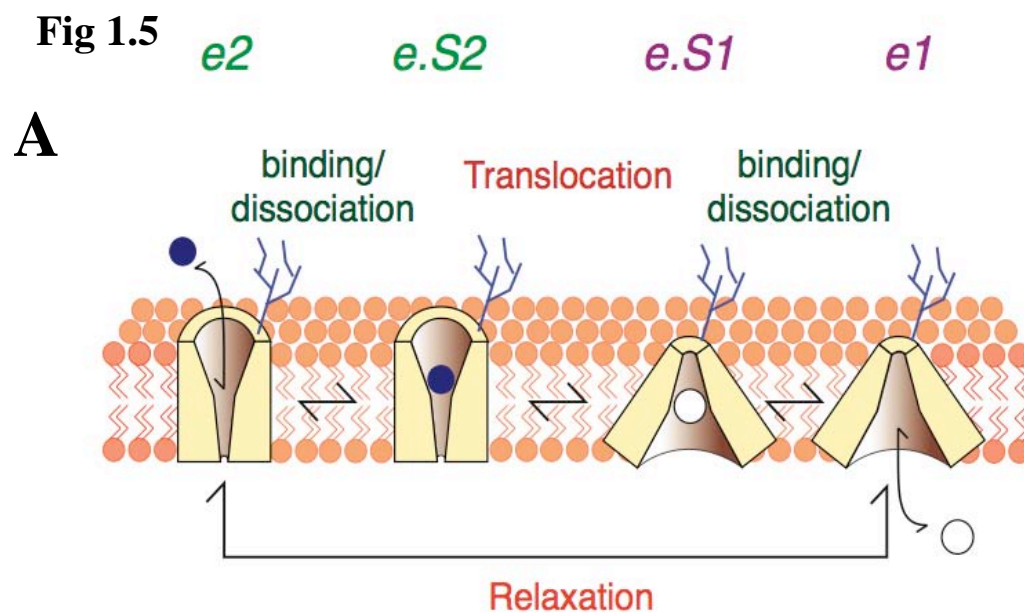
King - Altman Diagram: Simple Carrier
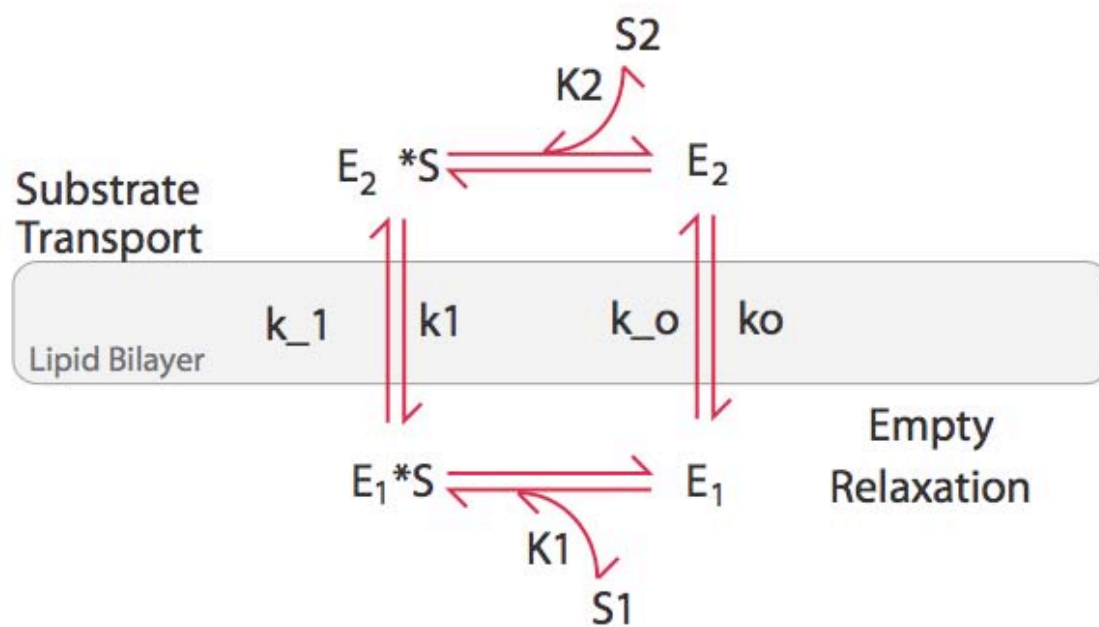
Figure 1.6 Common types of erythrocyte kinetic sugar flux measurements, with graphical representations of sugar flux.

Experimental conditions, binding affinities, and rates of reaction measured are listed to the right of each representation. **A.** Zero-Trans Uptake is when radiotracer sugar uptake in the interstitum is allowed to equilibrate with sugar-depleted cells. After a fixed time, the reaction is stopped, cells are lysed, and the radiotracer is counted. **B.** Zero-trans efflux is when cells preloaded with radiotracer sugar and varying concentrations of unlabeled sugar are diluted into media containing no sugar. **C.** Infinite-cis efflux describes an experiment in which cells are loaded with saturating concentrations of sugar and are resuspended in medium containing zero or increasing amounts of unlabeled sugar. When net exit is monitored by light scattering this experiments reports the concentration of sugar that inhibits net exit by 50%. If unidirectional exit is monitored by radiolabeled sugar efflux, this experiments reports that concentration of sugar that stimulates unidirectional exit half-maximally. Aliquots of the extracellular media are counted after stopping the reaction to measure the rate of sugar efflux. **D.** Equilibrium exchange transport is measured when the concentrations of sugar in the cell and the extracellular medium are equal. Unidirectional sugar fluxes are measured using radiotracer amounts of sugar.

Adapted from *Carruthers et al.* (*12*)

Fig 1.6

A — Zero-Trans Uptake

Sugar

Procedure
$[Sugar]_o$ Varied
$[Sugar]_i = 0$

Measures
$K_{m (entry)}$
$V_{max (unidirectional entry)}$

B — Zero-Trans Efflux

Procedure
$[Sugar]_i$ Varied
$[Sugar]_o = 0$

Measures
$K_{m (exit)}$
$V_{max (unidirectional exit)}$

C — Infinite Cis Exit

Procedure
$[Sugar]_o$ Varied
$[Sugar]_i = Fixed$

Measures
$[Sugar]_{50\% Inhibition}$
$V_{max (net exit)}$
$K_{m (entry)}$

D — Equilibrium Exchange

Procedure
$[Sugar]_o =$
$[Sugar]_i$

Measures
$K_{m (eq exch)}$
$V_{max (eq exch)}$

medium, and at 20ºC has a K_m of 4.6 mM and a V_{max} of 154 mmol L^{-1} min^{-1} (*91*). Infinite-cis exit measurements measure V_{max} for sugar exit and the concentration of extracellular sugar that reduces net exit by 50%. Transport rates may be determined either by light-scattering analysis or radiotracer sugar exit. Light-scattering infinite-cis exit of erythrocytes has a K_m of 2.0 mM and a V_{max} of 179 mmol L^{-1} min^{-1} (*90*). The rate of sugar entry as determined by zero trans uptake is almost tenfold lower than the rate of equilibrium exchange at the same temperature, while the rate of infinite-cis exit is only twofold lower than exchange. For advocates of the simple carrier hypothesis, this observed transport asymmetry results from different site affinities and rates of protein conformational change. Faster equilibrium exchange may be accounted for because the carrier bypasses a slower relaxation phase, or in this case $k_{-1} > k_{-0}$, and $k_1 > k_0$, as seen in Fig 1.5. Upon closer mathematical analysis, however, the simple carrier model breaks down in terms of predicting affinities and maximum transport rates.

Carruthers (*92*) analyzed in detail mathematical expressions derived from the simple carrier (Fig. 1.5). He found the simple carrier could successfully predict K_m for zero trans uptake and exit (1.6 mM and 10 - 25 mM respectively). However, the experimental data for glucose at 20 ºC, K_m for infinite cis uptake (2 mM; saturated sugar uptake into cells loaded with varying [D-glucose]) is significantly lower than the simple carrier's predicted values of 15 mM. The predicted equilibrium exchange value of 8.15 mM also underestimates the measured value of 27.2 mM (*92*). These observations are consistent with reservations about the simple carrier model expressed by Nafatlin & Holman, who proposed that the sheer density of erythrocyte GLUT1 (10% by mass,

(*93*)) creates an unstirred layer of substrate just below the cytoplasmic surface of the membrane. This would artificially increase the concentration of cytoplasmic glucose at the e1 binding site during an uptake experiment, as well as reduce the effective e1 concentration during an exit experiment (*94*). Experimental support for the unstirred layer hypothesis shows that net 3MG uptake displays biphasic kinetics in erythrocytes. This suggests rapid equilibration with an unstirred layer followed by slower diffusion into bulk cytosol (*95*). Given all the data, Carruthers hypothesized that extant measuring techniques were too slow to correctly determine binding constants. *Blodgett and Carruthers (96)*, Carruthers utilized a rapid quench flow system to further resolve 3MG uptake (50μM, 22ºC) in red cells into three sequential phases, a rapid phase (rate constant $k = 69s^{-1}$) thought to represent sugar sequestration within the protein, a fast phase ($k = 0.13s^{-1}$) of translocation and release, and a slow phase ($k = 0.0021s^{-1}$, or .12 min^{-1}) of diffusion into bulk cytosol (*96*). However, even with the modifications imposed upon the simple carrier model by the unstirred layer hypothesis, the simple carrier remains inadequate to explain all the structure function data obtained, leading to the development of the fixed, two-site carrier.

Alternating Conformer Model

Carruthers et al. found that in the presence of increasing concentrations of an e2 site inhibitor, such as maltose, the K_i (inhibitor affinity constant) for an e1 site inhibitor increases in a saturable manner that is quite inconsistent with the competitive inhibition predicted by the simple carrier model (*97*). The reverse situation was also true; increasing

Figure 1.7 Graphical representation of substrate translocation and conformational changes within an alternating conformer or fixed site carrier model.

　　A. There are four possible conformational changes in dimer translocation: empty dimer, dimer with one substrate transporting inward, dimer with one substrate transporting outward, and dimer with two substrates traveling simultaneously in opposite directions. E represents the dimer with its left subunit facing the outside of the cell, while F represents its functional equivalent after both monomers have exchanged orientation.

　　B. King-Altman Diagram of the fixed two site carrier model of obligate, antiparallel dimer transport. Rates of translocation are indicated by small case k constants, while binding affinities are shown as uppercase K constants. Any motion implied by a small k constant crosses the lipid bilayer, while any arrow with a large K constant indicates a substrate binding event. Empty dimer is E, in the top left corner of the inner square. Fully complexed dimer is S_1ES_2, in the bottom right corner of the outer square.

Fig 1.7

A

The Fixed-Site Carrier

B

concentrations of an e1 inhibitor, such as cytochalasin B, increased K_i for maltose in a hyperbolic manner (*97*). The simple carrier model predicts that an exofacial inhibitor at e2 should reduce the concentration of e1 sites available for endofacial inhibitor at site 1, and vice versa. However, the simple carrier model cannot account for the observed allosteric communication between e1 and e2 sites. *Hamill et al.* went on to show that low concentrations of extracellular maltose increase the rate of 3-OMG import (*7*). These observations argue for the presence of at least two coordinating exofacial e2 sites. Similarly, *Cloherty et al* (*16*) demonstrate that low concentrations of cytochalasin B or forskolin stimulate sugar uptake, which argues for the presence of at least two coordinating endofacial e1 sites.   If we assume that each GLUT1 protein alternately presents e2 and e1 sites, and that maltose and cytochalasin B bind at e2 and e1 sites respectively, together these findings argue that tetrameric GLUT1 is the minimal membrane complex that may accommodate the data.

Further evidence for tetramer subunit-subunit interactions comes from mononucleoside adenosine triphosphate (ATP) interactions with the transporter. At its simplest, the cytosolic side of GLUT1 e1 monomer presents at least one ATP binding site, which when occupied by ATP promotes sugar transport asymmetry. However, when red cells become ATP depleted, are artificially acidified, or excess AMP is present, this sugar transport asymmetry is lost. V_{max} for sugar exit is increased, K_m for exit is reduced, and both K_m and V_{max} for sugar uptake are increased (*88, 89, 93, 98, 99*). The net effect is increased total glucose transport capacity at physiological glucose (5-10 mM).

ATP binding to GLUT1 is cooperative. While binding of the first ATP molecule

is a low affinity event ($K_{d(app)}$=250 µM), the second ATP molecule binds with 15-fold

greater affinity ($K_{d(app)}$=15µM, (*89*)), suggesting communication between sites. Upon

reconstitution into pH 6 proteoliposomes, GLUT1 displays only high affinity binding for

ATP and loses ATP-modulation of transport as well as cooperative function(*88, 99*).

Under conditions of low pH, all four subunits expose an ATP-binding site and,

paradoxically, they become insensitive to ATP (*89*). This underscores the importance of

conformational change to cooperative binding.

The simplest explanation for the observed cooperative binding of ligands is the

obligate, functionally antiparallel association of two sugar uniporters. The fixed, two site

model (Fig 1.6A) posits that the glucose transporter is a homo-oligomer, typically a

dimer or tetramer, with equal numbers of e1 and e2 sites facing opposite sides of the

membrane. Binding of a sugar in the substrate-binding pocket of one subunit results in a

coordinated conformational change in which the entire oligomer switches its functional

orientation, whether or not other subunits contain substrate (*63*).   Thus a tetramer

comprising e1.e2.e1.eS2 becomes e2.e1.e2.eS1. Subunit-subunit contacts provide an

intuitive model for the cooperativity seen between substrate binding sites. These affinity

constants are represented in the King-Altman diagram in Fig 1.6 as uppercase

dissociation constants, with isomerization rates represented as lower case constants (*63,

92*).

Small Molecule Modulators of GLUT1 Function

Due to the utility and availability of the human erythrocyte glucose transporter in

erythrocytes, the properties of many sugars and ligand modulators have been extensively

characterized (Tables 1.2, 1.3 and 1.4) GLUT1 transports the sugars D-glucose, 2-deoxy glucose, galactose, sorbose, dehydroascorbic acid, and 3-O-methyl glucose. (Table 1.2) GLUT1 behavior is modulated by sugars in three ways; 1) sugars compete for binding at the same site (cis competition), 2) Binding of sugars allosterically modulates sugar binding at different sites at the same surface of the membrane (cis-allostery), and 3) binding of sugar at the surface of the membrane allosterically modulates sugar binding at the opposite side of the membrane (trans-allostery) (*97*).

What comprises a transportable sugar? To further elucidate determinants of sugar binding to the e2 site, *Munday, et al* studied the hydrogen bonding preferences of the exofacial sugar binding pocket by measuring the ability of substituted sugars to inhibit L-sorbose uptake. (Table 1.4) *Munday et al* deduced key structural requirements for glucose transport asymmetry: they concluded that the hydroxyl group at carbon 1 and carbon 3 of glucose were hydrogen bond acceptors, while the hydroxyl at carbon 4 was a hydrogen bond donor. Spatial requirements around carbon 2 are considered tight, since 2-O-Methyl Glucose binds with low affinity. Glucose-6-phosphate poorly inhibits L-sorbose uptake, suggesting that a strongly hydrophobic region surrounds the area that interacts with glucose at carbon position 6 (Fig 1.7)(*6, 111*).

The most extensive and varied research into other GLUT1 ligands has been done by *Naftalin et al,* analyzing ligands such as testosterones, estrogens, and green tea cathechins to fathom the complex interregulatory effects of hormones and drugs on this ubiquitously

Table 1.2

Sugar	Measurement	Action[a]	K_m[b]	V_{max}[c]	Ref
D-Glucose 20C	ZT Uptake	K_m e2 V_{max} Influx	1.6	36	(*90*)
	IC Exit	K_m e1, V_{max} efflux	2.0	179	(*90*)
	Eq Exch	K_m, V_{max} exchange	17	352	(*90*)
D-Galactose 20C	ZT Uptake	K_m e2 V_{max} Influx	31.8	28.6	(*63*)
	IC Exit	K_m e1, V_{max} efflux	19.2	-	(*63*)
	Eq Exch	K_m, V_{max} exchange	138	432	(*63*)
DHA 20C	ZT Uptake	K_m e2 V_{max} Influx	3.5	4.8	(*100*)
D-Glucose 0-4C	ZT Uptake	K_m e2 V_{max} Influx	0.2	0.21	(*90*)
	IC Exit	K_m e1, V_{max} efflux	0.39	8.6	(*101*)
	Eq Exch	K_m, V_{max} exchange	25	30	(*101*)
3MG 0-4C	ZT Uptake	K_m e2 V_{max} Influx	0.38	0.18	(*12*)
	ZT Exit	K_m e1, V_{max} efflux	4.35	1.62	(*12*)
	Eq Exch	K_m, V_{max} exchange	22.6	9.17	(*12*)

Table 1.2 Transportable Sugars and their Kinetic Properties in Erythrocytes.

[a] Properties of the transporter directly measured by the experimental analysis. [b] Affinity in mM. [c] Rate expressed as (mmol*L)/min.

Table 1.3

Inhibitor	Site	K_i (inh)	T	Inhibits / Measured	Ref
Cytochalasin B	e1	0.1 μM	22C	14C CB to Ghosts	(*102*)
	e1	0.35 μM	21C	IC D Glucose Efflux	(*103*)
	e1	0.26 μM	21C	D Glucose Eq Exch	(*103*)
	e1	0.46 μM	25 C	IC D Glucose Efflux	(*104*)
+ATP	e1	0.76 μM	25 C	IC D Glucose Efflux	(*104*)
Phloretin	e2	10 μM	37C	ZT D Glucose Upt	(*105*)
	e2	0.37 μM	25 C	IC D Glucose Efflux	(*104*)
	e2	0.48 μM	21 C	ZT D Glucose Upt	(*106*)
Forskolin	e1	7.5μM	21C	ZT 3MG Uptake	(*107*)
p-butyl phenol	e2	660 μM	37C	ZT D Glucose Upt	(*105*)
Phloretic Acid	e2	1.42 mM	37C	ZT D Glucose Upt	(*105*)
Phlorpropophenone	e2	142 μM	37C	ZT D Glucose Upt	(*105*)
Phloroglucinaldehyde	e2	5 mM	37C	ZT D Glucose Upt	(*105*)
Naringenin	e2	142 μM	37C	ZT D Glucose Upt	(*105*)
Hexestrol	e2	14.2 μM	37C	ZT D Glucose Upt	(*105*)
Stilbestrol	e2	6.25 μM	37C	ZT D Glucose Upt	(*105*)
Dienestrol	e2	66 μM	37C	ZT D Glucose Upt	(*105*)
Tamoxifen	e1	0.76 μM	25 C	IC D Glucose Efflux	(*104*)
Oestradiol	e1	4.71 μM	25 C	IC D Glucose Efflux	(*104*)
Genistein	e1	4.2 μM	25 C	IC D Glucose Efflux	(*104*)
Quercetin	e2	16 μM	37 C	ZT 3MG Uptake	(*108*)
	e2	1.04 μM	21 C	ZT D Glucose Upt	(*106*)
Myricetin	e2	33.5 μM	37 C	ZT 3MG Uptake	(*108*)
Catechin-gallate	e2	90 μM	37 C	ZT 3MG Uptake	(*108*)
AzitriFluoroethylbenzoyl bismannose	e2	338 μM 360 μM	0 C 20 C	D-Galactose Binding	(*109*)
Phenobarbital	e2*	0.91 mM	21 C	ZT D Glucose Upt	(*110*)
Aniracetam	e2*	1.05 nM	21 C	ZT D Glucose Upt	(*110*)
Benigride	e2*	10.2 μM	21 C	ZT D Glucose Upt	(*110*)
Montirelin	e2*	45.7 μM	21 C	ZT D Glucose Upt	(*110*)
Sunifferam	e2*	26 μM	21 C	ZT D Glucose Upt	(*110*)
Levriacetam	e2*	3.19 mM	21 C	ZT D Glucose Upt	(*110*)
Galanin Peptide	e2*	19.6 μM	21 C	ZT D Glucose Upt	(*110*)
L-Pyroglutamic Acid	e2*	13.8 mM	21 C	ZT D Glucose Upt	(*110*)
Methamphetamine	e2*	118 μM	21 C	ZT D Glucose Upt	(*110*)
Diazepam	e2*	50 μM	21 C	ZT D Glucose Upt	(*110*)

Inhibitor	Site	K_i (inh)	T	Inhibits / Measured	Ref
Thiamylal	e2*	0.22 mM	21 C	ZT D Glucose Upt	(*110*)
Melatonin	e2*	155 μM	21 C	ZT D Glucose Upt	(*110*)
Testosterone	e2	39.2 μM	21 C	ZT D Glucose Upt	(*106*)
Andostrenedione	e2	29.6 μM	21 C	ZT D Glucose Upt	(*106*)
5 Andostenediol	e2	50 μM	21 C	ZT D Glucose Upt	(*106*)
Androsterone	e2	44 μM	21 C	ZT D Glucose Upt	(*106*)
Epianderosterone	e2	33 μM	21 C	ZT D Glucose Upt	(*106*)
Etiocholanone	e2	1.25 μM	21 C	ZT D Glucose Upt	(*106*)
Dehydroepiandrosterone 3 acetate	e2	4.8 μM	21 C	ZT D Glucose Upt	(*106*)
Dehydroepiandrosterone Sulfate	e2	189.1 μM	21 C	ZT D Glucose Upt	(*106*)
Flutamide	e2	73.4 μM	21 C	ZT D Glucose Upt	(*106*)
Green Tea Extract (Whole)	e2	1.31 μM	21 C	ZT D Glucose Upt	(*106*)
Epigallochatechin 3-gallate	e2	0.97 μM	21 C	ZT D Glucose Upt	(*106*)
Epichatechin	e2	1.74 μM	21 C	ZT D Glucose Upt	(*106*)
Epichatechin 3-gallate	e2	0.14 μM	21 C	ZT D Glucose Upt	(*106*)
Epigallochatechin	e2	111 μM	21 C	ZT D Glucose Upt	(*106*)

Table 1.3 Summary of Ligand Interactions With GLUT1.

All experiments were made in erythrocytes, and are inhibition of D-Glucose

transport by GLUT1 except where noted.

Table 1.4

#C[a]	Sugar Name	Transportable	Site	K_i L-Sorbose[b]
1	D-Glucose	Y	Both	7.6
1	1-Deoxy D Glucose	Y	Both	76
2	2-Deoxy D Glucose	Y	Both	3.2
2	2-O-Methyl D Glucose	Y	Both	119
2	D-Mannose	N	E2	36
3	3-Deoxy D Glucose	Y	Both	71.5
3	3-O-Methy D Glucose	Y	Both	12
3	D-Allose	N	E2	N.D.[c]
4	D-Galactose	Y	Both	85
4	Maltose	N	E2	19
4	Cellobiose	N	E2	51
4	Lactose	N	E2	>250
6	6-Deoxy D-Glucose	Y	Both	6.7
6	Glucose 6-Phosphate	N	E2	N.D.[c]
5	D-Xylose	Y	Both	69
5	D-Galactose	Y	Both	85

Table 1.4 Summary of the inhibition of L-Sorbose uptake into erythrocytes by modified Sugars(*6*).

[a] Carbon position on the glucose molecule that has been modified, as compared to D-Glucose. [b] All K_i constants are in mM. [c] No detectable inhibition of uptake.
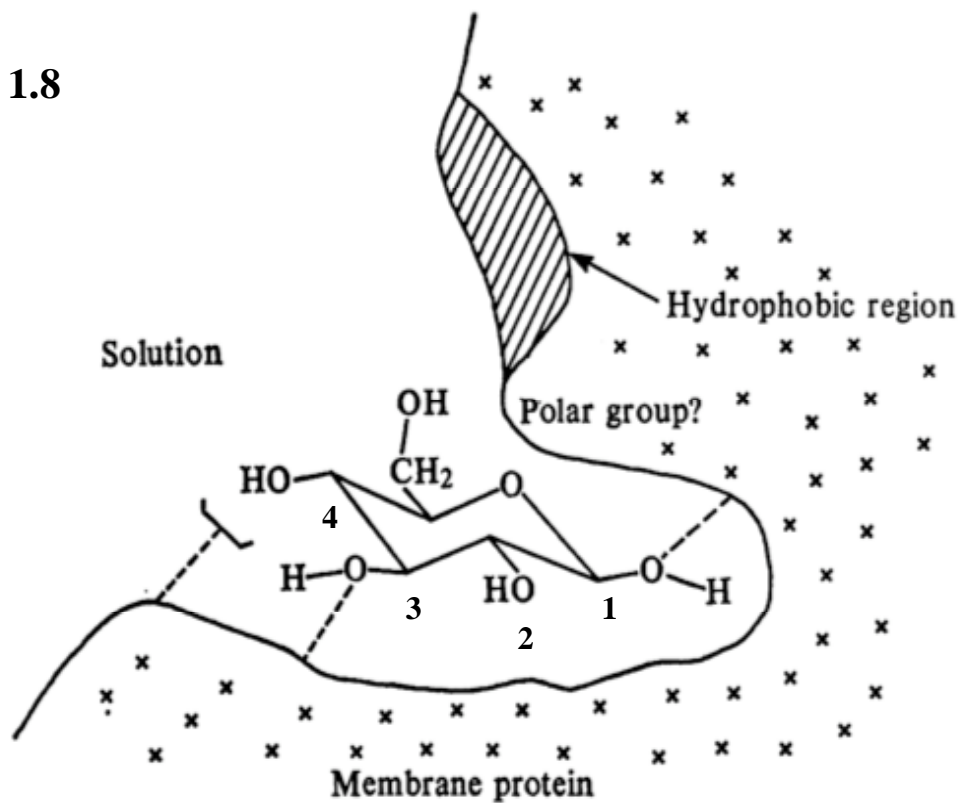
Figure 1.8 Rendition of exofacial sugar binding site taken from Munday, et al. (*6*)

  The first four carbons of the D-Glucose molecule pictured are numbered. It is postulated that D-Glucose slides through the transporter in the pyranose ring form, emerging in the same orientation at the other side. The membrane protein surface has been sketched in to approximate the results from L-sorbose inhibition data.

expressed protein (*104, 106, 110, 112*). The results of these studies are summarized in Table 1.3. However, the most widely studied small molecule modulators of sugar transport are discussed here in more depth: cytochalasin B, forskolin, phloretin, and ATP.

CYTOCHALASIN B

Cytochalasin B (CB) is a cell-permeable fungal toxin which also inhibits glucose transport by interacting with the e1 conformation of GLUT1. This ligand binds with an approximate erythrocyte K_d of 0.1μM (*102, 104, 113*). Other cellular activities include the strong inhibition of actin polymerization, restriction of cellular movements, as well as inhibition of cytokinesis (*114*).

Documented interactions of CB inhibition of GLUT1 include the following. 1) A common clinical missense case of GLUT1DS arising by point mutation at position R126 (H, E, L, K, C) results in decreased CB affinity (*115*). 2) Cytochalasin B at low concentrations (5nM) is a mild stimulator of sugar uptake by GLUT1 (*88*). This behavior in conjunction with maltose stimulation of glucose uptake refutes the simple carrier hypothesis as mentioned above (*97*). 3) Mutation of W387 and W412 separately decreases CB photolabeling of GLUT1, and together eliminates labeling by CB (*44, 116, 117*). 4) *Salas-Burgos et al* mapped one endofacial cytochalasin B binding site on their homology-modeled GLUT1 structure, suggesting involvement of residues L85, N88, R89, R92, K225, Q250, M251, and R400 (*5*). 5) *Holman and Rees* uv-photolabeled GLUT1 with a radiolabeled cytochalasin B, then digested labeled transporter with chymotrypsin. The smallest ^{3}H-CB photocrosslinked fragment found on the gel corresponded to GLUT1 residues 388-412, indicating that the GLUT1 endofacial sugar

binding site lies within or adjacent to that sequence. (*13*)

FORSKOLIN

Forskolin (FSK) is a cell-permeable diterpenoid that competitively inhibits glucose transport at the e1 site with a $K_{i(app)}$ of 7.5μM for inhibition of red cell transport. FSK is also a high-affinity inhibitor of GLUT4 mediated sugar transport in cardiac and skeletal muscle. (*107, 118*). Forskolin acts as an activator of adenylyl cyclase, and sees broad use in cell culture as a stimulator of cyclic adenosine monophosphate production (*119, 120*). Further documented interactions of FSK with GLUT1 include 1) IAPS forskolin has also been used to photolabel GLUT1; like CB, its photolabeling site is near W388 (*121, 122*). 2) *Salas-Burgos et al* docked forskolin to their homology modeled GLUT1 structure at two sites: the exofacial residues are N34, K38, W65, S285 and P306 while the endofacial residues are F81, V83, G84, G138, G398, and R400 (*5*).

PHLORETIN

Phloretin is the aglucon (sugarless form) of phlorizin, a compound originally known to induce glycosuria(*123*), and later shown to inhibit glucose transport in erythrocytes with a K_I of 10μM at 37ºC (*105, 124*). Phloretin is a competitive, temperature dependent inhibitor of the e2 site of both Group 1 and Group 2 human sugar porters. (*104, 106, 125*). It also blocks L-type Ca^{2+} channels, and may activate Ca^{2+}-activated K^+ channels in amphibian myelinated nerve fibers. (*114*) *Salas-Burgos et al* mapped two phloretin binding sites on their GlpT homology modeled version of GLUT1: an exofacial binding site at residues N34, W65 and S285, and an endofacial one at S80, F81, L85, G183, R400, and G398 (*5*).

ADENOSINE TRIPHOSPHATE

GLUT1 is an ATP binding protein that does not engage in ATP hydrolysis. GLUT1-ATP interactions appear to regulate GLUT1 function to meet the metabolic needs of the cell. As mentioned previously, if ATP dips below normal physiological levels, GLUT1 transport asymmetry is lost. (*88, 89, 93, 98, 99, 126-131*) It is tempting to speculate that this system evolved to permit tissues in which glycolysis is used for fast energy metabolism in order to respond rapidly to metabolic stress.

Several lines of evidence point to the cooperativity of ATP binding. Binding is cooperative as measured by fluorescence quenching with at least two binding sites per oligomer. (*88*) ATP binding is known to induce significant conformational changes when bound to GLUT1, for covalent labeling of GLUT1 lysine residues by NHS esters, GLUT1-sensitivity to trypsin and IgG binding to Loop 7 or the C terminus are inhibited when GLUT1 is exposed to saturating ATP. (*89, 99*) Proteolytic digestion followed by mass spectrometric analysis confirms global conformational changes of GLUT1 by ATP. Briefly, sulfo-NHS-biotin, a lysine-reactive reagent, was reacted with GLUT1 ± ATP, digested, and protected lysines determined by MALDI-TOF analysis. Loop 6-7 lysines 225, 229, and 230 are not protected, but labeling of lysines 244, 255, and 256 are inhibited by the presence of ATP. Substitution of GLUT4 loop 6-7 sequence greatly reduced ATP inhibition of c-terminal IgG binding, although two of three sensitive lysines remained present. Taken together, this suggests loop 6-7 lysines do not play a direct role in ATP regulation of glucose transport, though they possess an altered conformation in response to ATP binding. (*132*) It is possible the strong cooperativity shown in ATP

binding serves to fine-tune the regulation of GLUT1 function.

Overall Conclusions and Research Purpose

Protein-mediated sugar transport is vital for cellular growth. Dissecting and delineating transporter structure/function relationships is imperative to understand of GLUT1 function *in vivo*, essential to efforts to develop small molecules that target specific transporters for inhibition (or activation) and is fundamental to efforts aimed at understanding the molecular basis of carrier-mediated transport. Remaining gaps in our understanding addressed in this thesis include how cellular context affects function, as well as characterization of the e1 binding site from a ligand binding or mutagenic perspective.

GLUT1 has been studied in different tissues and in varied heterologous expression systems and is characterized by a complexity that is unexplained by the available hypotheses for carrier-mediated sugar transport (*9*). It is possible that the operational properties of GLUT1 are determined by host cell environment. A glucose transport-null strain of *Saccharomyces cerevisiae* (RE700A) was transfected with GLUT1. Its growth on glucose media, selectivity, and sugar transport kinetics were characterized. Unlike erythrocyte transport, the $K_{m(app)}$ for RE700A-resident GLUT1 2-deoxy- D-glucose uptake equals $K_{i(app)}$ for 2-deoxy-D-glucose inhibition of 3-*O*-methylglucose uptake. Unidirectional sugar uptake in RE700A-GLUT1 is neither inhibited by reductant nor stimulated by intracellular sugar. Net uptake of subsaturating 3-*O*-methylglucose by RE700A-GLUT1- HA-H6 is a first-order process. These findings support the hypothesis that the observed red cell sugar transport complexity is host cell-

specific.

Cytochalasin B (CB) and forskolin (FSK) inhibit GLUT1-mediated sugar transport in red cells by binding at or close to the GLUT1 sugar export site. Paradoxically, very low concentrations of these inhibitors produce a modest stimulation of sugar transport *(16)* This result is consistent with the hypothesis that the glucose transporter contains multiple, interacting, intracellular binding sites for e1 ligands CB and FSK. By screening a library of cytochalasin and forskolin analogs, asks what structural features of exit site ligands determine binding site affinity and cooperativity. Some forskolin derivatives and cytochalasins inhibit equilibrium [³H]-CB binding to red cell membranes depleted of peripheral proteins. Others produce a modest stimulation of [³H]-CB binding when introduced at low concentrations, but inhibit binding as their concentration is increased. Yet other analogs modestly stimulate [³H]-CB binding at all inhibitor concentrations applied. These findings are best explained by a carrier that presents at least two interacting endofacial binding sites for CB or FSK. We discuss this result within the context of GLUT1 quaternary structure and evaluate the major determinants of ligand binding affinity and cooperativity.

As mentioned above, cytochalasin B (CB) inhibits GLUT1 substrate transport at or near the endofacial sugar binding site. N-bromosuccinamide digestion combined with ³H-CB photolabeling implicates the region between Trp388 and Trp412 in ligand binding. Although its structure has been modeled(*5*), the specific residues which comprise the sugar binding site are unknown. A series of alanine point mutants were made and characterized for CB inhibition of 2DOG uptake. Expression was verified by

Western blot and surface localization by immunofluorescence. GLUT1Phe88Ala,

GLUT1Arg92Ala and GLUT1Trp412Ala mutants were weakly expressed, while

GLUT1Ser80Ala did not express at the membrane. The ranking of 2-DG uptake by

construct was GLUT1Arg126Ala > GLUT1Cys421Ala > GLUT1Arg400Ala as

compared to untagged GLUT1 expressed in HEK cells. The CB inhibition of 2-DG

uptake of the constructs GLUT1Arg126Ala, GLUT1Cys421Ala , and GLUT1Arg400Ala

were not statistically different from that of c-myc tagged GLUT1. Since point mutations

proved insufficient to abrogate CB binding, chimeras of GLUT1 Trp388 to Trp 412

sequence were exchanged with the equivalent GLUT4 and GLUT5 sequence.

GLUT1/GLUT4/GLUT1 was a point mutation (Iso404Met) whose 2-DG uptake had a

similar CB sensitivity profile to untagged GLUT1. GLUT1/GLUT5/GLUT1 shows

enhancement of 2-DG uptake at 50nM CB but its overall CB dose response is

indistinguishable from WT GLUT1. We conclude the W388 to W412 sequence is

necessary for CB photolabeling, but not inhibition of 2 deoxyglucose uptake by CB. We

discuss these results with their implications for structure-function sequence localization

of the CB binding site, and by extension, the e1 sugar binding site.

CHAPTER II

PROPERTIES OF THE HUMAN ERYTHROCYTE GLUCOSE TRANSPORT PROTEIN ARE DETERMINED BY CELLULAR CONTEXT

This chapter was published in the journal Biochemistry in 2005, and can be found using the following reference:

Levine, K. B., Robichaud, T. K., Hamill, S., Sultzman, L. A., and Carruthers, A. (2005) Properties of the human erythrocyte glucose transport protein are determined by cellular context, Biochemistry 44, 5606-5616.

Data presented in this chapter found in Tables 2.1 and 2.2, as well as Figures 2.5 B and C were contributed to by myself, Trista K Robichaud; the remaining work was a collaboration with Kara B Levine, Ph.D. based upon original observations by Lisa Sultzman, Ph.D.

ABSTRACT

Human erythrocyte hexose transfer is mediated by the glucose transport protein GLUT1 and is characterized by a complexity that is unexplained by available hypotheses for carrier-mediated sugar transport (Cloherty, E. K., Heard, K. S. and Carruthers, A. (1996), *Biochemistry, 35*, 10411-10421). The current study examines the possibility that the functional properties of the transport protein are determined by the host cell. A glucose transport-null strain of *S. cerevisiae* (RE700A) was transfected with the p426 GPD yeast expression vector containing DNA encoding wild-type human glucose transport protein (GLUT1), mutant GLUT1 (GLUT1$_{3338A3}$) or carboxy-terminal hemagglutinin-polyHis-tagged GLUT1 (GLUT1-HA-H6). GLUT1 and GLUT1-HA-H6 are expressed at the yeast cell membrane and restore 2-deoxy-D-glucose, 3-O-methylglucose, and D-glucose transport capacity to RE700A. GLUT1-HA-H6 confers GLUT1-specific sugar transport characteristics to transfected RE700A including inhibition by cytochalasin B and high affinity transport of the nonmetabolized sugar 3-O-methylglucose. GLUT1$_{338A3}$ – an engineered GLUT1 mutant that cannot catalyze transport in mammalian cells – is expressed but does not restore RE700A sugar uptake capacity. In contrast to sugar transport in human red cells, $K_{m(app)}$ for uptake of a primary sugar by RE700A-GLUT1-HA-H6 is very close to $K_{i(app)}$ for inhibition of import of a second sugar by the primary sugar (e.g. $K_{m(app)}$ for 2-deoxy-D-glucose uptake = $K_{i(app)}$ for 2-deoxy-D-glucose inhibition of 3-O-methylglucose uptake). Unlike transport in human red cells or in human embryonic kidney cells transfected with GLUT1-HA-H6, RE700A-GLUT1-HA-H6 sugar uptake is not inhibited by reductant and is not stimulated by intracellular sugar. The time-

course of net sugar uptake at subsaturating 3-O-methylglucose concentrations is monophasic in RE700A-GLUT1-HA-H6. These findings support the hypothesis that red cell sugar transport complexity is host cell specific.

THE ABBREVIATIONS USED ARE: GLUTs, glucose transporters, GLUT1; human erythrocyte glucose transporter; 2DOG, 2-deoxy-*D*-glucose; C-Ab, rabbit polyclonal antiserum raised against a synthetic peptide comprised of GLUT1 residues 480-492; CB, cytochalasin B; 3MG, 3-O-methyl-D-glucopyranoside; DTT, dithiothreitol; EDTA, ethylenediaminetetraacetic acid; FOA, 5-fluoroorotic acid; HA-Ab, mouse monoclonal antibody directed against the hemagglutinin sequence LYPYNVPNYA; HEPES, (N–[2–Hydroxyethyl]piperazine–N'–[2–ethanesulfonic acid]); RBC, red blood cell; SDS-PAGE, sodium dodecyl sulfate -polyacrylamide gel electrophoresis ;Tris–HCl, tris(hydroxymethyl)aminomethane hydrochloride; Dpmp1p, dolichol phosphate mannose synthase.

INTRODUCTION

The facilitated diffusion of glucose across cell membranes is mediated by a family of integral membrane proteins named <u>Glu</u>cose <u>T</u>ransporters ([1]GluTs). Twelve mammalian glucose transport proteins have been identified, differing in primary structure, tissue distribution and substrate specificity (*1*). GLUT1, the human erythrocyte glucose transport protein, mediates sugar transport in red blood cells, in endothelial cells lining the vasculature and contributes to basal glucose transport in adipose and cardiac muscle (*40, 133-135*). Membrane-associated GLUT1 is multimeric (*65, 87*) and cytoplasmic ATP interacts directly and cooperatively with GLUT1 to modify transporter affinity for substrate and net sugar flux through the transport complex (*93, 136, 137*).

Red cells are uniquely suited to steady-state sugar transport determinations because they provide a geometrically uniform population of cells in which to measure sugar fluxes. The human red blood cell is also a particularly rich source of GLUT1, with the transporter representing 6% or more of total erythrocyte integral membrane proteins. Erythrocyte GLUT1is not directly amenable to mutagenesis and *in situ* expression. Manipulation of GLUT1-mediated sugar transport through mutagenesis, has required the development of heterologous expression systems for mutant GLUT1 expression. GLUT1 has been successfully expressed in mammalian cells (CHOK1(*65*), Cos-7 and HEK293 (*99*)), *Xenopus* oocytes (*138*) and in insect cells(*139*). None of these systems has achieved an efficiency of protein expression that yields sufficient GLUT1 to facilitate detailed

biochemical analysis. Only the oocyte presents a relatively uniform cell geometry and thereby permits detailed kinetic analysis of GLUT1-mediated sugar transport.

Previous heterologous expression studies have suggested that *S. cerevisiae* can express a relatively homogeneously glycosylated form of human GLUT1(*140*). Yeast, a eukaryotic organism, contains a superfamily of sugar transporters (35 genes) that includes maltose, inositol, and glycerophosphoinositol transport proteins(*68*). *S. cerevisiae* contains a subfamily of 18 hexose transporters (HXT 1-17 and galactose permease (Gal2)) which, like the GLUTs, catalyze the facilitated diffusion of sugars across cell membranes(*141*). Sequence alignment indicates that the HXT proteins are similar to GLUT1, containing 12 putative transmembrane domains and intracellular amino and carboxyl termini (*70*). Yeast may, therefore, present a suitable expression system in which to produce wild type and mutant recombinant human red blood cell glucose transport proteins.

Deletion of *S. cerevisiae* HXT 1-7 produces a strain of yeast (RE700A) that is unable to grow on glucose media (*142*). This suggests that HXT 1-7 are the major hexose transporters in S. cerevisiae. *Wieczorke et al* (*141*) have suggested that a minimum of 20 hexose transporter genes (hxt 1-17, Gal2, maltose permeases Y9DL247w, YJR160c) must be eliminated in *S. cerevisiae* order to produce a yeast strain completely lacking in sugar transport capacity. However, in contrast to RE700A, the yeast strain used in their study (CEN.PK2-1C) appears to possess a greater capacity for respiration and consequently,

may be able to grow by utilizing residual levels of sugar present in the cells (*143*). The galactose permease (Gal2), which is a member of the hexose transporter family, has also been shown to transport glucose. Although it remains in the RE700A strain, Gal2 is tightly controlled by the presence of galactose and is inhibited by high intracellular glucose(*144*). Expression of the maltose permeases (YDL247w, YJR160c) which may modulate glucose transport in *S. cerevisiae*, is also repressed by glucose (*145*).

The present study characterizes human GLUT1 expression in *S. cerevisiae* using RE700A - the HXT 1-7 null yeast strain. RE700A transfected with exogenous, human GLUT1 is selectable by its ability to grow on, and transport glucose. Expressed GLUT1 interacts with human GLUT1-directed C-terminal antisera, co-localizes with yeast plasma membrane markers, displays a functional stereochemistry similar to erythrocyte-resident GLUT1 and is inhibited by inhibitors of GLUT1-specific sugar transport. This heterologous expression system may provide a rapid screening vehicle for mutant GLUT1 proteins. Significant kinetic differences between sugar transport in GLUT1 expressing human red cells and RE700A cells suggest that the complexity of human erythrocyte sugar transport (*9*) may be cell context-specific.

MATERIALS & METHODS

MATERIALS

[^{14}C]-D-Glucose, [^{14}C]-3-0-methyl-glucose, and [^{3}H]-2-deoxy-glucose were purchased from Dupont NEN (Wilmington, DE). Complete protease inhibitor tablets were purchased from Roche (Mannheim, Germany). Supersignal ECL reagents were obtained from Pierce (Rockford, Il). Centricon concentrators were acquired from Millipore (Bedford, MA). SCM-URA dropout mix was purchased from Bufferad (Newark, NJ). Nitrocellulose and Immobilon-P were obtained from Fisher Scientific, (Pittsburg, PA).

RED CELLS

De-identified, washed red blood cells and whole blood stored in CPDII AS-1 preservative solution were obtained from Biological Specialties Corporation (Colmar, PA). Red cells were isolated by repeated wash/centrifugation cycles in ice-cold saline. One volume of whole blood was mixed with 3 or more volumes of saline and centrifuged at 10,000 x g for 5 minutes at room temperature. Serum and the buffy coat were aspirated and the wash/centrifugation cycle repeated until the supernatant was clear and the buffy coat was no longer visible. Cells were resuspended in 20 volumes of saline and were incubated for 30 minutes at 37 ˚C in order to deplete intracellular sugar levels.

HEK923T Cells

HEK cells were maintained in Dulbecco's Modified Eagle Medium (DMEM) supplemented with 10% FBS , 100 units/mL penicillin, and 100 μg/mL streptomycin in a 37 ˚C humidified 5% CO_2 incubator.

Antisera

A peptide corresponding to GLUT1 residues 480-492 was synthesized by the University of Massachusetts Medical School Peptide Synthesis facility. This peptide was conjugated to keyhole limpet hemocyanin using a kit purchased from Pierce. Rabbit antisera (C-Ab) against this GLUT1 peptide were obtained from Animal Pharm Services Inc (Healdsburg, CA). Anti-GLUT1 antisera reacting exclusively with extracellular epitopes of GLUT1 (∂-Ab) were prepared as described previously (*146*). Goat anti rabbit IgG horseradish peroxidase was purchased from Biorad (Hercules, CA). Anti-yeast dolichol phosphate mannose synthase (Dpm1p) antiserum was obtained from Molecular Probes (Eugene, OR).

Solutions

Phosphate-buffered saline (PBS) contained 140 mM NaCl, 10 mM Na_2HPO_4, 3.4 mM KCl, 1.84 mM KH_2PO_4 (pH 7.3), and 5 mM EDTA. 2X Spheroplasting buffer contained 2.8 M sorbitol, 0.1 M potassium phosphate buffer (pH 7.4), and 10 mM NaN3. Membrane buffer was composed of 0.8 M sorbitol, 1 mM EDTA, and 25mM HEPES). Sample buffer (2X) contained 0.125M Tris-HCl, (pH 6.8), 4% SDS, 20% glycerol, and 50 mM DTT. Phosphate Buffer (PB) pH 6.5 included 0.329 mM KH_2PO_4.

Buffer A consisted of 300 mM NaCl, 10 mM imidazole, 20% Glycerol, and 50 mM NaH$_2$PO$_4$.

REAGENTS

Restriction enzymes were purchased from New England Biolabs. The glucose transport null strain of S. cerevisiae, RE700A, was generously provided by Dr. M. Johnston (University of Washington, St. Louis). p426 and p416 yeast expression vectors, as described in(*89*), were provided by Dr. C. Hirschberg (Boston University, the Goldman School of Dentistry, Department of Molecular and Cell Biology).

GENETIC ENGINEERING

A 1.7 kbp fragment of GLUT1 cDNA was subcloned into BamH1 site of the high copy number yeast expression vector p426. Removal of the 5'-untranslated region of the GLUT1 sequence was accomplished by using PCR to insert a unique Spe1 restriction site 3 bps prior to the GLUT1 start codon. This construct was subcloned into the Spe1-BamH1 restriction site of the p426 yeast expression vector. The triple alanine GLUT1 mutant, GLUT1$_{338A3}$ in which GLUT1 residues 338, 339 and 340 were each replaced with alanine, was engineered using the Stratagene Quickchange^{tm} Site Directed Mutagenesis Kit and confirmed by sequence analysis.

TRANSFECTION OF RE700A WITH GLUT1

Stable expression of GLUT1 in yeast was accomplished using RE700A, a strain of *S. cerevisiae* in which 7 of 20 hexose transporters are disrupted (*142*). This results in a

yeast strain incapable of using glucose as a primary carbon source and subsequently unable to grow on glucose media. Briefly, cells were prepared for electroporation using the following protocol. RE700A (250 mL) grown to an OD600 of 1.3-1.5 in YP-maltose were pelleted by spinning at 1,500 x g for 5 min at 4 °C. Following two washes in ice cold sterile water (250 mL followed by 125 mL), the cells were washed in 20 mL of ice cold 1M sorbitol than resuspended in 1 mL of 1M sorbitol. A portion of the cell slurry (80-100μL) was mixed with 5-20μg of DNA, equilibrated on ice for 10-20 minutes, then transferred to a pre-chilled 0.2 cm electroporation cuvette. The yeast were pulsed at 1.5 kV, 25 μF, and 200 Ohms. Immediately, 1mL of ice cold sorbitol was added to the cuvette and the cells were plated onto SCM-URA maltose selective media. Growth was observed after 2-4 days at 30 °C.

TRANSIENT EXPRESSION OF GLUT1 IN HEK CELLS

GLUT1-HA-H6 was subcloned into the BamH1 site of the pcDNA3.1+ mammalian expression vector as described previously (*147*). Sub confluent HEK923T cells were transfected with GLUT1-HA-H6 cDNA using the Fugene 6 transfection reagent system. Following transfection, cells were maintained in DMEM for 24 hours, at which time, 0.72 mM G418 (Geneticin) was added to the media and the cells were allowed to continue growing for an additional 48 hours.

MEMBRANE ISOLATION

Yeast grown to late log phase were washed in an equal volume of cold 10 mM NaN_3 and resuspended in 20 mL each of 10 mM NaN3 and 2X spheroplasting buffer.

Zymolase 20T was added (25mg/15mL) and the suspension was incubated at 30 ˚C for 1-2 hours. Successful cell wall removal was monitored by measuring yeast optical density periodically throughout the incubation period. Yeast were centrifuged at 3000 x g for 10 min and the pellet was resuspended in a small volume of membrane buffer containing protease inhibitors. Yeast were lysed by repetitive pipetting and were then diluted to 100mL by addition of membrane buffer plus protease inhibitors. Lysed cells were spun at 3,000 x g for 10 minutes to isolate the P1 fraction; at 8,000 x g for 20 minutes to pellet the P2 Fraction, and at 100,000 x g for 30 minutes to sediment the plasma membrane containing P3 fraction. Membranes were resuspended in membrane buffer with protease inhibitors and stored at -70 ºC until use.

To harvest HEK923T cell membranes, 6 culture plates of cells (150 mm) were washed twice with PBS + 5 mM EDTA, than scraped into 20 mL of lysis buffer mixed with 1 mM PMSF. Membranes were prepared according to (*148*). Briefly, cells were homogenized for five minutes with a Fisher Dyna-Mix, then spun at 5000 x g for 10 minutes at 4 ˚C. The supernatant was decanted and centrifuged at 100,000 x g for 1 hour to pellet crude membrane fractions. Membranes were resuspended in 300 μL Buffer A with 1mM PMSF and frozen at ⁻70ºC until use.

RENOGRAFIN DENSITY GRADIENTS

Crude yeast membranes were resolved on Renografin gradients as previously described in (*149*). Briefly, the P3 fractions isolated from RE700A and RE700A-GLUT1-HA-H6 were combined with an equal volume of Renografin-76. The Renografin gradient

was constructed on top of 0.8mL of sample (38% Renografin) by sequentially layering

0.8 mL of 34, 30, 26, and 22% Renografin-76 diluted in 50 mM Tris-HCl pH 7.4.

Gradients were centrifuged in a 50.1Ti rotor at 40,000 rpm for 20 hours at 4 $^{\circ}$C. Samples

were isolated from the top down in aliquots of 500 μL, and stored at -70 ˚C until use.

Fractions containing GLUT1, the yeast endoplasmic reticulum marker OST, and the yeast

plasma membrane marker Ste1p were determined by Western Blotting.

POLYACRYLAMIDE GEL ELECTROPHORESIS AND WESTERN BLOTTING

Proteins were resolved on 10% polyacrylamide gels as described previously in

(*150*). Recombinant human GLUT1, Dpm1p, and Ste1p were detected by Western Blot

analysis. Peptides separated by SDS-PAGE were transferred electrophoretically to

nitrocellulose membranes, which were subsequently blocked for 1 hour in PBS-T (PBS +

0.1% tween detergent) with 20% Carnation nonfat dry milk. Following four washes of 5

minutes in PBS-T, membranes were incubated for 1 hour in primary antibody. C-Ab was

diluted 1:10,000 in 3% nonfat dry milk/PBS-T, anti Dpm1p was diluted 4μg/ml in 3%

nonfat dry milk/PBS-T, and anti-Ste1p was diluted 1:2000 in 3% nonfat dry milk/PBS-T.

Following four wash cycles to remove primary antibody, membranes were exposed for 45

minutes to secondary antibody (goat anti-rabbit IgG or goat anti mouse IgG) diluted

1:5000 in PBS-T containing 3% nonfat dry milk. Detection of antigen-antibody

complexes was achieved by chemiluminescence using Pierce Supersignal ECL reagents.

Sugar Transport Measurements

ZERO-TRANS UPTAKE

RE700A and RE700A-GLUT1 (wild type and mutant 338) were grown to an

OD_{600} of 0.6 in YP-maltose and SCM-URA-maltose respectively. 50 mL of culture was

centrifuged at 5,000 x g, then washed twice in phosphate buffer (PB). Samples were

resuspended in 1 mL of PB. 100 μL aliquots of cells at room temperature were exposed to

4 volumes of room temperature PBS containing [^{3}H] D-glucose. Uptake of 100μM D-

glucose was measured at 5 minute intervals then 10 volumes of ice cold PBS were added

to the samples to stop the reaction. The yeast suspension was sedimented by

centrifugation (14,000 x g for 30sec), the supernatant was aspirated, and the

wash/centrifugation/aspiration cycle was repeated. The resulting pellet was extracted in

500μL of 3% perchloric acid. The acid extract was centrifuged, and duplicate samples of

the clear supernatant were counted. Time zero uptake points were prepared by addition

of ice cold PBS to cell suspensions prior to addition of medium containing sugar and

radiolabel. Cell suspensions were immediately processed. Radioactivity associated with

yeast suspensions at time zero was subtracted from the activity associated with cell

suspensions following the uptake period. Uptake assays were performed using solutions

and tubes pre-equilibrated to 20 ^{o}C.

2-Deoxy-D-glucose (2DOG) uptake in yeast was carried out as described D-

glucose uptake. 100μL aliquots of cells at room temperature were exposed to 2 volumes

of room temperature PBS containing [^{3}H]2-deoxy-D-glucose. Uptake of 100μM 2DOG

was measured at 2 minute intervals, and quenched by addition of 10 volumes of ice cold PBS buffer containing 50mM maltose.

Zero-trans sugar uptake experiments in intact human red blood cells were made at 4 ˚C (to slow transport and thereby permit accurate determinations of transport) as described previously (*9*). Briefly, sugar-free cells or erythrocyte ghosts (at ice temperature) were exposed to 5 volumes of saline (ice temperature) containing variable concentrations of unlabeled sugar plus labeled sugar. Uptake was permitted to proceed over intervals of 30sec then 50 volumes (relative to cell volume) of stopper solution (PBS containing 10µM CB and 100µM phloretin) were added to the cell suspension. Cells were sedimented by centrifugation (14,000 x g for 30 sec), washed once in stopper, collected by centrifugation and extracted in 500µL 3% perchloric acid. The acid extract was centrifuged and duplicate samples of the clear supernatant fluid were counted. Zero-time uptake points were prepared by addition of stopper to cells prior to addition of medium containing sugar and radiolabel. Cells were immediately processed. Radioactivity associated with cells at zero-time was subtracted from the activity associated with cells following the uptake period. Uptake assays were performed using solutions and tubes pre-equilibrated to 4 ˚C. Triplicate or quadruplicate samples were processed at each time point. Cell counts were obtained from a calibration curve relating red cell absorbance at 417nm to cell numbers (obtained using a hemocytometer).

Michaelis Menten parameters for sugar uptake by recombinant human GLUT1 expressed in yeast were calculated by measuring the concentration dependence of 2DOG transport (100µM to 100mM 2DOG). 3MG inhibition of 2DOG transport in wild-type yeast and RE700A-GLUT1 was analyzed by measuring 2DOG uptake (100µM) in the presence or absence of increasing concentrations (100µM - 100mM) of 3MG.

ELISA

Purified, human erythrocyte GLUT1, and yeast membranes (isolated from RE700A +/- GLUT1 HA 6His) were attached to ELISA dishes by incubation at 37°C for 18-24 hours. Following absorption of proteins to the microtiter plates, each well was washed 3 times with phosphate buffer (PB) and then incubated for 90 minutes at 37°C with 250µL of 3% BSA in PB. GLUT1 was detected with rabbit antisera raised against a synthetic carboxyl-terminal peptide of the human red blood cell glucose transport protein (C-Ab) diluted 1:20,000 with 1% BSA in PB. The reporter molecule for rabbit IgG was goat anti-rabbit IgG peroxidase diluted 1:5000 with 1% BSA in PB. Bio-Rad peroxidase substrate kits were employed. Detection of product was determined by absorbance at 410nm using a Dynatech MR 700 plate reader. Nonspecific IgG binding was determined by processing wells lacking glucose transport protein.

Figure 2.1 GLUT1-HA-H6 expression in *S. cerevisiae*.

RE700Acells were transfected with HA-H6-tagged wild-type GLUT1 (GLUT1-HA-H6), with mutant GLUT1 (GLUT1338-A3), with an empty vector (p426 GPD), or without a vector (RE700A) and plated on SCM-URA maltose (A) or SCM-URA glucose (B). Plates were photographed after 3 days. (C) RE700A-GLUT1-HA-H6 grown on SCM-URA maltose. (D) RE700A-GLUT1-HA-H6 streaked onto 5-FOA-containing media. (E) RE700A-GLUT1-HA-H6 restreaked post-5-FOA exposure (3 days) onto YP-maltose. (F) RE700AGLUT1-HA-H6 restreaked post-5-FOA exposure (3 days) onto YPdextrose. (G) RE700A-GLUT1-HA-H6 restreaked post-5-FOA exposure (3 days) onto SCM-URA dextrose.

Fig 2.1

Maltose · D-Glucose

GLUT1-HA-H6 · GLUT1-HA-H6

p426 GPD · RE700A · p426 GPD

GLUT1$_{338-A3}$ · GLUT1$_{338-A3}$
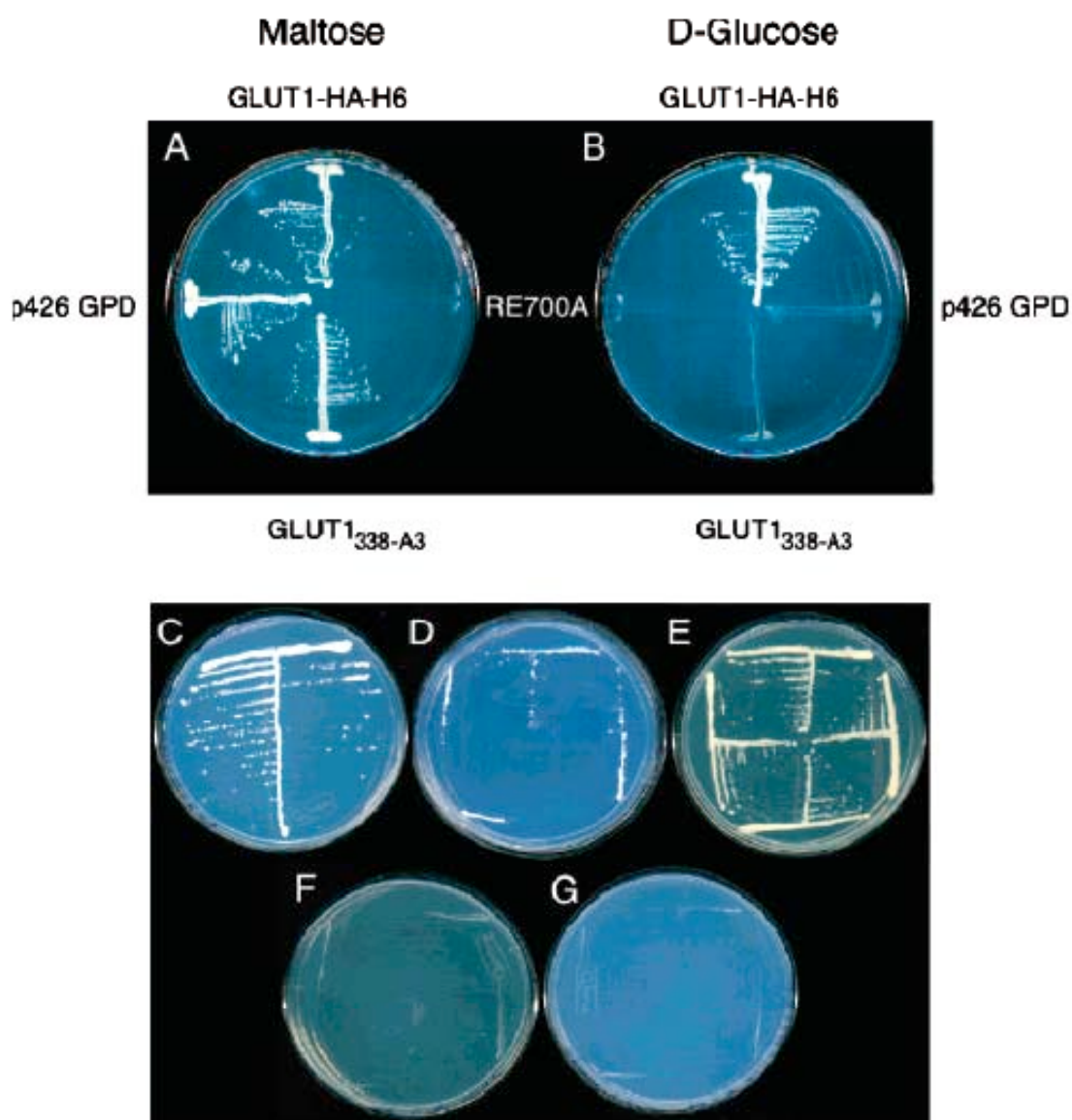
Figure 2.2 Human Expression of human GLUT1 in *S. cerevisiae*.

A Western blot using GLUT1 carboxyl-terminal IgGs (C-Ab) of GLUT1 expressed in RE700A. Membranes were isolated by differential centrifugation, resolved by 10% SDS PAGE, and transferred to nitrocellulose for western blotting. Lanes 2-7 each contain 35 µg total membrane protein. Lane 1 contains 1µg of purified erythrocyte GLUT1. Two fractions were obtained upon yeast lysis: The F2 fraction (lanes 2 and 3) was collected as the low speed (8,000 x g) pellet. The F3 membrane fraction (lanes 4,5 , 6 and 7) was obtained as the high speed (100,000 x g) pellet. Lane 2 contains membranes from the RE700A hxt-null mutant. Lane 3 contains membranes from -5'UTR-GLUT1-transfected RE700A; Lane 4 contains membranes from the RE700A hxt-null mutant; Lane 5 contains membranes from -5'UTR-GLUT1-transfected RE700A. Lane 6 contains membranes from RE700A transfected with GLUT1 containing the 5'UTR. Lane 7 contains membranes from -5'UTR-GLUT1-transfected RE700A. Lanes 6 & 7 were obtained from a separate gel. The migration and mass of molecular weight markers is shown to the left of Lane 1.

B Western blot using GLUT1 carboxyl-terminal IgGs (C-Ab) of GLUT1 expressed in RE700A. Membranes were isolated by differential centrifugation, resolved by 10% SDS PAGE, and transferred to nitrocellulose for western blotting. Lanes 2-4 each contain 35 µg F3 fraction membrane protein. Lane 1 contains 0.25µg of purified erythrocyte GLUT1. Lanes 2, 3 and 4 contain membranes from RE700A-5'UTR-GLUT1-HA-H6 grown on glucose (lane 2), maltose (early passage, Lane 3) or maltose (late passage, Lane 4). The migration and mass of molecular weight markers is shown to the left of Lane 1.

Fig 2.2
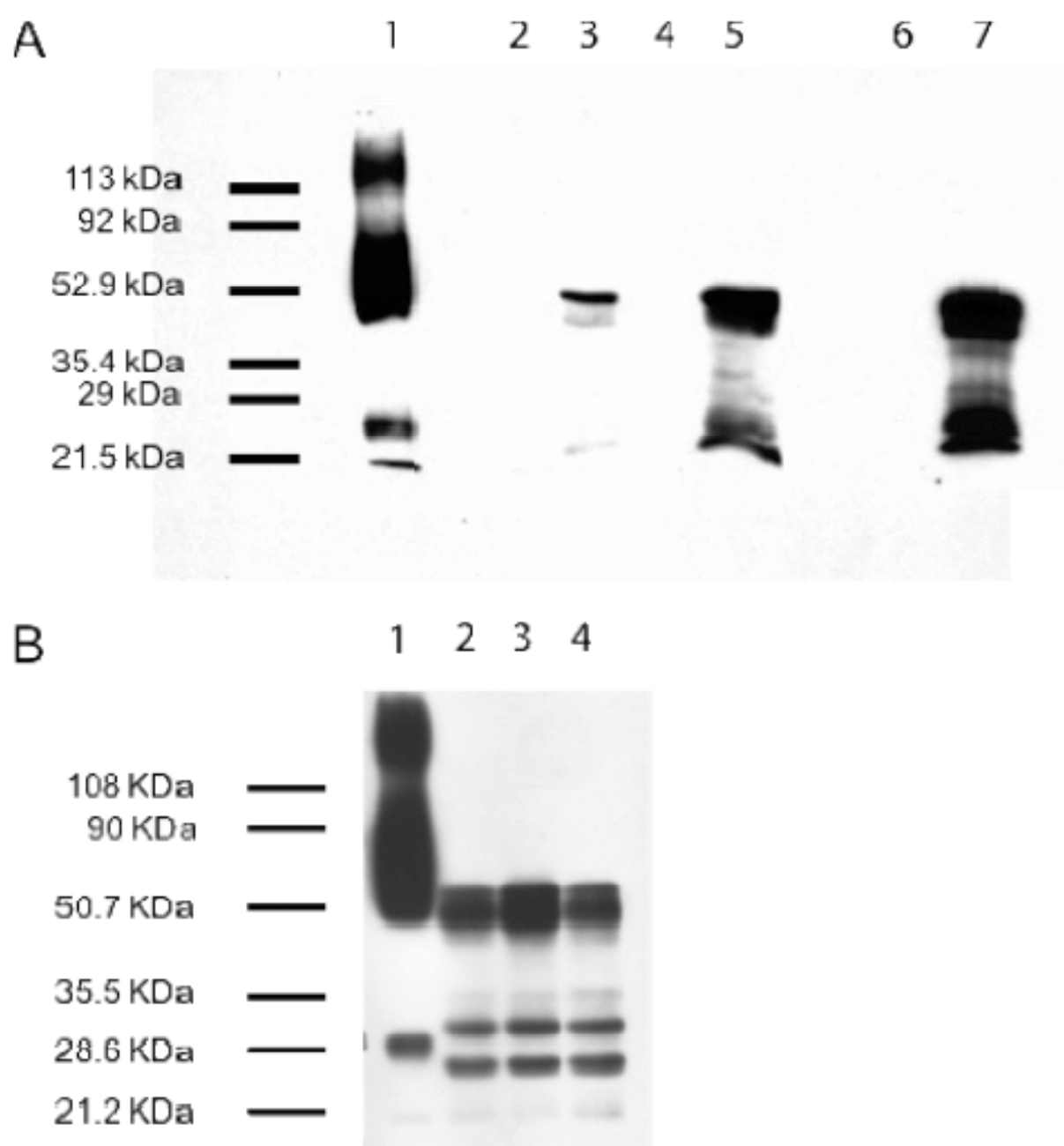
FOA Induced Vector Drop-Out

Clones of RE700A-GLUT1-HA-H6 that have lost the URA3 based p426-GPD plasmid were selected by plating on media containing 5-fluoroorotic acid (5-FOA; 0.1% for 2-3 days).

RESULTS

The disruption of seven of 20 hexose transporter genes in *S. cerevisiae* results in a strain of yeast (RE700A) that is capable of growing on maltose (a disaccharide imported by maltose-H+ symport then hydrolyzed to yield 2 glucose molecules), but incapable of growth on glucose (*142*).

RE700A were transfected with epitope-tagged GLUT1 cloned into the BamH1 site of the yeast expression vector p426 GPD and subsequently plated onto selective media containing maltose (SCM-URA maltose), and later glucose only (SCM-URA glucose). Transfection with either empty vector (p426 GPD), or p426-GLUT1-HA-H6 results in growth on maltose. Only p426-GLUT1-HA-H6-containing yeast grow on glucose (Figure 2.1). In the absence of vector, RE700A fails to grow (Figure 2.1). RE700A was also transfected with the GLUT1338-3A mutant (residues 338, 339 and 340 each replaced with alanine). Mammalian cells (Cos-7) transiently transfected with GLUT1338-3A exhibit sugar transport rates indistinguishable from untransfected control cells, yet GFP-tagged GLUT1338-3A is expressed at high levels at the plasma membrane suggesting that hGLUT1338-3A is targeted correctly but is catalytically impaired (*147*). Figure 2.1 demonstrates that RE700A-GLUT1338-3A grows on maltose, but lacks the

Figure 2.3 Sugar transport by RE700A expressing or lacking hGLUT1-HA-H6.

A. D-glucose transport in RE700A transfected with GLUT1 DNA containing the 5'UTR. D-glucose uptake was measured in transfected (▲) and untransfected (△) cells. Ordinate: mol sugar imported per 10^9 cells; Abscissa: time in minutes. Each point represents the mean of 4 or more separate determinations.

B. 3MG uptake in RE700A transfected with GLUT1 DNA lacking the 5'UTR. 3-O-methyglucose uptake (100 µM sugar) was measured in nontransfected (○) and transfected (●) cells. Ordinate: mol sugar imported per 10^9 cells; Abscissa: time in seconds. Each point represents the mean of 4 or more separate determinations.

Fig 2.3
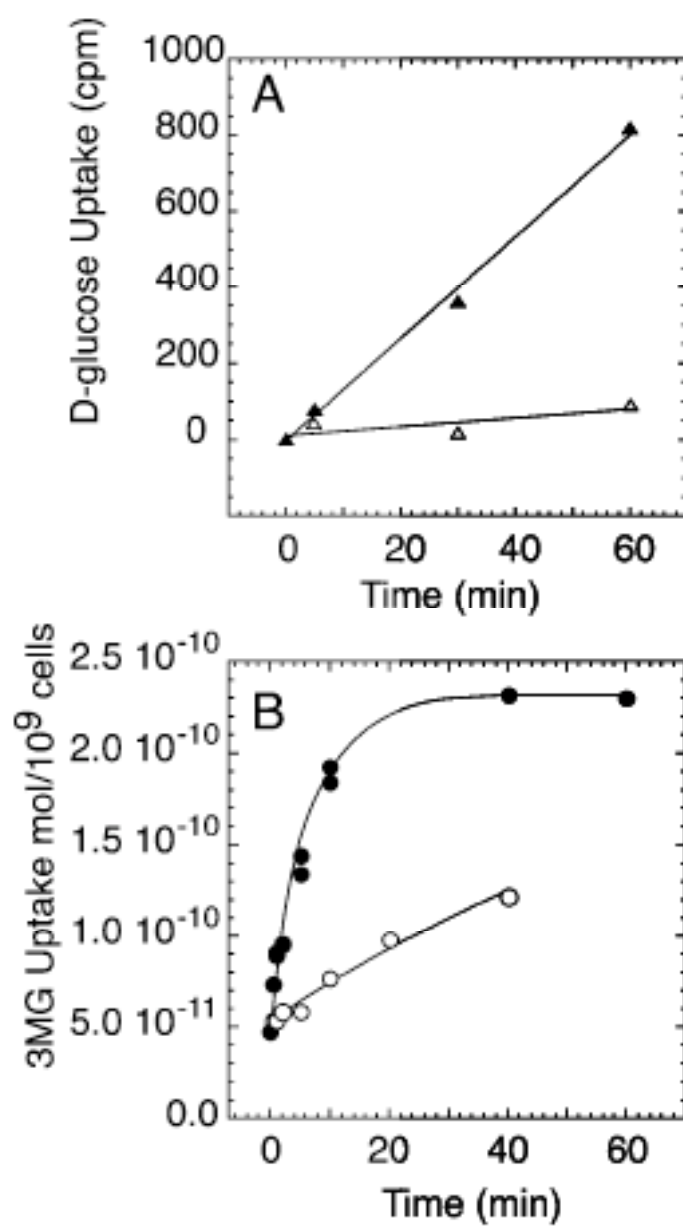
ability to survive on glucose. This result is consistent with previous observations in

mammalian cells suggesting that GLUT1 mutant GLUT1$_{338-3A}$ lacks the capacity to

transport D-glucose.

To determine that the RE700A-GLUT1-HA-H6 phenotype (growth on glucose)

results directly from the GLUT1-HA-H6 sequence carried on the p426 GPD vector, cells

containing p426 GLUT1-HA-H6 were plated onto media containing 5-fluoroorotic acid

(FOA). FOA is toxic to yeast expressing the URA-3 gene. This selection thus identifies

clones that have lost their URA-3 containing plasmid (p426 GLUT1-HA-H6). Following

exposure to FOA, growth of RE700A GLUT1 was observed on YP maltose, but not on

YP glucose, SCM-URA maltose or SCM-URA glucose (Figure 2.2) suggesting that the

yeast have lost both the GLUT1 containing vector (p426 GLUT1-HA-H6) and the

capacity to survive on glucose.

hGLUT1 Expression in RE700A

Yeast transfected with epitope-tagged GLUT1 were screened for protein

expression by immunoblot and sugar transport analyses. Initial attempts at RE700A

transfection resulted in yeast with slow growth rates (doubling time > 8 hr on glucose

medium) and undetectable GLUT1 expression by Western analysis of total yeast

membranes (lane 6, Figure 2.2A). In an effort to increase human GLUT1 expression, we

re-engineered the transporter construct by deleting the mammalian 5' untranslated region

(5' UTR). A unique Spe1 site 3 base pairs 5' to the GLUT1 start codon was introduced

by PCR. Excision, using Spe1 and BamH1, permits ligation of the resulting 1.5 kbp

fragment of epitope-tagged GLUT1 (–5'UTR-GLUT1-HA-H6) into the Spe1/BamH1

restriction site of the p426 GPD expression vector. RE700A was transfected with p426-

5'UTR-GLUT1-HA-H6 and plated as described previously. These yeast grow more

rapidly on glucose medium (doubling time ≈ 2 hours). C-Ab immunoblot analysis of

yeast membranes indicates the presence of a 50-55 kDa C-Ab reactive protein in

RE700A-5'UTR-GLUT1-HA-H6 (Figure 2.2A, Lanes 3,5) which is absent in

untransfected cells (Figure 2.2A, Lanes 2,4). Thus removal of the 5'UTR appears to

increase GLUT1 expression in RE700A. Densitometric analysis suggests that

recombinant GLUT1 (present in both the F2 (8,000 x g) and F3 (100,000 x g) membrane

fractions of RE700A-5'UTR-GLUT1-HA-H6 approaches 1% of total protein. It is also

apparent that GLUT1 expressed in yeast is characterized by a relatively narrow

electrophoretic mobility. In contrast, purified human red blood GLUT1 is

heterogeneously glycosylated and is resolved as a broader smear (Figure 2.2A, lane 1). C-

Ab reactive peptides of relatively low M_r (21-29 kDa) are detected in the F3 fraction of

RE700A GLUT1-5'UTR (Figure 2.2A, Lane 5) suggesting that proteolytic fragments of

GLUT1 or truncated versions of the transporter may also be present. GLUT1-HA-H6

expression is unaffected by growth medium (Figure 2.2B).

Net uptake at 24ºC of 100μM [^{3}H]-D-glucose by RE700A-5'UTR-GLUT1-HA-

H6 is 12-fold greater than uptake in nontransfected RE700A (Figure 2.3A). Uptake of

[^{14}C]3-O-methylglucose (3MG, a transported but nonmetabolizable sugar) is 10.5-fold

greater in RE700A-5'UTR-GLUT1-HA-H6 than in RE700A (Figure 2.3B).

Sites of hGLUT1 expression in RE700A

Renografin gradient separation of cellular membrane compartments was used to identify the cellular location of recombinant GLUT1-HA-H6 expression in RE700A. Membrane fractions from yeast with and without -5'UTR-GLUT1-HA-H6 were layered under a gradient of renografin-76. Samples were centrifuged for 20 hours at 40,000 rpm to allow proteins to migrate to regions of equivalent buoyant density. Fractions were then isolated in order of increasing density, and were immunoblotted by using GLUT1 C-Ab and antibodies directed against yeast plasma membrane (Ste1p) and endoplasmic reticulum (OST1p or Dpm1p) markers. Figure 2.4 indicates that the largest fraction of -5'UTR-GLUT1-HA-H6 in transfected RE700A co-fractionates with the yeast plasma membrane marker Ste1p. Very little of the expressed transporter is detected in the less dense, ER-dominated (OST1p or Dpm1p) membrane fractions.

Figure 2.4 Renografin gradient centrifugation of yeast membranes.

F3 fractions isolated from RE700A and RE700A-GLUT1 were combined with an equal volume of Renografin-76. The Renografin gradient was constructed over 0.8 mL of sample (38% Renografin) by sequentially layering 0.8 mL of 34, 30, 26, and 22% Renografin-76 diluted in 50 mM Tris-HCl pH 7.4. Gradients were centrifuged in a 50.1Ti rotor at 40,000 rpm for 20 hours at 4ºC. Samples were isolated from the top down in aliquots of 500 μL, and stored at -70°C until use. Fractions containing GLUT1 ($\triangle$), the yeast endoplasmic reticulum marker OST ($\blacksquare$), and the yeast plasma membrane marker Ste1p ($\circ$) were determined by Western Blotting. Ordinate: fraction of total GLUT1, OST or Ste1p in each sample. Abscissa: fraction number (samples closest to the top of the gradient have the greater numbers). The distribution of OST and Ste1p are unchanged by GLUT1 expression (nontransfected RE700A yeast give identical results for OST and Ste1p; not shown).

Fig 2.4

Legend

△ .˜ GLUT1

■ ER Marker

○ PM Marker
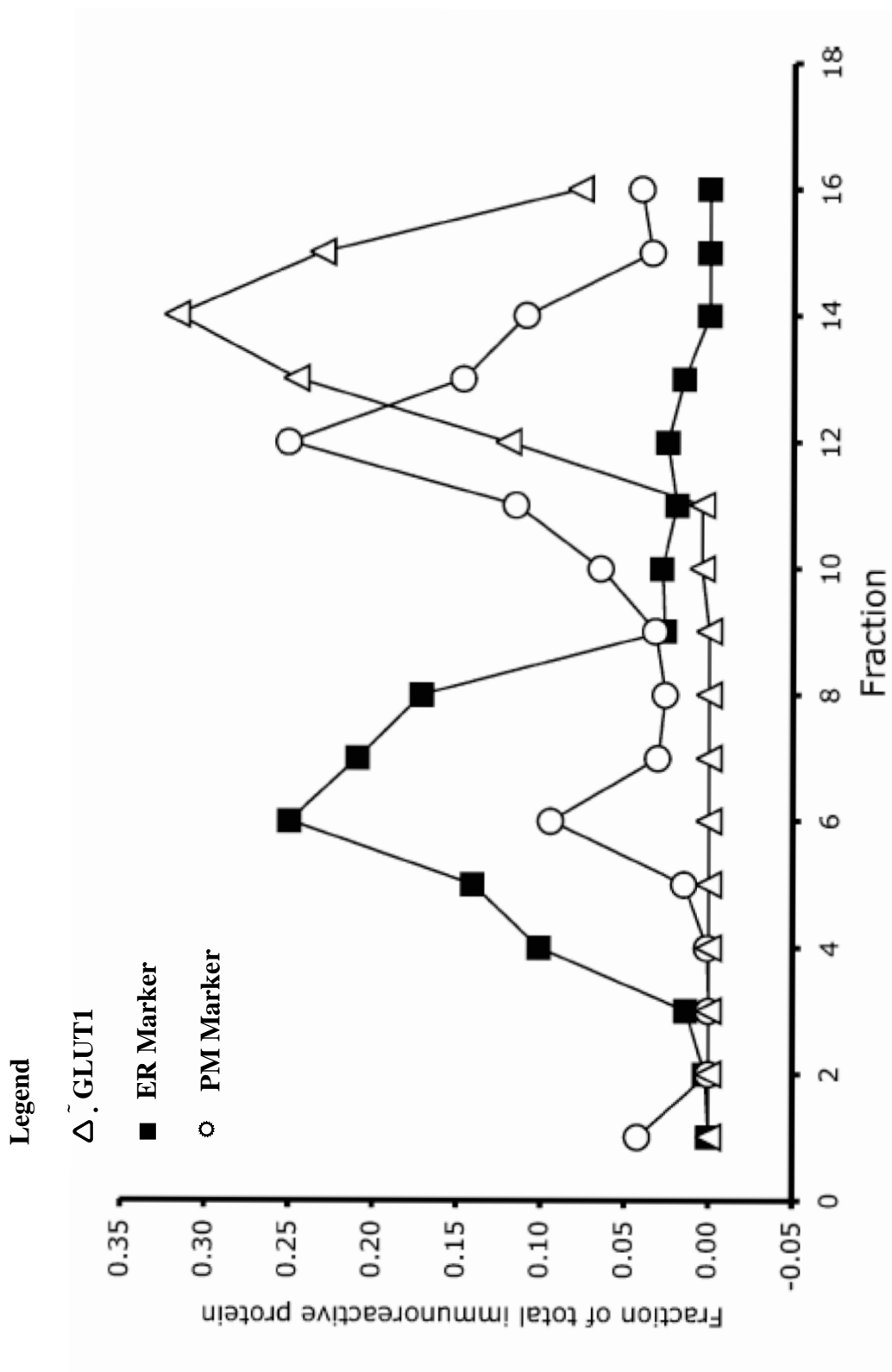
Figure 2.5 Yeast and Erythrocyte 2DG Uptake

A) Concentration dependence of 2-deoxy-D-glucose uptake and inhibition of D-glucose uptake by RE700A-5′UTR-GLUT1- HA-H6. Left ordinate: 2DG uptake [nmol/10^9 cells/min ($\bullet$)]. Right ordinate: uptake of 100 μM D-glucose [pmol/10^9 cells/min (O)]. Abscissa: [2DOG] (mM). Each point represents the mean of at least four separate determinations in triplicate. The curve drawn through the 2DOG uptake data points ($\bullet$) was computed by nonlinear regression assuming simple Michaelis-Menten sugar uptake kinetics and takes the form V) $V_{max[2DG]}/[K_{m(app)} + [2DOG]]$, where V is the rate of uptake at any [2DOG], V_{max} is the maximum rate of sugar uptake obtained at a saturating [2DOG], and $K_{m(app)}$ is that [2DOG] that results in uptake of $0.5V_{max}$. The curve has the following constants: $V_{max} = 2.35 \pm 0.09$ nmol/(10^9 cells)$^{-1}$ min^{-1}; $K_{m(app)} = 2.9 \pm 0.4$ mM 2DOG; $R^2 = 0.985$). The curve drawn through the D-Glucose uptake data points (O) was computed by nonlinear regression assuming simple Michaelis-Menten competitive inhibition of D-Glucose uptake by 2DOG and takes the form V = V_o - $V_i[2DOG]/[K_{i(app)} + [2DOG]]$, where V_o is the rate of D-Glucose uptake in the absence of 2DOG, V_i is the extent of inhibition produced at a saturating [2DOG], and $K_{i(app)}$ is that [2DOG] that results in 50% of the maximum inhibition of D-Glucose uptake. The curve has the following constants: $V_o = 72.9 \pm 4.5$ pmol (10^9 cells)$^{-1}$ min^{-1}; $V_i = 64.2 \pm 5.0$ pmol (10^9 cells)$^{-1}$ min^{-1}; $K_{i(app)} = 2.1 \pm 0.6$ mM 2DOG; $R^2 = 0.983$.

(B) Concentration dependence of CCB inhibition of 2DOG uptake by RE700A-5′UTR-GLUT1-HA-H6 and baker's yeast. Left ordinate: 2DOG uptake in RE700A-GLUT1-HA-

H6 [mol/10^9 cells/min (○)]. Right ordinate: 2DOG uptake in baker's yeast [mol/10^9

cells/min (■)]. Abscissa: [CB] (nM). Each point represents the mean of four triplicate

determinations of 2DOG uptake at 100 µM sugar. The curve drawn through the RE700A-

GLUT1-HA-H6 data points was computed by nonlinear regression assuming simple

Michaelis-Menten inhibition of sugar uptake and takes the form $V = V_o - V_i[CB]/[K_{i(app)}$

$+ [CB]]$, where V is the rate of uptake at any [CB], V_o is the rate of uptake in the absence

of CB, V_i is the maximum decrease in sugar uptake produced by a saturating [CB], and

$K_{i(app)}$ is that [CB] that inhibits uptake by 50% of V_i. The curve has the following

constants: $V_o = (6.99 \pm 0.24) \times 10^{-11}$ mol $(10^9$ cells$)^{-1}$ min^{-1}; $V_i = (3.68 \pm 0.27) \times 10^{-11}$

mol $(10^9$ cells$)^{-1}$ min^{-1}; $K_{i(app)} = 142 \pm 42$ nM CB; $R^2 = 0.969$.

(C) Inhibition of 2DOG uptake in RE700A-GLUT1-HA-H6 and in baker's yeast by

cytochalasin B. Ordinate: moles of 2-deoxy-D-glucose imported by 10^9 cells. Left

ordinate: uptake in nontransfected RE700A (● and ○) or in RE700A-GLUT1-HA-H6

(▲ and △). Right ordinate: uptake in baker's yeast (■ and □). Abscissa: time in

seconds. 2DOG uptake was assessed at 100 µM sugar in the presence (■, ●, and ▲) or

absence (□, ○, and △) of cytochalasin B. RE700A- 5′UTR-GLUT1-HA-H6 cells were

exposed to 10 µM CB, while wild-type *S. cerevisiae* cells were exposed to 100 µM CB.

Cells received CCB 10 min prior to 2DOG uptake initiation. The curves drawn through

the points were computed by nonlinear regression assuming uptake is described by the

expression $2DOG_t = 2DOG_\infty(1 - e^{-kt})$, where $2DOG_t$ is the amount of 2DOG associated

with the cells at time t, $2DOG_\infty$ is the amount of 2DOG associated with the cells at

equilibrium, and k is the first-order rate constant describing the rate of 2DOG uptake. The following constants were obtained: $2DOG_\infty = 2.5 \pm 0.2$ nmol/10^9 cells, $k = 0.007 \pm 0.001$ s^{-1}, and $R^2 = 0.999$ for baker's yeast; $2DOG_\infty = 4.3 \pm 0.4$ nmol/10^9 cells, $k = 0.0048 \pm 0.001$ s^{-1}, and $R^2 = 0.975$ for baker's yeast and CB; $2DOG_\infty = 2.1 \pm 0.2$ nmol/10^9 cells, $k = 0.00076 \pm 0.00033$ s^{-1}, and $R^2 = 0.992$ for RE700A-GLUT1-HA-H6; $2DOG_\infty = 2.1 \pm 0.3$ nmol/10^9 cells, $k = 0.00025 \pm 0.00001$ sec^{-1}, and $R^2 = 0.985$ for RE700A-GLUT1-HA-H6 and CB; $2DOG_\infty = 2.1$ nmol/10^9 cells, $k = (4.1 \pm 0.4) \times 10^{-5}$ s^{-1}, and $R^2 = 0.835$ for RE700A; and $2DOG_\infty = 2.1$ nmol/10^9 cells, $k = (4.2 \pm 0.5)\ 10^{-5}$ s^{-1}, and $R^2 = 0.770$ for RE700A and CB. With RE700A cells, $2DOG_\infty$ was assumed to be identical to RE700A-GLUT1-HA-H6.

Fig 2.5
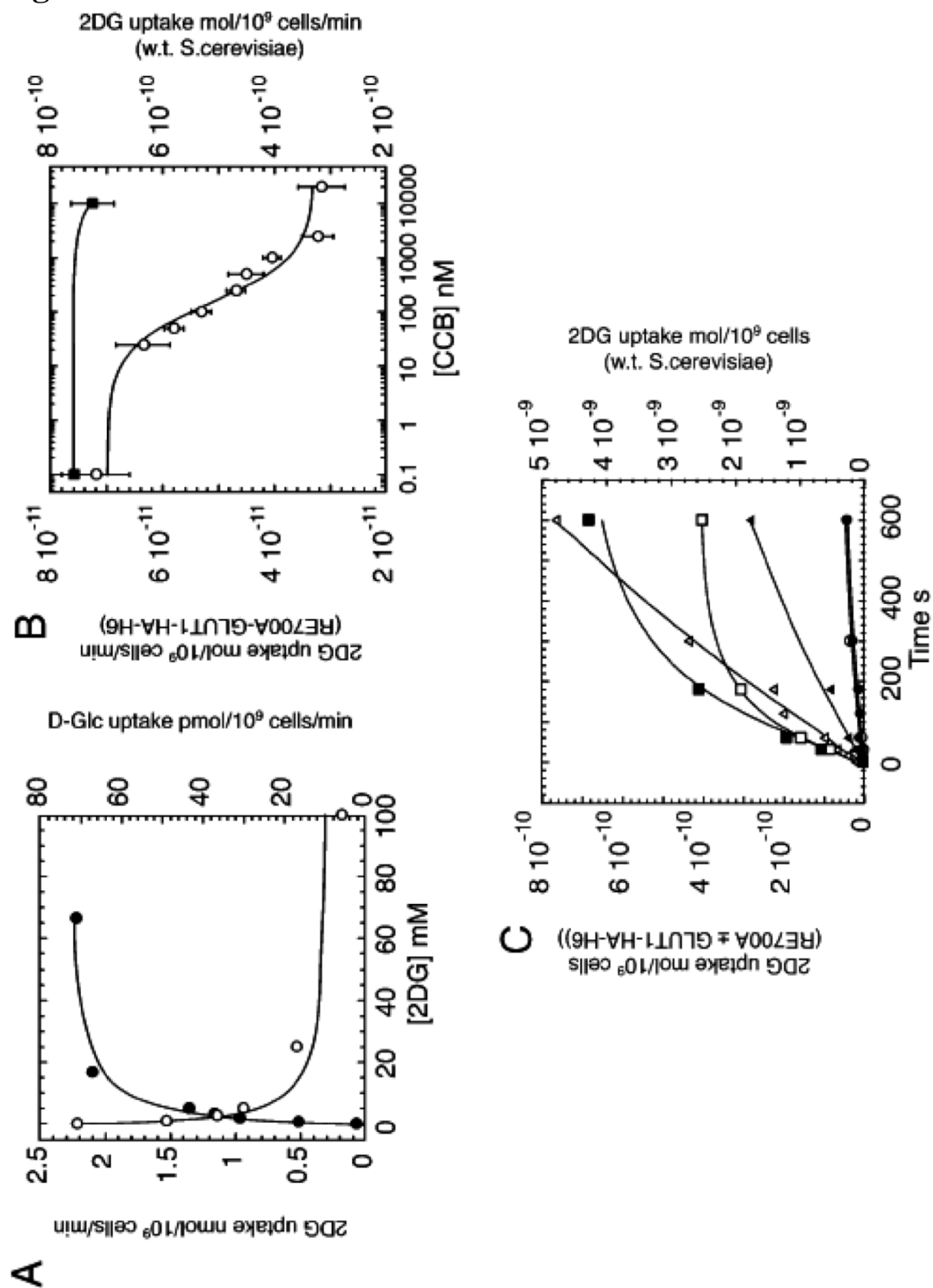
Table 2.1 Specificity of GluT1-mediated sugar transport

Sugar	Temp (ºC)	[a]RE700A-GluT1-HA-H6			[a]wt *S. cerevisiae*	[b]Human erythrocytes		
		$K_{m(app)}$ mM	[c]V_{max}	[d]$K_{i(app)}$	[d]$K_{i(app)}$	$K_{m(app)}$ mM	[c]V_{max}	[d]$K_{i(app)}$
2DOG	4					0.59 ± 0.27	19.14 ± 2.64	1.4 ± 0.4
	24	2.89 ± 0.42	2.35 ± 0.09	2.05 ± 0.57	5[e]	1.8 ± 0.2f		3.2[g]
3MG	4					0.38 ± 0.13	11.9 ± 1.32	1.9 ± 0.3
	24			10.1 ± 4.2	64.4 ± 3.8 / 250[e]	4.6 ± 0.3[g] / 3.1 ± 0.8[h] / 2[i] / 15-23[j]		13[g]
CB	4							126 ± 16
	24			142 ± 42	> 10,000			110[k]

[a] Sugar uptake was measured in wild-type (wt) and GluT1-HA-H6-transfected RE700A yeast at 20ºC. [b] Sugar uptake in red cells was measured at 4ºC. $K_{m(app)}$ is that concentration at which uptake is 0.5 V_{max}. [c]V_{max} is the maximal rate of sugar uptake in nmol*10^9cells*min. [d]$K_{i(app)}$ is that concentration of sugar (mM) or cytochalasin B (nM) that reduces sugar uptake by 50% of the maximal inhibition. In experiments where 2DOG was the inhibitory sugar, uptake of 66µM D-glucose was measured. In experiments where 3MG or CB were the inhibitors, uptake of 66µM 2DOG was measured. [e] From ref (*151*). [f] From ref (*152*). [g] From ref (*6*). [h] From ref (*153*). [i] From ref (*154*). [j] From refs (*155*) and (*96*). [k] (*156*)

Figure 2.6 Lack of hGluT1-HA-H6-mediated trans-acceleration in RE700A.

A) Ordinate: mol 2-deoxy-D-glucose imported by 10^9 cells per min. Abscissa: Intracellular [3MG] in mM. 2DOG uptake (100µM) was measured in RE700A-5'UTR-GluT1-HA-H6 (●) that had been pre-loaded for 1 hr with 0, 10, 20 or 40 mM 3MG. The rate of 2DOG uptake was then measured over a 5 minute interval. Results are shown as mean ± SEM of at least 3 separate determinations made in triplicate. The straight line drawn through the data points was computed by linear regression. The rectangular hyperbolae illustrate the fold stimulation and the [3MG] dependence of transport stimulation that is expected (*9*) if transport were measured in human red cells at 4ºC (solid line) or at 20ºC (dotted line).

B) Transacceleration is observed in HEK cells expressing GluT1-HA-H6. Ordinate: rate of 2DOG uptake in mol per µg cell protein per minute. Abscissa: experimental condition. 100µM 2DOG uptake was measured in control (HEK) or 3MG (40 mM) loaded HEK cells (HEK+3MG$_i$) or in HEK cells transiently transfected with GluT1-HA-H6 and preloaded with 0 (HEK-GluT1-HA-H6) or 40mM 3MG (HEK-GluT1-HA-H6+3MG$_i$). These results represent the mean ± SEM of three separate measurements. Uptake in nontransfected HEK cells (1.62 pmol/µg protein/min) was subtracted from the data.

Fig 2.6
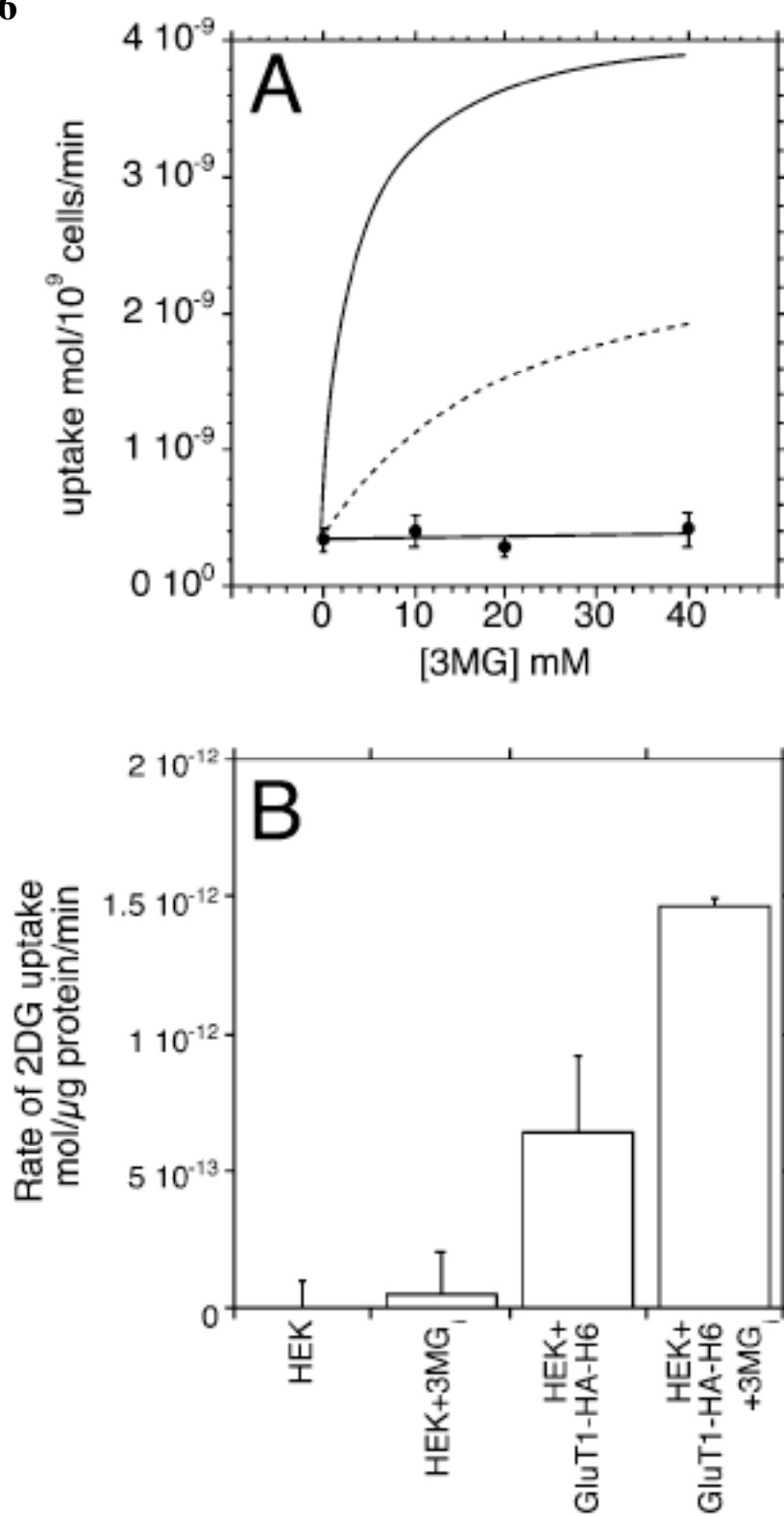
Table 2.2 Effect of DTT on sugar uptake by human red cells and RE700A.

Cell Type	2DG Uptake[a] control[b]	DTT[b]	CB[c]	n[d]	p[e]
RE700A-GluT1-HA-H6[f]	98.2 ± 2.6	144.0 ±11.6	42 ± 6	5	0.264
HEK293[g]	3.91 ± 0.21	3.61 ± 0.12	0.04 ± 0.003	4	0.153
HEK293+GluT1-HA-H6[g]	5.94 ± 0.16	4.63 ± 0.11	0.04 ± 0.01	4	0.002
GluT1-HA-H6 uptake[g,h]	0.20 ± 0.02	0.13 ± 0.01		4	0.013

[a] 2DOG uptake at 100 μM sugar was assessed in RE700A-GLUT1-HA-H6 cells and control (HEK293) or GLUT1-HA-H6-transfected HEK cells (HEK293+GLUT1-HA-H6). b 2DOG uptake was assessed at 20 °C following a 30 min pre-incubation at 30 °C in the absence (control) or presence (DTT) of 20 mM DTT at pH 7.4. [c] 2DOG uptake by HEK cells (control and transfected) is inhibited by >90% by 20 μM CB. [d] Number of separate measurements made in duplicate. [e] Probability that there is no difference between control and DTT conditions in each experiment calculated using the Student's t-test. This two-tailed test assumes that paired samples have equal variance. [f] Uptake is expressed as picomoles per 109 cells per minute and is shown as mean ± standard error of the mean. [g] Uptake was assessed as picomoles per microgram per minute and is shown as mean ± standard error of the mean. [h] GLUT1-HA-H6-specific 2DG was calculated as the difference between uptake in transfected versus nontransfected HEK293 cells.

Characterization of sugar transport in RE700A GLUT1

The concentration dependence of 2DOG uptake by RE700A-5'UTR-GLUT1-HA-H6 at 24 ℃ shows saturation kinetics with Michaelis and velocity constants of $K_{m(app)} = 2.64 \pm 0.40$ mM and $V_{max} = 2.25 \pm 0.08$ nmol/min/10^9 cells respectively (Table 2.1; Figure 2.6A). 2DOG transport rates in wild type yeast are at least 10-fold greater than in GLUT1-transfected RE700A (Fig 2.6B). 2DOG-inhibition of D-glucose uptake by RE700A-5'UTR-GLUT1-HA-H6 at 24 ˚C is characterized by $K_{i(app)} = 1.75 \pm 0.75$ mM (Table 2.1). $K_{i(app)}$ for 2DOG-inhibition of D-glucose uptake by human red cells is 1.4 ± 0.4mM while $K_{m(app)}$ for 2DOG uptake by red cells is 0.59 ± 0.17mM (Table 2.1).

3MG inhibition of 2DOG uptake by RE700A-5'UTR-GLUT1-HA-His6 (Figure 2.5B) is characterized by a $K_{i(app)}$ of 10.1 ± 4.2mM. In contrast, $K_{i(app)}$ for 3MG inhibition of 2DOG uptake by wild type S. cerevisiae is 64.4 ± 3.8 mM (Table 2.1). Cytochalasin B, an inhibitor of human red blood cell sugar transport, also inhibits 2DOG uptake by RE700A-5'UTR-GLUT1-HA-H6 with $K_{i(app)} = 60 \pm 17$nM (Figure 2.5C). Maximum inhibition of unidirectional uptake is 58%. The remaining uptake is similar to that observed in the presence of saturating concentrations of 3MG or D-glucose suggesting a non-mediated or leakage pathway. 2DOG uptake in wild-type *S. cerevisiae* is unaffected by 100 µM CB (Figure 2.5B).

Human red cell unidirectional sugar import is inhibited 5-fold by extracellular reductant (*65*) and is stimulated by 10 - 100-fold by intracellular sugar (*96, 155, 157,*

158). 2DOG uptake by RE700A-5'UTR-GLUT1-HA-H6 is not inhibited by DTT

exposure (10mM, 30min at 30ºC; Table 2.2). Unidirectional uptake of 100µM 3MG by

RE700A-5'UTR-GLUT1-HA-H6 is unaffected by preloading cells with 10, 20 or 40 mM

unlabeled 3MG (Fig 2.6A). Introduction of the carboxy-terminal HA-H6 tag to GLUT1

could influence (positively or negatively) the ability of the GLUT1 cytoplasmic C-

terminal domain to interact with other cytoplasmic regions of GLUT1. This, in turn,

could influence GLUT1-mediated sugar transport. We therefore expressed GLUT1-HA-

H6 in human embryonic kidney cells (HEK923T) and determined whether reductant or

intracellular sugar influences sugar transport in these cells. GLUT1-HA-H6 catalyzes

DTT-inhibitable 2DOG uptake in HEK cells (Table 2.2) where intracellular 3MG

stimulates GLUT1-HA-H6-mediated 2DOG unidirectional uptake (Figure 2.6B).

Uptake of the non-metabolizable sugar, 3MG, by human red cells is characterized

by multi-phasic import kinetics(*93, 101, 159, 160*). 3MG uptake by RE700A-5'UTR-

GLUT1-HA-H6 is a simple, exponential process (Figure 2.5A).

DISCUSSION

Sugar transport in S. cerevisiae

The *S. cerevisiae* genome contains seventeen hexose transporter genes (Hxt1-11, Hxt13-17, Gal2) and three maltose transporter homologs (Agt1, Mph2, Mph3) each of which can catalyze hexose transport (*141*). A recent analysis suggests that it is necessary to disrupt all 20 of these genes in order to prevent growth on glucose media (*141*). The present study confirms earlier observations that a yeast strain (RE700A) lacking Hxt1-7 is unable to grow on glucose as the sole carbon source (*142, 161, 162*). We further demonstrate that introduction of human GLUT1 into RE700A restores the ability of the organism to utilize glucose as an energy source.

GLUT1 is directly involved in promoting glucose transport in transfected RE700A cells since subsequent exposure to 5-FOA selects for cells that have lost the URA-3 containing plasmid and results in clones capable of growth on YP-maltose but not on YP-dextrose or SCM-URA dextrose. Sugar transport measurements also indicate that FOA-treated yeast have lost the ability to import 2-deoxy-D-glucose. This suggests that the selected RE700AGLUT1 clones have lost both the GLUT1 containing vector and the ability to use glucose as a carbon source.

One explanation for this result could be that RE700A responds to transfection with human GLUT1 by inducing the expression or activation of an endogenous yeast hexose transport protein. Ozcan *et al.* (*162*) have shown that two hxt-like genes in *S.*

cerevisiae (rgt2 and snf3) are not transporters but rather are glucose sensors that control expression of several members of the hxt family of genes. Furthermore, Wieczorke *et al.* (*141*) demonstrate that deletion of snf3 in the background of the 20 hexose transporter gene deletion, partially restores growth on hexoses suggesting the existence of even more yeast proteins that are capable of transporting hexoses. Thus recombinant GLUT1 may act in *S. cerevisiae* as a glucose sensor, introducing a signal for transcriptional induction of previously inactive or inhibited sugar carriers.

This seems unlikely for several reasons. 1) Glucose transport by wild-type yeast (grown under conditions required for GLUT1 expression in RE700A) is characterized by a lack of sensitivity to the sugar transport inhibitor cytochalasin B (see here and (*163*)). Expression of the cytochalasin B-sensitive, human GLUT1 gene confers acute CB sensitivity to RE700A sugar transport. Thus if GLUT1 expression induces the expression of an unrecognized sugar transporter, this transporter must differ from other yeast hexose transporters in being CB-inhibitable. This inhibitory action of CB on sugar transport is unlikely to result from inhibition of transcriptional activation by GLUT1 because the actions of the inhibitor on transport are acute (fully observable within 10 minutes of addition). 2) Wild-type yeast shows only very low affinity ($K_{i(app)} = 65mM$) for the nonmetabolized but transported sugar 3-O-methylglucose while human GLUT1 and RE700A yeast expressing GLUT1HAHis6 are characterized by 6-fold greater affinity for the sugar (see (*24*) and here). 3) The transport-deficient GLUT1 mutant $GLUT1_{338A3}$

does not catalyze sugar transport when expressed in mammalian cells or in RE700A. 4)

Identical results have been obtained with GLUT1[i] using the yeast strain employed by

Wieczorke *et al.* (*141*) in which all 20 hexose transporter genes are eliminated. Thus if

GLUT1 serves as a transcriptional activator, it must induce the expression of as yet

unrecognized glucose transporters. We conclude, therefore, that human GLUT1 directly

catalyzes glucose, 2-deoxy-D-glucose and 3-O-methylglucose transport when expressed

in yeast.

Previous studies have suggested that GLUT1 expression is limited to the

endoplasmic reticulum in yeast (*140, 164*). The present study not only shows that

GLUT1 expression increases sugar import by RE700A, but that expressed GLUT1 co-

migrates with yeast plasma membrane and endoplasmic reticulum markers upon

membrane fractionation by Renografin gradient density centrifugation. Similar results have

been described by Wieczorke et al. (*165*). However, in this case, GLUT1 was expressed

at the cell surface but was either inactive or misfolded (*165*). These workers demonstrated

that GLUT1-mediated transport could be activated in one of two ways. 1) By

mutagenesis of a cluster of amino acids (human GLUT1 residues 63, 67, 68 and 69) in

putative transmembrane domain two. 2) By selection of a Δhxt strain containing a

genomic mutation (fgy1-1) that now permits GLUT1 function. In the present study,

sequence analysis of the p426GPD-GLUT1-HA-H6 vector isolated from transfected

RE700A and amplified in *E. coli* indicates that the GLUT1-encoding sequence is

unaltered. We conclude that the use of the yeast expression vector p426 GPD and elimination of the hGLUT1 5'UTR results in sufficiently robust expression of GLUT1 to saturate any ER-sequestering mechanism and thereby permit leakage to the yeast plasma membrane. Furthermore, high expression of GLUT1 either saturates the mechanism (fgy1-1) that suppresses GLUT1 transport function or the RE700A yeast strain also contains the fgy1-1 genomic mutation proposed in (*165*) and thus permits full function of human GLUT1 when expressed at the yeast plasma membrane.

Properties of GLUT1 in S. cerevisiae and human red cells

Sugar transport in RE700A cells expressing hGLUT1 is a saturable process. Equilibrium exchange 2DOG import is characterized by $K_{m(app)} = 2.6\pm0.4$mM and $V_{max} = 2.3$ nmol/min/10^9 cells. 2DOG uptake is competitively inhibited by 3MG ($K_{i(app)} = 10$mM) and 2DOG and D-glucose uptake compete for sugar uptake (2DOG $K_{i(app)} = 1.75\pm0.75$mM). This measure of the apparent affinity of hGLUT1 for 2DOG compares with $K_{i(app)}$ for 2DOG inhibition of glucose entry in human red cells at 4 ˚C of 1.4 mM and with $K_{m(app)}$ for 2DOG uptake by red cells at 4 ˚C of 0.6 mM. $K_{i(app)}$ for 2DOG inhibition of sorbose entry in human red cells at 22˚C is 7 mM (*24*)

These observations in yeast illuminate a long-standing problem in the field of human erythrocyte sugar transport. The Michaelis parameters for D-glucose and 3MG uptake by human red cells are 1.6 mM and 5 mM respectively (*63*). However, $K_{i(app)}$ for glucose and 3MG inhibition of L-sorbose uptake by human red cells are 7 mM and 14

mM respectively (*6*). These discrepancies between half-saturation constants for transport and transport inhibition have led some to suggest that sugar transport measurements in human red cells are technically flawed owing to: 1) complications arising from interactions of transported sugar with intracellular sugar binding species and/or, 2) the extremely high sugar transport capacity of red cells which makes accurate estimates of initial rates of transport difficult to attain (*9, 157, 166, 167*). Support for this hypothesis is available from recent measurements of 3MG transport by human red cells at 22 ˚C made using a rapid quench device that permits msec resolution of transport. These studies indicate $K_{m(app)}$ for net 3MG uptake by red cells is 15 - 25mM (*101, 160*).

The transport properties of RE700-5'UTR-GLUT1-HA-H6 differ from those of human red blood cells in several important ways. These include: 1) $K_{m(app)}$ for net transport of sugar is indistinguishable from $K_{i(app)}$ for sugar-inhibition of transport of a second sugar. 2) Sugar uptake is unaffected by extracellular reductant. 3) Net sugar uptake at subsaturating [3MG] is a simple mono-exponential process ($\tau = 400sec$). 4) CB-inhibition of sugar uptake shows simple, saturable (Michaelis) inhibition. In human red cells, $K_{i(app)}$ for sugar inhibition of uptake of a second sugar is normally greater than $K_{m(app)}$ for net uptake of the sugar (summarized in (*24*)). Net sugar uptake in erythrocytes is inhibited by 50% by reductant (*65, 93*). 3MG uptake by human red cells is multiphasic consisting of sequential, rapid ($\tau = 44msec$), fast ($\tau = 12sec$) and slow ($\tau = 1400$ sec) phases at room temperature (*160*). Inhibition of erythrocyte sugar transport by CB is

characterized by complex cooperative kinetics at subsaturating [CB] where net sugar

uptake can be subject to a paradoxical stimulation by inhibitor (*16*). These differences are

significant and suggest that the functional properties of human GLUT1 may be

determined by cellular environment.

Properties of GLUT1 in other cells

The possibility that transporter phenotype could be determined by cellular

environment is not unexpected. GLUT1-mediated sugar transport in human red cells is

asymmetric (V_{max} and $K_{m(app)}$ for net sugar exit > V_{max} and $K_{m(app)}$ for net sugar entry), is

characterized by trans-acceleration (intracellular sugar stimulates unidirectional uptake of

radiolabeled sugar;(*158*)) and is inhibited by extracellular reductant (*65*). GLUT1-

mediated sugar transport in rabbit red cells and metabolically depleted avian erythrocytes

is symmetric, does not display trans-acceleration (*98, 168-170*) but is inhibited (in avian

red cells) by reductant (*98, 169*). These differences could be explained by subtle

differences between the primary structures of human and avian GLUT1 (85% identical)

or rabbit GLUT1 (97% identical to human). Rat erythrocyte GLUT1 is kinetically

symmetric and has been reported to lack (*171*) or to display (*172, 173*) accelerated

exchange transport. Rat GLUT1 is 98% identical to human GLUT1. Human GLUT1

expressed in *Xenopus* oocytes displays transacceleration (*174*) but is not inhibited by

extracellular reductant(*65*). Primary sequence differences cannot account for the disparate

behavior of human GLUT1 in yeast, *Xenopus* oocytes and human red cells. The absence

of transacceleration in RE700A-GLUT1-HA-H6 (Figure 2.7A) is unrelated to the introduction of a modified GLUT1 carboxy-terminal region because the same construct catalyzes transacceleration when expressed in HEK cells (Figure 2.7B).

Accelerated exchange and kinetic asymmetry are not obligate properties of carrier-mediated sugar transport. For example, rat GluT4 – the insulin-sensitive sugar transporter (*1*) – shares 65% identity and 83% similarity with GLUT1 but is kinetically symmetric and does not display accelerated exchange (*175*). Passive sugar transport in giant axons of *Loligo forbesi* is asymmetric but shows trans-inhibition(*176*). Passive sugar transport in isolated, striated muscle cells of *Balanus nubilis* is symmetric and lacks trans-acceleration or inhibition (*177*). Human erythrocyte sugar transport in red cell ghosts lacking ATP at 4 ℃ is symmetric (*versus* asymmetric in the presence of ATP) but continues to display accelerated exchange (*129*). At 37℃, ATP-containing red cells lose kinetic asymmetry and trans-acceleration . Trans-acceleration is also lost in rat red cells at 40℃(*172*). These observations indicate that cytoplasmic factors and temperature profoundly influence GLUT1 phenotype.

A model of GLUT1-mediated transport

We have proposed that human GLUT1 forms a reductant-sensitive GLUT1 homotetramer in the red cell membrane (*65*). When reduced, the transporter complex dissociates into GLUT1 dimers. Tetrameric GLUT1 interacts allosterically with cytoplasmic ATP(*88, 99, 147*). This interaction promotes conformational changes in GLUT1 cytoplasmic domains (*136*) leading to formation of a "cytoplasmic cage" that encloses the exit site of the translocation pathway and introduces a noncatalytic sugar

binding site within the cage thus delaying release of sugar into cytosol(*93*). Reductant

causes dissociation of tetrameric GLUT1, loss of GLUT1 ATP binding capacity (*99*) and

loss of the "cytoplasmic cage". In the absence of ATP, the "cytoplasmic cage" is relaxed,

the noncatalytic sugar binding site is lost and transport asymmetry (which is proposed to

result from substrate recycling within the cage) is reduced (*93, 101, 160*). We therefore

propose that RE700A-GLUT1-HA-H6 exists predominantly as a "reduced" GLUT1

homodimer. However, it should be noted that while the so-called "cage-hypothesis" can

account for ATP- and reductant-sensitivity of GLUT1 sugar transport asymmetry, it does

not account for the lack of human GLUT1-sensitivity to reductant in *Xenopus* oocytes

and *S. cerevisiae* - tissues where GLUT1 displays transacceleration and no trans-

acceleration respectively.

The RE700A GLUT1 heterologous expression system may provide a useful

model for systematic analysis of environmental factors and GLUT1 primary structural

details that influence GLUT1-mediated sugar transport. It may also prove useful in the

development of genetic and pharmacodynamic screens for molecules that modulate

GLUT1 activity. RE700A expresses hGLUT1 at a level approximately 10-fold lower than

that observed in human red blood cells. RE700A may, therefore, also serve a rich source

of recombinant hGLUT1.

CHAPTER III

AFFINITY AND COOPERATIVITY DETERMINANTS AT THE GLUT1 ENDOFACIAL BINDING SITE

This chapter will be submitted as a manuscript in November of 2008.

Derivatized forskolin analogues the kind gift of:

Peter Henderson
Institute of Membrane and Systems Biology,
Faculty of Biological Sciences,
University of Leeds,
Leeds, LS2 9JT
U.K.

[1]The abbreviations used are: GLUT1 - Human Glucose Transporter Type 1 (SCL2A), GLUT1DS - GLUT1 Deficiency Syndrome, CA - Cytochalasin A, CB - Cytochalasin B, CC - Cytochalasin C, CD - Cytochalasin D, CE - Cytochalasin E, CH - Cytochalasin H, CJ - Cytochalasin J, e1 - endofacial sugar binding site, e2 - exofacial sugar binding site, 3MG - 3-O-Methyl Glucose, FSK - Forskolin, 1,6DiA-FSK - 1,6 Di Acetyl Forskolin, 6A-FSK - 6 Acetyl Forskolin, 7FPPNEA-FSK - 7-{2-[3-(4-Fluorophenyl)propanamido]-N-ethyl-7-aminocarbonyl} Forskolin, 7DeA-FSK - 7 Deacetyl Forskolin, 7-FPA-FSK - 7-(4-Fluorophenyl)acyl Forskolin, 1DeO-FSK - 1 Deoxy-Forskolin, 9DeO-FSK - 9 Deoxy Forskolin, 7FA-FSK - 7-Fluoroacetyl Forskolin, 1A-FSK - 1 Acetyl Forskolin, 14,15DiH-FSK - 14, 15 Dihydro Forskolin, 7FPP-FSK - 7-[3-(4-Fluorophenyl)propionyl] forskolin, 6A,7DeA-FSK - 6 Acetyl, 7 DeAcetyl Forskolin.

ABSTRACT

Cytochalasin B (CB) and forskolin (FSK) inhibit GLUT1-mediated sugar transport in red cells by binding at or close to the GLUT1 sugar export site. Paradoxically, very low concentrations of these inhibitors produce a modest stimulation of sugar transport *(Cloherty, E. K., Levine, K. B., & Carruthers, A. (2001). The red blood cell glucose transporter presents multiple, nucleotide-sensitive sugar exit sites. Biochemistry, 40(51), 15549-15561).* This result is consistent with the hypothesis that the glucose transporter contains multiple, interacting, intracellular binding sites for CB and FSK. The present study tests this hypothesis directly and, by screening a library of cytochalasin and forskolin analogues, asks what structural features of exit site ligands determine binding site affinity and cooperativity. Like CB, FSK competitively inhibits exchange 3-O-methylglucose transport (sugar uptake in cells containing intracellular sugar) but non-competitively inhibits sugar uptake into cells lacking sugar. This refutes the hypothesis that FSK binds at the sugar import site in addition to the sugar export site. Some forskolin derivatives and cytochalasins inhibit equilibrium [^{3}H]-CB binding to red cell membranes depleted of peripheral proteins. Others produce a modest stimulation of [^{3}H]-CB binding when introduced at low concentrations but inhibit binding as their concentration is increased. Yet other analogs modestly stimulate [^{3}H]-CB binding at all inhibitor concentrations applied. These findings are explained by a carrier that presents at least two interacting endofacial binding sites for CB or FSK. We discuss this result

within the context of GLUT1 quaternary structure and evaluate the major determinants of

ligand binding affinity and cooperativity.

INTRODUCTION

Cellular exchange of nutrients, ions and metabolites proceeds via membrane-spanning proteins called channels and carriers (*24*). The Major Facilitator Superfamily of carriers is responsible for the largest portion of nutrient transport in cells (*46*) and among these carriers, the sugar porter sub-family is one of the oldest and largest family classifications.

Sugar porters catalyze both cellular sugar import and export but net sugar transport always proceeds from high to low sugar concentration. The first human sugar transporter to be isolated was the erythrocyte membrane protein GLUT1 (*133, 178*). GLUT1 is primarily expressed in the cardiovascular system and astrocytes and mediates glucose transport across blood-tissue barriers (*179*). Any one of several mutations in GLUT1 results in GLUT1 Deficiency Syndrome (GLUT1DS) in which reduced glucose transport into the brain leads to developmental defects and seizures (*43*).

Hydropathy analysis, scanning glycosylation mutagenesis and proteolytic digestion studies confirm that GLUT1 (a 55 kDa protein) contains twelve alpha-helical transmembrane domains (*73*). Each GLUT1 polypeptide is thought to function as a simple carrier *(85)*, presenting either a sugar uptake or a sugar exit site at any given moment. However, the simple carrier model does not explain the complex behavior of GLUT1 in human red cells (*9*) where the association of GLUT1 monomers into cooperative oligomers promotes an obligate, functionally antiparallel arrangement of

subunits such that any given GLUT1 complex displays uptake and efflux sites simultaneously (*158*).

Scanning cysteine mutagenesis analysis (*80*) suggests that the GLUT1 sugar uptake site involves portions of alpha-helical, transmembrane spanning regions 1, 5, 7, 8 and 11. Peptide mapping studies of affinity labeled GLUT1 suggest that the exit site contains a subdomain of membrane spanning regions 10 and 11 (*13*). However, specific GLUT1 residues contacting glucose in GLUT1 import (e2) and export (e1) conformations are unknown.

The present study characterizes the GLUT1 export conformation by analysis of inhibitor binding to the GLUT1 exit site. Comprehensive analysis of GLUT1 interaction with a library of inhibitors may reveal details of the complementary relationship between ligand and binding pocket structures. We selected GLUT1 endofacial site inhibitors and their derivatives for this analysis. Cytochalasin B (CB) is a cell-permeable alkaloid that disrupts actin filaments and inhibits glucose transport (*180*). Forskolin (FSK) is a cell-permeable diterpenoid that inhibits GLUT1 and activates adenylate cyclase (*107*). Both CB and FSK are thought to bind to the endofacial orientation of GLUT1 where they act as noncompetitive inhibitors of erythrocyte glucose uptake and competitive inhibitors of exit (*(17, 97 , 107)* and this work). These e1 inhibitors have also been docked to an homology-based, theoretical GLUT1 structure where they are proposed to bind to cytoplasmic domains of the carrier *(5)*. Our findings confirm that export-site inhibitors inhibit ligand binding by two mechanisms - direct competition and cooperative inhibition - and provide new insights into the molecular determinants of each type of inhibition.

MATERIALS AND METHODS

SOLUTIONS:

Kaline consisted of 150 mM KCl, 5 mM MgCl2, 5 mM EGTA, 5mM HEPES, pH 7.4. Lysis buffer contained 10 mM Tris-HCl, 2mM EDTA, pH 8.0. Stripping solution contained 2 mM EDTA, 15.4 mM NaOH, pH 12. Sugar-stop solution consisted of ice-cold Kaline containing 20 µM CB and 200 µM phloretin.

MATERIALS:

$[^3H]$-3-O-methylglucose, $[^3H]$-cytochalasin B, and $[^3H]$-forskolin were purchased from Sigma Chemicals. Human blood was purchased from Biological Specialties Cooperation. Other reagents were purchased from Sigma Chemicals.

RED CELLS:

Red cells were isolated from whole human blood by centrifugation as described previously(*9*).

RED CELL MEMBRANES:

Red cell membranes depleted of peripheral membrane proteins (including the cytochalasin B binding protein actin) were prepared as described in (*93*).

3-O-METHYLGLUCOSE UPTAKE:

Zero trans 3MG uptake (3MG uptake into cells lacking intracellular sugar) and equilibrium exchange 3MG sugar uptake (unidirectional $[^3H]$-3MG uptake in cells where intracellular [3MG] = extracellular [3MG]) were measured at 4 ºC as described previously (*(9); (131)*).

FORSKOLIN OR CYTOCHALASIN B INHIBITION OF 3MG TRANSPORT

3MG uptake was measured as described above in the absence and presence of cytochalasin B, forskolin or their derivatives. Inhibitor concentrations ranged from 10^{-9} - 10^{-4} M using ethanol or dimethylsulfoxide as carriers. Carrier concentration never exceeded 0.1% (vol:vol) and is without effect on sugar transport rates. Cells were pre-incubated with inhibitor of 15 minutes on ice before starting uptake measurements. When transport inhibition was profound (> 75%), the uptake interval was extended to permit more accurate determinations of uptake.

LIGAND BINDING COMPETITION ASSAY

Stripped ghosts (peripheral protein-depleted membranes) were diluted to 2 mg/ml in 50 mM Tris medium, pH 7.4 at 4°C. Ligand binding assay solutions comprised Tris medium plus 50 nM unlabeled CB, 1 μCi/ml [^{3}H]-CB plus a range of inhibitor (I) concentrations (0 - 100 μM). Some ligand binding assays substituted 50 nM forskolin and 1 μCi/ml [^{3}H]-forskolin for cytochalasin B. Binding assays were as described previously (*96*). Membranes (50 μL) and ligand binding solutions (50 μL) were mixed in a micro centrifuge tube and, following 15 minutes of inversion at 4°C, two 10 μL aliquots were sampled (Total dpms). The tubes were centrifuged at 14,000 rpm for 5 minutes, and two 10 μL aliquots of the supernatant were sampled (Free dpms). 'Bound' dpms were calculated as the difference between 'total' and 'free' dpms. Each inhibitor concentration was tested three times in triplicate.

LIGAND BINDING TO GLUT1 - THEORY

Equilibrium cytochalasin B and forskolin binding to GLUT1 display non-Michaelis kinetics at low ligand concentrations (*(16); (7)*).   The simplest model that accounts for this behavior (see Scheme 1) assumes that the glucose transporter complex presents two interacting binding sites for e1 ligands. This could be explained either by two sites on one transport protein or two interacting transport proteins each with one site. When presented with a binary mixture of ligands (e.g. radio-ligand plus inhibitor I), the transporter, *e*, may form several liganded states: e (unliganded transporter), 2(I. e), 2(L.e), 2(I.e.L), L.e.L and I.e.I.

Inhibition Scheme 3.1

$$
\begin{array}{ccccc}
\text{I.e.I} & \xrightarrow{\gamma K_i} & \text{I + I.e + L} & \xrightarrow{\beta K_L} & \text{I.e.L} \\
\Big\uparrow \gamma K_i & & \Big\downarrow K_i & & \Big\downarrow \beta K_i \\
| & & | & & | \\
+ & & + & & + \\
\text{e.I} & \xrightarrow{K_i} & \text{I + e + L} & \xrightarrow{K_L} & \text{e.L} \\
+ & & + & & + \\
\text{L} & & \text{L} & & \text{L} \\
\Big\uparrow \beta K_L & & \Big\downarrow K_L & & \Big\downarrow \alpha K_L \\
\text{L.e.I} & \xrightarrow{\beta K_i} & \text{I + L.e + L} & \xrightarrow{\alpha K_L} & \text{L.e.L}
\end{array}
$$
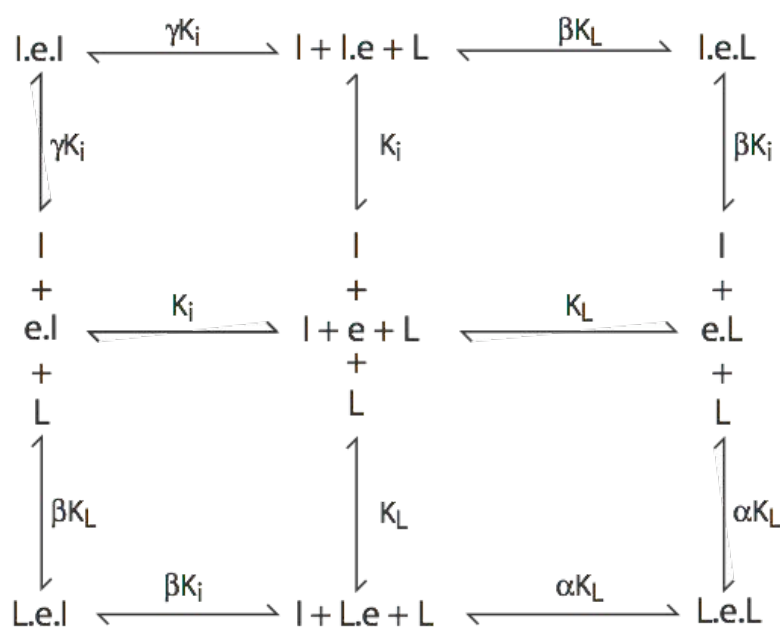
Cooperative interactions between binding sites (positive or negative cooperativity) may depend on whether the first and second ligands to bind are identical or different. For example, the ligand CB might enhance binding of the remaining site for CB ($\alpha < 1$; positive homo-cooperativity) but reduce the affinity of the remaining site for inhibitor I ($\beta > 1$; negative hetero-cooperativity).

Ligand (L) binding to GLUT1 in the presence of a competing e1 inhibitor I is described by:

$$b = \frac{B_{\text{max}} L}{K_{d(app)} + L}$$

where $B_{\text{max}} = 0.5[\text{GLUT1}]$ and $K_{d(app)}$ is given by:

$$\frac{K_L \left\{ 1 + \frac{I}{K_i} \left\{ 2 + \frac{I}{\gamma K_i} \right\} \right\}}{\left\{ 2 + \frac{L}{\alpha K_L} + \frac{2I}{\beta K_i} \right\}}$$

and where K_L, K_I, α, β and γ are shown in scheme 1. In a typical experiment, the ratio of bound : free ligand is measured as a function of competing e1 inhibitor I. The ratio of inhibited : control binding (b'/b) is thus obtained as:

$$\frac{b'}{b} = \cfrac{\left\{ \cfrac{K_L}{\left\{2 + \cfrac{L}{\alpha K_L}\right\}} + L \right\}}{\left\{ \cfrac{K_L\left\{1 + \cfrac{I}{K_i}\left\{2 + \cfrac{I}{\gamma K_i}\right\}\right\}}{\left\{2 + \cfrac{L}{\alpha K_L} + \cfrac{2I}{\beta K_i}\right\}} + L \right\}} = \cfrac{L + \cfrac{\alpha K_L^2}{2\alpha K_L + L}}{L + \cfrac{\alpha\beta K_L^2(I^2 + 2\gamma K_i I + \gamma K_i^2)}{\gamma K_i(2\alpha K_L(I + \beta K_i) + \beta K_i L)}}$$

This analysis assumes that all binding and dissociation steps are rapid with respect to the time of measurement and that free and bound ligand achieve true equilibrium. These assumptions are most likely satisfied because cytochalasin B binding to GLUT1 occurs with a time constant of 1 sec at 4ºC (*(158); (181)*) whereas binding was measured over a period of 15 minutes (> 1,000 half-lives).This model allows for several possible effects of inhibitor (I) on ligand (L) binding.

1   ***Binding is not cooperative.*** When binding of L and I at any single site is mutually exclusive and lacks hetero-cooperativity ($\beta = 1$; Figure 3.1, curve a), the inhibitor I will serve as a simple competitive inhibitor of L binding.

2   ***Binding is negatively cooperative.*** When binding of L and I at any single site is mutually exclusive and displays negative hetero-cooperativity ($\beta > 1$; Figure 3.1, curve b), the inhibitor I will appear to serve as a simple competitive inhibitor of L binding although the inhibition dose response is shifted to the left.

3   ***Binding is positively cooperative.*** When binding of L and I at any single site is mutually exclusive but displays positive hetero-cooperativity between sites ($\beta < 1$;

Figure 3.1, curve c), the inhibitor I will enhance L binding at low [I] where I and L bind

at adjacent sites. When [I] is increased further such that I and L compete for binding to

the same site, L binding is inhibited.

4   Zero hetero-cooperativity and positive or negative homo-cooperativity.

When binding of L and I at any single site is mutually exclusive but displays zero hetero-

cooperativity but positive homo-cooperativity (i.e. $\beta = 1$ and $\gamma < 1$; Figure 3.1, curve d),

the inhibitor I will inhibit L binding more effectively (the inhibition curve is left-shifted).

If the inhibitor I displays negative homo-cooperativity, I will be a less effective inhibitor

and maximum inhibition will be reduced (i.e. $\beta = 1$ and $\gamma > 1$; Figure 3.1, curve e).

5   Positive hetero-cooperativity and positive or negative homo-

cooperativity. When binding of L and I at any single site is mutually exclusive but

displays positive-hetero-cooperativity and positive homo-cooperativity (i.e. $\beta \ll 1$ and γ

$\ll 1$; Figure 1, curve f), the inhibitor I will enhance L binding at low [I] and inhibit

binding at greater [I]. If the inhibitor I displays negative homo-cooperativity ($\gamma \gg 1$) but

strong positive hetero-cooperativity ($\beta \ll 1$), I will enhance ligand binding at all [I]

(Figure 3.1, curve g).

Ligand binding was calculated as the ratio ligand bound in the presence of

inhibitor (b') to ligand bound in the absence of inhibitor (b). b'/b was plotted against [I]

(see Figure 1) and binding was analyzed using eqn 3 and the method of least squares

using the software programs Kaleidagraph (v 4.03, Synergy Software) or ProFit (v 6.13,

Quantum Soft). When cytochalasin B inhibition of [^{3}H]-cytochalasin B binding (or

forskolin inhibition of [^{3}H]- forskolin) was measured, the analysis simplifies considerably

because $\alpha = \beta = \gamma$ and $K_L = K_i$. Thus the homo-inhibition experiment allow the

unambiguous calculation of K_L and α for cytochalasin B and forskolin (Table 3.1). These

values may then be substituted directly into eqn 3 leaving only 3 parameters to solve for

in hetero-inhibition experiments: β, γ and K_i.

Figure 3.1 Simulations of effects of inhibitors on cytochalasin B binding to GLUT1

when each transporter complex contains two interacting binding sites .

Ordinate: CB binding in the presence of an inhibitor/CB binding in the absence of

inhibitor (calculated using equation 3). Abscissa: inhibitor concentration in μM (note the

log scale). Seven (a-g) scenarios were simulated. In each instance K_L for CB binding, K_i

for inhibitor binding and α (cooperativity between CB binding sites when only the CB is

present) were set at 0.25 μM, 1 μM and 1 respectively. The curves show: a, β = γ = 1; b β

=10, γ = 1; c β = 0.1, γ = 1; d β = 1, γ = 0.1; e β = 1, γ = 10; f β = γ = 0.1; g β = 0.1, γ =
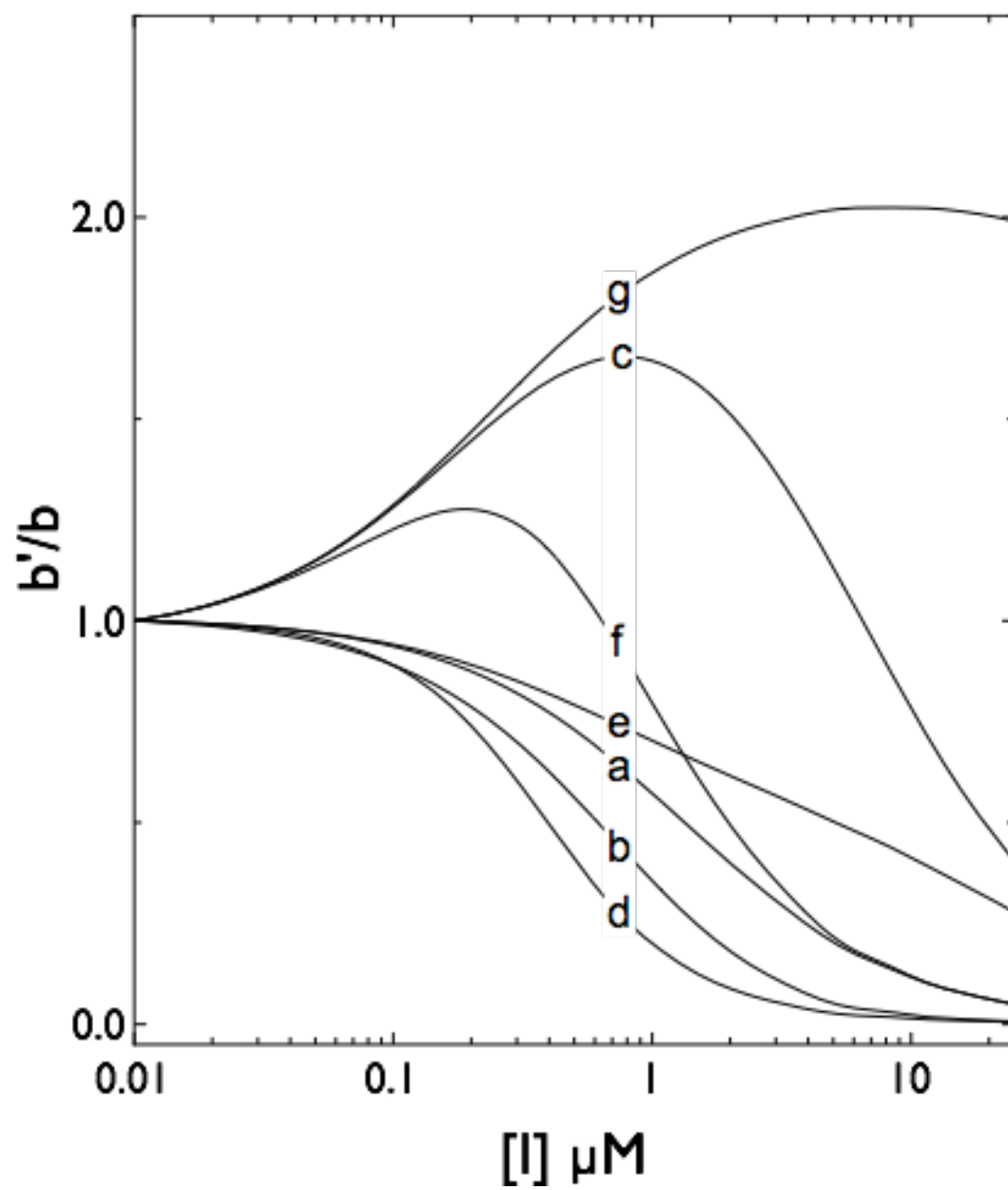
100.

Fig 3.1

Figure 3.2 Erythrocyte sugar transport inhibition by forskolin.

Panels A & B, Ordinate: initial rate of 3MG uptake (mmol/L cell water/min). Abscissa: [3MG] mM. Results are shown as mean $\pm$ SEM of at least 3 experiments made in quadruplicate. Uptake was measured in the absence ($\circ$) and presence ($\bullet$) of 2 μM FSK. Curves drawn through the points were computed by nonlinear regression assuming that 3MG uptake follows simple Michaelis-Menten kinetics. A Zero-trans 3MG uptake (cells lack intracellular sugar). Control: $K_{mapp} = 1.51 \pm 0.22$ mM; $V_{max} = 0.114 \pm 0.009$ mM/L/min; $R^2 = 0.995$. FSK: $K_{mapp} = 1.09 \pm 0.15$ mM; $V_{max} = 0.055 \pm 0.004$ mM/L/min., $R^2 = 0.994$. B Equilibrium-exchange 3MG uptake (intracellular [sugar]= extracellular [sugar]). Control: $K_{mapp} = 17.8 \pm 4.7$ mM; $V_{max} = 6.5 \pm 0.7$ mM/L/min, $R^2 = 0.981$. FSK: $K_{mapp} = 48.5 \pm 7.3$ mM; $V_{max} = 8.3 \pm 0.7$ mM/L/min, $R^2 = 0.997$.

Fig 3.2
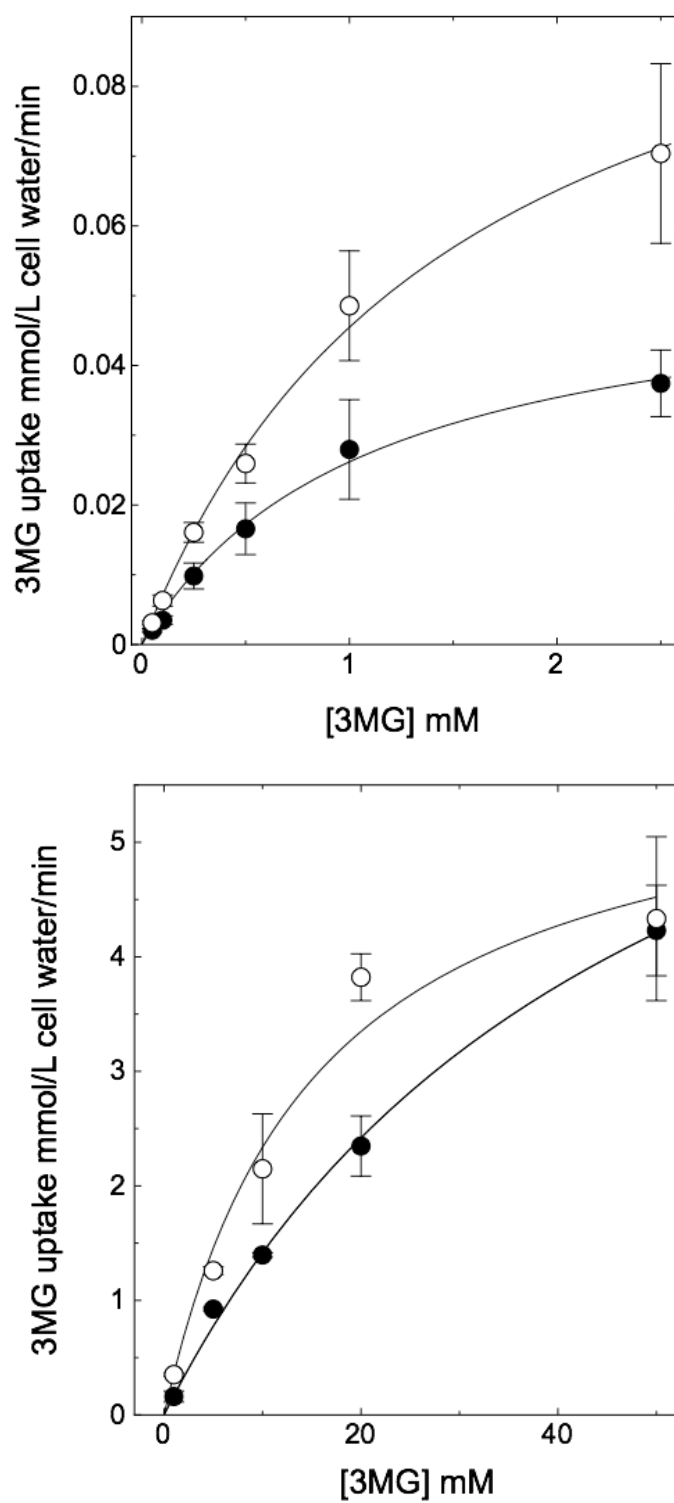
RESULTS

Cytochalasin B is a competitive inhibitor of equilibrium exchange transport in erythrocytes (*156*) and a noncompetitive inhibitor of net sugar uptake into red cells lacking sugar (*97*). Equilibrium exchange transport is a condition in which intra- and extracellular [sugar] are identical and unidirectional fluxes are monitored through use of tracer sugar. Competitive inhibition by cytochalasin B indicates that extra- or intracellular sugar compete with cytochalasin B for binding to the transporter. Noncompetitive inhibition of uptake into cells lacking sugar indicates the absence of competition between extracellular sugar and inhibitor at the uptake site. This aggregate behavior is characteristic of an inhibitor that binds at (or whose binding site is mutually exclusive with) the sugar export site (*(97)*).

Forskolin is a competitive inhibitor of cytochalasin B binding to the human erythrocyte sugar transporter (*182*) suggesting that forskolin, like cytochalasin B binds at or close to the transporter sugar export site. In support of this hypothesis, we observe that forskolin acts as a noncompetitive inhibitor of net sugar uptake (Figure 3.2A) and as a competitive inhibitor of exchange sugar uptake (Figure 3.2B) in human erythrocytes. Forskolin reduces V_{max} for sugar uptake by sugar-depleted cells but increases $K_{m(app)}$ for equilibrium exchange transport. Assuming noncompetitive and competitive inhibition of 3MG zero-trans and equilibrium exchange transport respectively, $K_{i(app)}$ for FSK inhibition of net and exchange transport are 1.9 ± 0.4 μM and 1.2 ± 0.6 μM respectively.

Figure 3.3 A Modulation of [^{3}H]-CB binding to red cell membranes by forskolin and its derivatives.

Ordinate: The ratio CB binding in the presence of forskolin to CB binding in the absence of forskolin. Abscissa: [forskolin], μM (note the log scale). Results are shown as mean of at least 3 separate measurements made in quadruplicate. Standard errors about the mean are ≤ 10% of the averaged data. CB binding was measured at 50 nM [^{3}H]-CB. Results are shown for inhibition by FSK (○), 7DAFSK (●) and 1DOFSK (Δ). Curves drawn through the points were computed by nonlinear regression using equation 3. Based on CB inhibition of [^{3}H]-CB, Kl and α were set at 0.25 ± 0.03 μM and 0.52 ± 0.26 respectively. The results are: FSK, $K_i = 2.13 \pm 0.45$ μM, $\beta = 0.48 \pm 0.05$, $\gamma = 1.13 \pm 0.26$, $R^2 = 0.979$. 7DeA-FSK, $K_i = 0.07 \pm 0.01$ μM, $\beta = 0.36 \pm 0.01$, $\gamma = \infty$, $R^2 = 0.86$. 1DO-FSK, $K_i = 0.20 \pm 0.10$ μM, $\beta = 0.34 \pm 0.01$, $\gamma = 58 \pm 29$, $R^2 = 0.975$. B Modulation of [3H]-FSK binding to red cell membranes by unlabeled forskolin. Ordinate: The ratio [^{3}H]-FSK binding in the presence of forskolin to [^{3}H]-FSK binding in the absence of forskolin. Abscissa: [forskolin], μM (note the log scale). Results are shown as mean ± SEM of 3 separate measurements made in quadruplicate. [^{3}H]-FSK binding was measured at 50 nM [3H]-FSK. The curve drawn through the points was computed by nonlinear regression using equation 3. The results are:, $K_i = K_L = 2.13 \pm 0.45$ μM and $\alpha = \beta = \gamma = 0.88 \pm 0.31$, $R^2 = 0.939$.

Fig 3.3
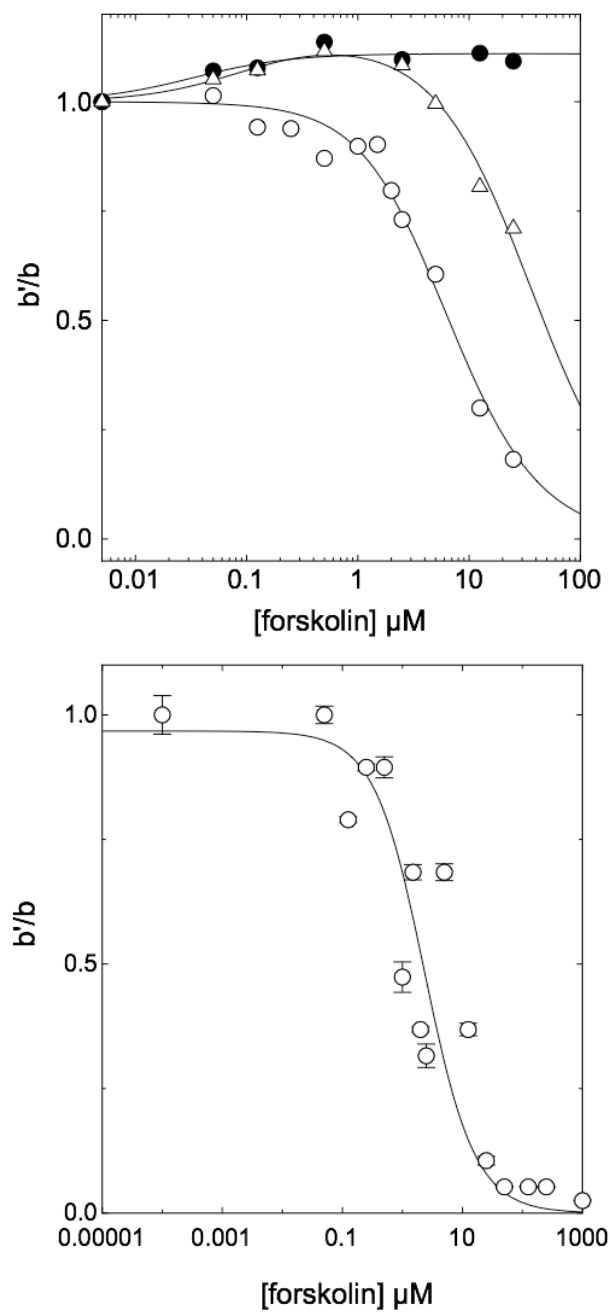
We screened the ability of forskolin and its derivatives to displace cytochalasin B from GLUT1 by measuring forskolin inhibition of equilibrium ^{3}H-cytochalasin B binding to red cell membranes depleted of peripheral membrane proteins. Cytochalasin B binding to peripheral membrane protein-depleted human red cell membranes, is competitively displaced by D-glucose and other GLUT1 substrates and is quantitatively accounted for by ligand binding to GLUT1 (*(183); (86)*).

Forskolin and its derivatives modify cytochalasin B (50 nM) binding to GLUT1 in several interesting ways (Figure 3.3). Some forskolins (see Figure 3.3A and Table 3.1) appear to function as simple inhibitors of cytochalasin B binding in which inhibition is a saturable function in [forskolin]. Other forskolins (see Figure 3.3A and Table 3.1) first enhance then inhibit cytochalasin B binding as the concentration of the inhibitor is raised. Yet other inhibitor analogs simply increase cytochalasin B binding (see Figure 3.3A and Table 3.1) while others appear to be without effect.

These behaviors are predicted by a simple binding model (Scheme 1) in which each transporter complex presents two cytochalasin B or forskolin binding sites that interact in ways that are dependent upon the nature of the bound ligands. For example, if binding of a forskolin derivative at the first site increases the affinity of the second site for cytochalasin B or the forskolin derivative, cytochalasin B binding may be enhanced at low [forskolin] then inhibited as [forskolin] is raised and competes more effectively with cytochalasin B for binding at the second site. Other permutations are possible (see Scheme 1 and Figure 3.1) and, according to the model, the net effect of any [forskolin] on cytochalasin B binding is determined by 5 parameters: K_L (K_d for cytochalasin B

binding), K_i (K_d for forskolin derivative binding), α (a cooperativity factor indicating how cytochalasin B binding at the first site impacts $K_{d(app)}$ for cytochalasin B binding at the second site), β (a cooperativity factor indicating how cytochalasin B binding at the first site impacts $K_{d(app)}$ for forskolin binding at the second site and vice versa) and γ (a cooperativity factor indicating how forskolin binding at the first site impacts $K_{d(app)}$ for forskolin binding at the second site). In homo-inhibition studies where, for example, the radioligand and unlabeled competing ligand are the same species (e.g. cytochalasin B or forskolin), $K_L = K_i$ and $\alpha = \beta = \gamma$ thereby simplifying analysis of experimental data to the resolution of two affinity parameters - K_L and α. These values may then be explicitly inserted into binding equation 3 thereby reducing the challenge of non-linear curve fitting of forskolin-modulation of cytochalasin B binding (hetero-inhibition) to the resolution of 3 parameters - K_i, β and γ.

Tests for internal consistency mandate that studies of unlabeled forskolin inhibition of [^{3}H]-forskolin binding to GLUT1 (forskolin homo-inhibition) provide values for K_L and α (2.12 ± 0.35 µM and 0.88 ± 0.31 respectively, see Figure 3.3B) that that are indistinguishable from K_i and γ (2.13 ± 0.45 µM and 1.13 ± 0.26 respectively) obtained in studies of forskolin-modulation of [^{3}H]-cytochalasin B binding (hetero-inhibition).

Table 3.1 summarizes the results of hetero-inhibition studies in which the effects of a wide range of forskolin analogues on [^{3}H]-cytochalasin B binding were measured. Figure 3.4 and Table 3.1 summarize the results of similar studies in which the effects of a number of cytochalasin analogues on [^{3}H]-cytochalasin B binding were measured.

Table 3.1 Modulation of ^{3}H cytochalasin B binding to red cell membranes by cytochalasins and forskolins - summary of findings.

The results of analyses such as those in Figures 3 and 4 are summarized for the cytochalasins and the forskolins. The concentration of radioligand ($[^3$H]-CB) was 50 nM in all experiments. [a]The concentration of unlabeled competing ligand was varied from 0 to 100 μM. Analysis of binding inhibition was carried out as described in Figures 2 and 3 using equation 3. [b]Ki (μM) represents the affinity of unoccupied GLUT1 for ligand. [c]Gº was calculated as RT ln(1/Ki). [d]ΔΔGº was calculated as the change in ΔGº using the lowest Ki for cytochalasins or foskolins as the baseline. [e,f,g]Analysis according to equation 3 also permits computation of the cooperativity parameters β and γ and yields a correlation coefficient R^2. [h]Types of inhibition are: Michaelis like inhibition (curves a & e, Figure 3.1); stimulation followed by inhibition (curves c & f, Figure 3.1); high and low affinity inhibition (curve d, Figure 3.1); stimulation (curve g, Figure 3.1) and no effect. [i]These types of inhibition are related to the product β*γ. . [j]KL (μM) and [k]α for CB binding were computed in studies of CB inhibition of [3H]-CB binding and assume that α = β = γ. [l]While γ parameters are ligand dependent, β parameters appear to be invariant and are averaged for the cytochalasins and forskolins (mean ± SEM). [m]No effect on binding was observed. In all experiments, at least three complete dose responses were performed with each data point in triplicate and averaged at each concentration to perform the final analysis. Ligand structures shown in Tables 3.2 and 3.3.

Table 3.1

[a]Ligand	[b]K_I μM	[c]ΔG kcal/mol	[d]ΔΔG kcal/mol	[e]β	[f]γ	[g]R^2	[h]Inh. Scheme	[i]β*γ
CB	0.25 ± 0.03	-8.37	0.00	0.52 ± 0.26	0.52 ± 0.26	0.995	f	0.4
CD	111.7 ± 14.8	-5.01	3.36	1.00 ± 0.12	0.67	0.906	f	0.7
CH	2.08 ± 0.39	-7.20	1.17	0.34 ± 0.03	7.1 ± 0.55	0.946	f	2.4
CJ	1.37 ± 3.11	-7.43	0.94	0.55 ± 0.13	41.4 ± 66.3	0.927	c	22.8
CE	0.53 ± 0.31	-7.95	0.41	0.47 ± 0.04	363 ± 44	0.823	c	170.6
CA	1.44 ± 0.88	-7.40	0.96	0.35 ± 0.12	93.365	0.999	f	31627.8
CC	1.87 ± 1.11	-7.26	1.11	0.34 ± 0.08	∞	0.915	g	∞
CB [j]KL μM	0.25 ± 0.03		[l]mean	0.510				
CB [k]α	0.52 ± 0.03			± 0.088				
FSK	2.13 ± 0.45	-7.19	2.73	0.48 ± 0.05	1.13 ± 0.26	0.979	f	0.5
14,15 DiH-FSK	1.27 ± 0.03	-7.47	2.44	0.467 ± 0.031	4.49 ± 0.68	0.969	f	2.1
1A-FSK	0.99 ± 0.31	-7.61	2.31	0.32 ± 0.18	21 ± 7	0.850	f	6.7
9DeO-FSK	0.269 ± 0.25	-8.33	1.59	0.37 ± 0.01	127 ± 119	0.852	f	10.8
7FA-FSK	0.651 ± 0.45	-7.84	2.08	0.375 ± 0.012	29.2 ± 1.9	0.972	f	11.0
1DeO-FSK	0.20 ± 0.10	-8.49	1.43	0.34 ± 0.01	58 ± 29	0.975	f	19.7
6A-FSK	0.015 ± 0.021	-9.92	0	0.36 ± 0.01	555 ± 27	0.994	c	199.8
1,6DiA-FSK	0.018 ± 0.58	-9.82	0.10	0.38 ± 0.01	621 ± 46	0.976	c	236.0
7FPA-FSK	0.109 ± 0.35	-8.82	1.09	0.43 ± 0.01	1230 ± 404	0.823	c	528.9
7FPPNEA-FSK	0.02 ± 0.04	-9.76	0.16	0.33 ± 0.01	36858 ± 83397	0.748	g	12073.1
7DeA-FSK	0.07 ± 0.10	-9.07	0.85	0.36 ± 0.01	∞	0.860	g	∞
6A,7DeA-FSK	NA[m]			NA	NA	NA	c	
7FPP-FSK	NA			NA	NA	NA	e	
			[l]mean	0.378 ± 0.016				

Table 3.1 – Modulation of GLUT1 Cytochalasin B binding by cytochalasins and forskolins

Figure 3.4 Modulation of cytochalasin B binding to red cell membranes by cytochalasins.

Ordinate: The ratio CB binding in the presence of forskolin to CB binding in the absence of cytochalasins. Abscissa: [cytochalasin], µM (note the log scale). Results are shown as mean of at least 3 separate measurements made in quadruplicate. Standard errors about the mean are $\leq 10\%$ of the averaged data. CB binding was measured at 50 nM [^{3}H]-CB. Results are shown for inhibition by CB (○), CC (●) and CH (Δ). Curves drawn through the points were computed by nonlinear regression using equation 3. The results are: CB, $K_i = K_L = 0.25 \pm 0.03$ µM and $\alpha = \beta = \gamma = 0.52 \pm 0.26$, $R^2 = 0.995$. CC, $K_i = 1.87 \pm 0.11$ µM, $\beta = 0.34 \pm 0.06$, $\gamma = \infty$, $R^2 = 0.915$. CH, $K_i = 2.08 \pm 0.39$ µM, $\beta = 0.34 \pm 0.03$, $\gamma = 7.1 \pm 0.55$, $R^2 = 0.946$.

Fig 3.4
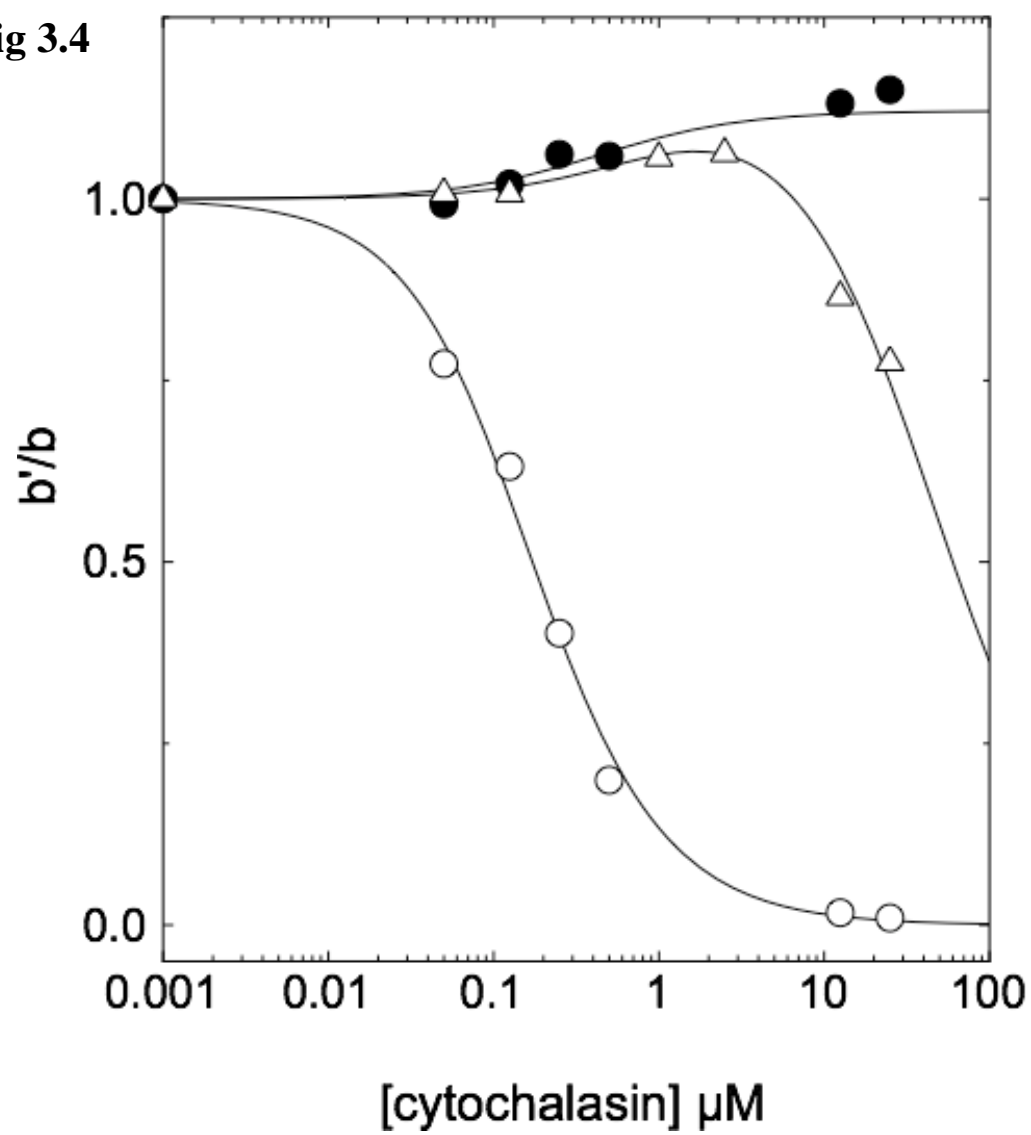
DISCUSSION

GLUT1 LIGANDS & TETRAMERIC COOPERATIVITY

The human type 1 glucose transporter (GLUT1) is inhibited by diverse natural compounds. Methylxanthines and ATP act as mixed-type inhibitors of sugar exit reducing V_{max} and increasing $K_{m(app)}$ *(98, 184, 185)*. Cytochalasins and forskolins increase $K_{m(app)}$ for exchange transport and reduce V_{max} for net entry (see here and *(97, 107, 156))*. Tyrosine kinase inhibitors are competitive inhibitors of sugar import (*186*) and the androgens and catechins reduce V_{max} for exit and increase $K_{m(app)}$ for uptake (*106*). These observations are consistent with the hypothesis that cytochalasins and forskolins bind at or close to the sugar export site and that the tyrosine kinase inhibitors, androgens and catechins bind at or close to the sugar import site (*106*). Methylxanthines and ATP appear to modulate transport by acting at a site(s) distinct from import and exit sites.

Recent studies have revealed an unexpected complexity in transport inhibition by import and export site inhibitors. When presented at very low concentrations, the import site inhibitor maltose or the exit site inhibitors cytochalasin B (CB) or forskolin (FSK) modestly stimulate sugar import in human red blood cells *(7, 16)*. As inhibitor concentration is increased, sugar import stimulation is replaced by transport inhibition. The simplest explanation for this behavior is that the sugar transporter contains 2 interaction sites for import site inhibitors and two sites for export site inhibitors. When one import or export interaction site is occupied by inhibitor, the transporter is converted into a high affinity, high capacity sugar transporter that catalyzes greater net transport (*7*).

As the concentration of inhibitor is increased further, the second import or export site is occupied and transport is fully inhibited.

This behavior is consistent with the structural and functional properties of GLUT1. Each GLUT1 protein functions as a sugar transport pathway by isomerizing rapidly between two states - e2, exposing an exofacial, sugar import site and e1, exposing an endofacial, sugar export site(*8*). Overall behavior, however, is determined by transporter quaternary structure. Red cell GLUT1 is a dimer of GLUT1 dimers (*65*). Each dimer always contains one subunit presenting the e2 state and one subunit presenting the e1 state (*12*). CB binding to the e1 subunit of any dimer inhibits transport through each subunit of the occupied dimer but stimulates transport through the neighboring unoccupied dimer. As the concentration of cytochalasin B is increased, an e1 subunit within the neighboring unoccupied dimer becomes complexed with cytochalasin B and transport via both dimers is inhibited (*7, 16*). The goals of the present study were to understand the structural features of cytochalasin B and forskolin that determine ligand binding affinity and dimer-dimer cooperativity.

CYTOCHALASIN AND FORSKOLIN DERIVATIVE ANALYSIS

The cytochalasins (Table 3.2) share a common rigid bicyclic isoindoline core fused to a macrocycle. CB shows the greatest affinity for GLUT1 ($K_{d(app)} = 0.25 \ \mu M$), and an auto-inhibition profile consistent with scheme f in Fig 3.1. Dehydration of the macrocycle hydroxyl group to form cytochalasin A (CA) maps to scheme g, and results in a 6-fold loss of affinity for GLUT1 ($\Delta \Delta G^\circ = 1$ kcal/mol). This group may serve as a

Table 3.2 Cytochalasin derivative structures.

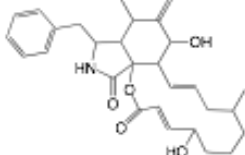KL and γ are also shown (taken from Table 3.1) to facilitate comparison.
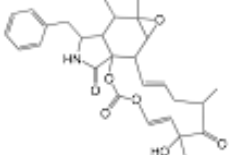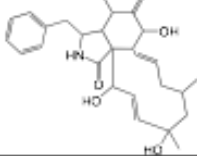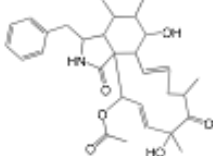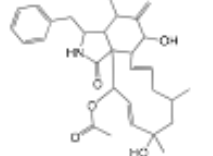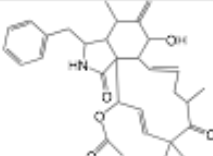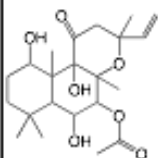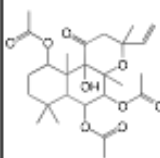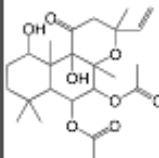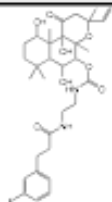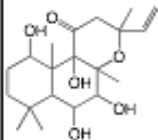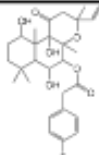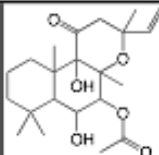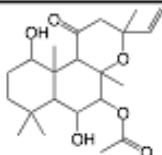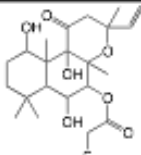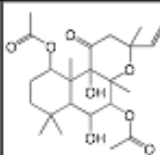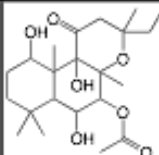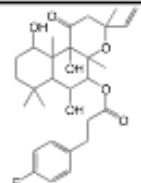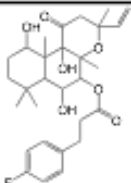
Cytochalasin B (CB)		Cytochalasin E (CE)	
$K_L = 0.25\ \mu M$ $\gamma = 0.5$		$K_L = 0.5\ \mu M$ $\gamma = 363$	
Cytochalasin J (CJ)		Cytochalasin A (CA)	
$K_L = 1.37\ \mu M$ $\gamma = 41.4$		$K_L = 1.44\ \mu M$ $\gamma = 90,365$	
Cytochalasin C (CC)		Cytochalasin H (CH)	
$K_L = 1.87\ \mu M$ $\gamma = \infty$		$K_L = 2.08\ \mu M$ $\gamma = 7$	
Cytochalasin D (CD)			
$K_L = 111\ \mu M$ $\gamma = 0.7$			

Table 3.3 Forskolin derivative structures.

KL and γ are also shown (taken from Table 3.1) to facilitate comparison.

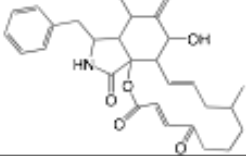| FSK	1,6DiA-FSK	6A-FSK	7FPPNEA-FSK
$K_L = 2.1$ μM $\gamma = 1.13$	$K_L = 0.02$ μM $\gamma = 621$	$K_L = 0.02$ μM $\gamma = 555$	$K_L = 0.02$ μM $\gamma = 36,858$
7DeA-FSK	**7FPA-FSK**	**1DeO-FSK**	**9DeO-FSK**
$K_L = 0.07$ μM $\gamma = \infty$	$K_L = 0.11$ μM $\gamma = 1230$	$K_L = 0.2$ μM $\gamma = 58$	$K_L = 0.27$ μM $\gamma = 127$
7FA-FSK	**1A-FSK**	**14,15DiH-FSK**	
$K_L = 0.6$ μM $\gamma = 29.2$	$K_L = 1$ μM $\gamma = 21$	$K_L = 1.3$ μM $\gamma = 4.5$	
7FPP-FSK	**6A,7DeA-FSK**		
$K_L = NA$	$K_L = NA$		

hydrogen bond donor. Shortening the macrocycle by three carbon atoms reduces GLUT1 affinity for ligands by 5- to 8-fold (cytochalasins C, H and J; $\Delta\Delta G^o$ = 0.9 - 1.2 kcal/mol). This may result from the loss of van der Waal's interactions or from the resultant mis-location of the macrocycle hydroxyl group within the binding site. Addition of an acetyl group to the macrocycle ketone does not affect ligand binding (CC and CH versus CA). Addition of a carbonyl at position 5 of a shortened macrocycle is without effect on binding affinity (compare CJ and CC). However, subsequent methyl substitution at position 5 of the bicyclic isoindoline reduces binding affinity by 55-fold (compare CD and CC; $\Delta\Delta G^o$ = 2.25 kcal/mol). This suggests that the cytochalasin binding pocket can tolerate reduced molecular motion at each position but not at both.

The forskolins (FSK; Table 3.3) are a family of labdane diterpenes known primarily for their activation of adenylyl cyclase (*187*). FSK derivatives containing acetyl groups at positions 6 and 7 show greatest affinity for GLUT1. Substitution of both groups with hydroxyl groups results in a 3-fold loss in FSK binding affinity ($\Delta\Delta G^o$ = 0.9 kcal/mol). Deacylation at position 7 results in the complete loss of FSK binding affinity whereas loss of the acyl group at position 6 (to form the parent molecule FSK) results in a 500-fold loss of affinity ($\Delta\Delta G^o$ = 3.6 kcal/mol). Deacylation at position 6 is partially mitigated by introduction of an acetyl group at position 1 (10-fold recovery in affinity), by removal of hydroxyl groups at positions 1 (50-fold recovery of affinity) or 9 (30-fold recovery of affinity) or, by conversion of the acetaldehyde to a formyl fluoride (16-fold recovery). FSK binding tolerates hydroxyl, acetyl, formyl fluoride, fluorophenylacetyl and fluorophenyl propanamidoethylcarbamic group additions at position 7.

Cytochalasins and forskolins show a similar cooperativity parameter ($\beta = 0.44 \pm$ 0.05) for binding to the second site when the first site is occupied by CB. This positive hetero-cooperativity means that forskolin or cytochalasin occupancy of the first site increases the affinity of the second site cytochalasin B by two-fold and *vice versa*. CB-inhibition of radiolabeled CB binding also displays positive cooperativity ($\alpha = 0.5 \pm 0.3$, Fig 3.1 scheme f) whereas forskolin inhibition of radiolabeled forskolin binding is not cooperative ($\alpha = 0.9 \pm 0.3$, Fig 3.1 scheme d). This suggests that β - the cooperativity factor describing binding site interactions when different ligands bind at sites 1 and 2 - is determined by the ligand whose binding is experimentally measured (in this case the radioligand). This is consistent with the observation that the cooperativity parameter γ - describing the effect of occupancy of the first site by unlabeled inhibitor on unlabeled inhibitor binding to the second site - is determined by the nature of the unlabeled inhibitor.

Cytochalasin D, while displaying only poor affinity for GLUT1, shows the same homo-cooperativity ($\gamma = 0.7$, scheme f) for binding to GLUT1 as does CB ($\gamma = 0.52 \pm$ 0.26, scheme f). Cytochalasin C differs from CD only at position 5 of the bicyclic isoindoline but has a homo-cooperativity γ parameter of infinity. This means that CD cannot bind at the second site when the first site is occupied by CD. Dehydration of the CB macrocycle hydroxyl group to form CA results in 180,000-fold increase in γ suggesting that loss of a hydrogen bond donor at this position promotes negative cooperativity between sites (Fig 3.1, scheme g). Addition of an acetyl group to the macrocycle ketone is without great effect on γ.

Addition of a single acyl group to forskolin at positions 1 or 6 or extension of the acyl group at position 7 significantly increase γ. Simultaneous additions of acyl groups at positions 1 and 6 have neither additive nor synergistic effects on γ, and both map to cooperativity scheme f in Fig 3.1. Elimination of hydroxyl groups at positions 1 or 9 (schemes f, Fig 3.1) or elimination of the acyl group at position 7 (scheme e, Fig 3.1) greatly increase γ. γ and $K_{i(app)}$ appear to be inversely related.

CURRENT VS. CLASSIC CYTOCHALASIN STUDIES

Previous studies have examined cytochalasin and forskolin inhibition of sugar transport and cytochalasin B binding in human red cells *(107, 121, 182, 188)* and forskolin inhibition of energized D-galactose transport by the GalP sugar-H+ symport protein of Escherichia coli (*189*). The present study differs from previous studies in that our analysis of inhibition of ligand binding to GLUT1 allows for two interacting ligand binding sites.

In their study of cytochalasin inhibition of [^{3}H]-cytochalasin B binding to GLUT1 in red cell membranes (*188*) Rampal and coworkers revealed that only CA and CB inhibit CB binding with high affinity. The remaining cytochalasins (CC through CH) were extremely low affinity inhibitors ($K_{i(app)} > 100$ μM). While this result appears to contradict our observations, closer inspection reveals that $K_{i(app)}$ for occupation of the second ligand binding site by cytochalasin analogs (provided in our study as the product γK_i), corresponds to $K_{i(app)}$ observed by Rampal et al (*188*). For example, CE inhibition of CB binding is characterized by β, γ and K_i parameters of 0.47 ± 0.04, 363 ± 44 and 0.53 ± 0.31 μM respectively. This means that CB binding is inhibited by $\leq 5\%$ over the CE

concentration range 0 to 0.5 µM then by an additional 6% over the CE concentration

range 1 to 25 µM. Analysis assuming a single ligand binding site would result in $K_{i(app)}$ of

222 ± 76 µM. Rampal et al report that $K_{i(app)} \geq 100$ µM. As with our previous studies

showing that low concentrations of "inhibitors" can produce a paradoxical stimulation of

transport (*7, 16*), the key to these observations is the use of inhibitor concentrations that

span $K_{d(app)}$ by ± 2 log units.

CLASSIC VS. COOPERATIVE ANALYSIS

When considering cooperativity, the 'gold standard' measure in the literature is

the application of the Hill equation, derived by A.V. Hill to model the binding of oxygen

to hemoglobin (*190*). While many variants on the Hill equation are utilized to measure

binding site interactions, this analysis is not useful to the current study for the following

reasons. 1) The Hill equation does not allow for appreciable concentrations of binding

intermediates in competitive analysis, 2) is it not intended to measure competition

analysis between ligands of varying natures, and 3) the Hill equation was designed with

the assumption of strong positive cooperativity between ligand sites as in the hemoglobin

model; negative cooperativity reduces the Hill coefficient to a minimum of 1(*191*). The

model derived from Scheme 1 allows for analysis of positive and negative homo- and

hetero- cooperativity, which closely reflects observed stimulatory and inhibitory binding

behavior seen in our dose-response data.

LIGAND BINDING SITE NUMBER AND POTENTIAL LOCATIONS

GLUT1 three-dimensional structure has been modeled using the crystal structure

of GlpT (an E. Coli MFS protein) as an homology template and human glucose-6-

phosphate translocase as an "evolutionary template" to correct for missing residue assignments in the homology-based analysis (*5*). The resulting structure has been docked with a variety of GLUT1 ligands (cytochalasin B, forskolin, glucose, galactose, mannose, quecertin and phloretin) to reveal potential substrate binding sites *(5, 112)*.

Salas-Burgos et al. suggest that GLUT1 presents two binding sites (exofacial and endofacial) for forskolin, phloretin and glucose but only one endofacial site for cytochalasin B. (*5*)An exofacial phloretin and glucose binding site is consistent with the observed competition between substrate and phloretin during sugar uptake. However, forskolin is a noncompetitive inhibitor of sugar uptake (see here and (*107*)), hence the red cell sugar import site and the putative exofacial site are not functionally analogous because docking analysis predicts that glucose and forskolin compete for binding. Forskolin is proposed to make H-bond acceptor contacts with the GLUT1 endofacial site via hydroxyl or carbonyl groups at forskolin positions 6, 9 and 11. Contrary to this suggestion, elimination of the hydroxyl group at position 9 is observed to enhance the affinity of ligand binding but also increases homo-negative-cooperativity (γ) by 130-fold. Deviations between experimental and modeled behavior are not unexpected. A recent study demonstrates that the use of homology-based threading to model LacY and GlpT structures results in the correct overall transporter architecture but incorrect alignment of key residues within active sites (*192*).

CB is proposed to dock with GLUT1 at a single site comprising portions of GLUT1 cytoplasmic loops 2, 6 and 10 (*5*). The available experiment data suggest that CB interacts with GLUT1 transmembrane helices 10 and 11 and loop 10 *(13, 116, 163)*.

Photo activation of CB complexed with loop 2 of one subunit could react covalently with loop 10 of the same subunit or with loop 10 of an adjacent subunit provided that loops 2 and 10 approach within approximately 1.6 nm. The lone hydroxyl group on the CB macrocycle is postulated to form a hydrogen bond with the backbone carbonyl of leucine 85 (5). This is consistent with our observation that macrocycle shortening or dehydration of the macrocycle OH results in a significant loss of binding affinity. Reduced binding affinity may cause the ligand to extend its molecular envelope into the cytochalasin binding pocket of an adjacent subunit thereby inhibiting ligand binding at the second site (negative cooperativity; Figure 3.5 A-B)

Figure 3.5 Model of Cooperative Inhibition Interactions.

Panel A shows a GLUT1 tetramer (see (*11*)) viewed from the interstitium. Two subunits (blue) are shown in the e2 conformation each presenting an import site and two subunits (a and b) are shown in the e1 conformation (their sugar binding sites are not visible because they are exposed to the cytoplasm). Panel B shows the e1 subunits a and b viewed normal to the bilayer and each sectioned directly through its catalytic center. According to Salas-Burgos et al (*5*), the cytochalasin binding site is located close to TM3. These subunits are oriented such that TM 3 on subunit a faces TM3 on subunit b (subunit b is rotated 180º relative to subunit a about the central axis of the tetramer). If the molecular envelope of cytochalasin bound to subunit a overlaps with that of cytochalasin bound to subunit b, this could account for strong negative cooperativity as observed, for example, with CA. Holman and Rees (*13*) suggest that the CB binding site lies closer to TMs 10 and 11 which would require that the opposite half of each GLUT1 molecule (TMs 9 and 12 most likely) form the oligomerization interface. Panel C hypothesizes that ligand interaction with subunit a promotes a conformational change in both subunits which, in this instance enhances the affinity of subunit b for ligand.

Fig 3.5
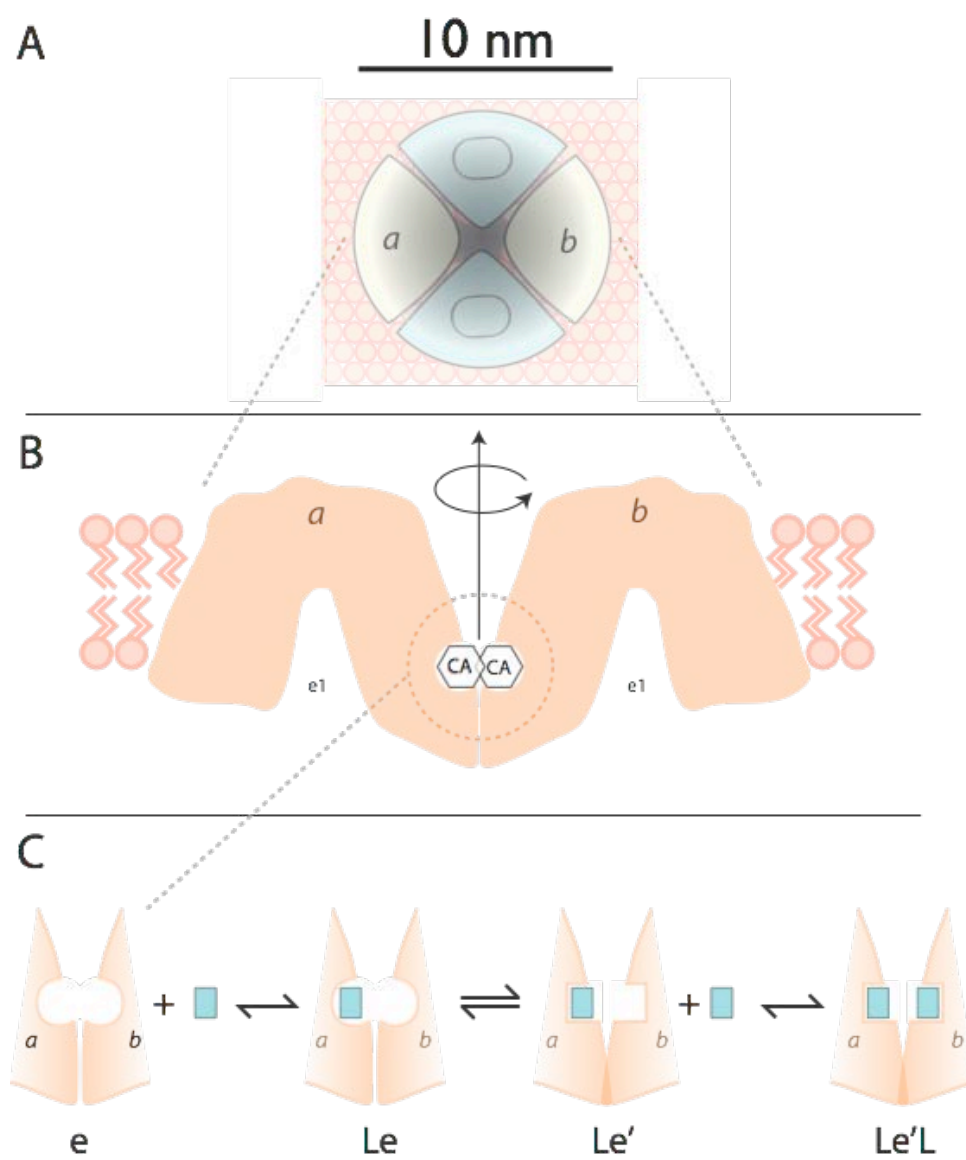
CHAPTER IV

MUTAGENIC AND CHIMERIC ANALYSIS OF LIGAND BINDING DETERMINANTS AT THE GLUT1 ENDOFACIAL BINDING SITE

This work will be submitted as a manuscript in December of 2008.

ABSTRACT

Cytochalasin B (CB) inhibits GLUT1 substrate transport by binding at or near the endofacial sugar binding site. N-bromosuccinamide analysis combined with ^{3}H-CB photolabeling implicates the region between Trp388 and Trp412 in ligand binding (*13*). Although the GLUT1 structure has been modeled(*5*), the specific residues comprising the sugar binding site are unknown. Constructs of mutant, exofacially myc tagged GLUT1 were expressed in HEK293 cells to test residues for effective CB inhibition of 2 deoxy glucose uptake (2-DG). A series of alanine point mutants were made at residues implicated by docking studies to be involved in cytochalasin B binding: Ser80, Arg400, and a double mutant Phe88,Arg92 (*5*). In addition, alanine substitutions were made at the proposed CB photolabeling site Trp412 (*117*), and at sites where missense GLUT1 DS point mutants are observed - Arg126 and Cys421 (*44, 193*). Expression was verified by Western blot and surface localization by immunofluorescence.   Phe88, Arg92 and Trp412 alanine mutants only weakly expressed, while Ser80 does not express at the membrane. The ranking of 2-DG uptake by construct is GLUT1Arg126Ala > GLUT1Arg200Ala > GLUT1Cys421Ala as compared to myc tagged GLUT1 expressed in HEK cells. CB inhibition of 2-DG uptake by GLUT1Arg126Ala and GLUT1Cys421Ala is significantly different (α=0.05) to inhibition of myc tagged GLUT1 mediated sugar uptake. GLUTArg400Ala also shows a moderate decrease in affinity for CB, suggesting its involvement in CB binding. In addition, GLUT1 chimeras were made by exchanging the sequence Trp388-Trp412 with the corresponding region of either

GLUT4 or GLUT5. GLUT5 shows very low affinity for CB. GLUT1/GLUT4$_{388-412}$/GLUT1 is a point mutation (Ile404Met) which shows statistically reduced sensitivity to CB inhibition. The GLUT1/GLUT5$_{388-412}$/GLUT1 chimera shows enhanced 2-DG uptake at 50nM CB but normal inhibition by higher concentrations of CB. We conclude that point mutants in this region are insufficient to abrogate CB binding, that the Trp388 to Trp412 sequence is necessary for CB photolabeling and binding affinity, but is not the major determinant of high affinity inhibition of 2 deoxyglucose uptake by CB.

INTRODUCTION

The structural mechanisms of integral membrane protein mediated nutrient transport are unknown. Two superfamilies of nutrient transport proteins or carriers mediate cellular import and export of metabolites: the ATP Binding Cassette (ABC) superfamily comprised of primary active carriers, and the Major Facilitator Superfamily (MFS) containing primary and secondary active, single-polypeptide, integral membrane carriers. The oldest and largest subfamily of the MFS is the sugar porter family. To date thirteen hexose transporters (GLUT1-12, HMIT) have been characterized in humans, each of which exhibits its own tissue distribution and unique catalytic properties. These thirteen porters may be further subdivided by sequence similarity into three groups. Group 1 (1-4) transporters primarily mediate glucose flux, were the first sugar porters discovered, and are the best characterized to date. GLUT2 expressed in liver, pancreas, and the intestine transports glucose with low affinity, while GLUT1 expressed in erythrocytes, endothelial and smooth muscle cells, GLUT3 expressed in neurons and GLUT4 expressed in adipocytes and skeletal muscle cells transport glucose with high affinity. Group 1 transporters are inhibited by phloretin, forskolin, and cytochalasin B. Since carcinomas typically up regulate GLUT1 and glycolysis, chemical inhibition of carrier-mediated sugar may be instrumental in starving tumorigenic masses.

Group 2 GLUTs (5,7,9,11) and Group 3 GLUTs (6,8,10,12,HMIT) are less well studied. Group 2 porters primarily transport fructose. GLUT5 and GLUT7 are expressed in the intestine, and GLUT9 and GLUT11 are expressed in the kidney, liver, heart, and

pancreas. Group 3 porters have an enlarged exofacial loop between transmembrane helices 10 and 11 and transport glucose or fructose. The exception is HMIT, a neuronal H+/myo inositol symporter highly expressed in the brain. Neither Group 2 nor Group 3 sugar porters are inhibited by cytochalasin B. This inhibitor is hypothesized to compete for sugar efflux by binding at the endofacial (e1) sugar binding site of the Group 1 primary glucose transporters.

Human GLUT1 has been extensively characterized; it comprises twelve transmembrane-spanning alpha helices (TMs)(*73*), is heterogeneously glycosylated at N-45 (*40*), presents both N- and C- termini to the cytosol, and TMs 6 and 7 are linked by a large intracellular loop. Each GLUT1 molecule is a functional sugar uniporter(*85*), and is thought to present only one sugar binding site, endofacial or exofacial, at any point in time (*7, 16*). GLUT1 self-associates in lipid bilayers as dimers or tetramers (*65, 87*). Kinetic analyses have suggested that the functional arrangement of subunits provides an obligate, antiparallel arrangement of binding sites such that the GLUT1 tetramer presents two endofacial and two exofacial binding sites at all times(*98, 158*). *Salas-Burgos et al* threaded the GLUT1 sequence through the GlpT folding scaffold providing a convenient model for hypothesis testing (*5*). Docking analysis of this structure and cytochalasin B (CB) suggests that CB binds near the edge of the endofacial sugar binding vestibule. Moreover, CB can photo-crosslink specifically to GLUT1 under UV light. Holman and Rees used n-bromosuccinamide proteolysis in combination with radiolabeled CB and peptide mapping to determine the smallest fragment of GLUT1 bound to CB. This fragment is between W387 and W412 of GLUT1, in TM's 10 and 11 (*13*). Mutation of

tryptophan residues flanking the CB-labeled peptide abrogates CB photolabeling (*117, 122*).

CB competes for glucose efflux and may directly interact with the e1 sugar binding site (*180, 194*). Point mutations in GLUT1 result in a heritable heterozygous disease known as GLUT1 deficiency syndrome (GLUT1DS), characterized by growth defects, mental retardation, and epileptic-like seizures (*19*). A few clinical cases of GLUT1DS present with reduced sensitivity to CB inhibition, readily testable via erythrocyte uptake of radiotracer glucose (*42, 44*). Some of these point mutants, such as C421(*195*) or R126(*193*), may be within the e1 binding site. Systematic exploration of these sequences may target domains important in endofacial sugar binding.

GLUT5 shares approximately 50% sequence similarity with GLUT1 (*2, 196*) and is proposed to resemble GLUT1 in its helical packing arrangement. Although transport of high fructose concentrations ($\geq$1mM) in GLUT5-expressing oocytes is not inhibited by CB (*197, 198*), GLUT5-mediated transport of low concentrations (~100μM) of radiolabeled glucose (*199*) or fructose (this work) is inhibited by CB but with greatly increased $KI_{(App)}$. This suggests a strategy for isolating determinants of CB binding to Group 1 transporters – the construction of Group 1 – Group 2 chimeras. *Inukai et al* expressed chimeras of GLUT1 and GLUT5 in *X. laevis* oocytes, and found the second half of GLUT1 (i.e. TM's 7-12) is crucial to glucose transport and CB photolabeling (*200*).

The aim of this work is to further deduce the location of the e1 binding site in GLUT1 by analysis of GLUT1 mutant sensitivity to inhibition by CB. To this end we

express point mutants and W388-W412 chimeras in HEK293 cells, and determine CB's

ability to inhibit 2-deoxyglucose uptake.

MATERIALS & METHODS

REAGENTS

Unless otherwise stated, all tissue culture medium and reagents, including Dubelco's Modified Eagle Medium (DMEM) ± glucose, trypsin, and 1X sterile PBS, were purchased from Gibco. Tissue culture dishes obtained from Nunc. Fetal Bovine Serum was obtained from Hyclone. Lipofectamine and Herculase were purchased from Invitrogen. PCR primers were ordered from Integrated DNA Technologies (IDT), and restriction endonucleases, phosphorylases, and ligases purchased from New England Biolabs (NEB). ^{3}H 2 deoxy glucose (^{3}H 2-DG), Cytochalasin B and all other salts and nonradioactive reagents were purchased from the Sigma Chemical Company. Vectashield^{TM} immunofluorescence mounting agent was purchased from Vector Labs. BioMol C-myc primary antibody was purchased from BioMol, and secondary antibodies goat anti rabbit HRP, and goat anti mouse HRP from BioRad, while secondary goat-anti-mouse FITC was from Caltag Laboratories. Protease Inhibitor Cocktail tablets (-EDTA) were obtained from Roche. Competent cells used were either XL-1 Blue Supercompetent Cells from Stratagene, or lab-grown strains of DH5α treated with the Zymo Z-Competent Cells kit.

SOLUTIONS

Unless stated otherwise, all buffers used were GIBCO sterile phosphate buffered saline supplemented with 5mM $MgCl_2$ pH 7.4 (PBS).

³H 2DG Uptake Radioactive uptake solution is 100 μM 2-deoxy glucose supplemented with ³H 2-DG in PBS, or 100μM fructose supplemented with C¹⁴ labeled fructose. Radiolabel was typically added to 2 μCi/mL uptake. 'Stop' medium is 100 μM CB and 100μM phloretin in PBS. Assays in which increasing doses of CB were added to the uptake medium also included an identical concentration of cytochalasin in both the pre-uptake and radiolabeled uptake solution. CB solutions were all diluted from a parental stock solution containing a maximum of 10% DMSO or ethanol; dose solutions were normalized to contain 0.1% ethanol or DMSO. Triton lysis solution contains PBS + 5mM $MgCl_2$ pH 7.4 treated with 0.5% Triton and 10X Roche Protease Inhibitor Cocktail.

Immunofluorescence Solutions A stock solution of 5% gelatin in PBS was made, and diluted into PBS for 1% block solution, or diluted to 0.5% and mixed with 1:350 BioMol C-Myc Antibody or 1:900 Caltag Goat Anti-Rabbit antibody. 4% paraformaldehyde made in PBS.

HEK Cell Maintenance

HEK-293 cell stocks were grown using 10cm Nunc tissue culture dishes. Medium was GIBCO High Glucose DMEM, supplemented with 10% fetal bovine serum and 1x GIBCO penicillin/streptomycin. (D10) Cell confluence before splitting was visually judged using a light microscope; cells were considered 50% confluent when the area covered by cells was equal to that yet uncolonized. 90% confluent stock plates were typically split using a 1 minute incubation with Trypsin 1X (GIBCO), followed by aspiration. The dishes were gently knocked against each other, after which the cells were easily washed free with D10.   Cells were separated by resuspension using a 200μL

plastic tip placed over a 10 mL sterile pipet; the media was pipetted up and down a minimum of three times against the tissue culture dish to dislodge and separate cells. Stock plates were typically split 1:5 mother: daughter, and would usually grow to 90% confluence within five days. After passage 22, cells were discarded and stock parental cells would be thawed.

HEK CELL FREEZING

Low passage number (<5) cells were split as above and grown to almost 100% confluence, typically in units of 10 plates. These cells were trypsinized, suspended in media, pelleted in a 4ºC centrifuge, and resuspended in antibiotic free media supplemented with 10% DMSO to a volume of 1mL/10cm dish. 500 µL were aliquoted into cryo-vials and stored in liquid nitrogen.

HEK CELL TRANSFECTION

Hemocytometer counted HEK cells were seeded at a density of one million cells per well of a 12 well Nunc tissue culture multi-dish (approximately 2.9 x 105 cells/cm3) and grown overnight at 37ºC (up to 16 hrs) to 70-80% confluence. HEK cells were transiently transfected using Invitrogen's Lipofectamine 2000 reagent in accordance with the package directions. Briefly, 1.6 µg of DNA was diluted in 100 µL serum-free tissue culture media, and 4 µL of Lipofectamine was diluted into an equal volume of media. After five minutes at 21ºC, these working reagents were combined and incubated for a minimum of 30 minutes at ambient temperature. During the reagent incubation, the media covering the cells was changed from D10 to 37ºC High Glucose DMEM with 10% Fetal Bovine Serum lacking antibiotic. After the media change, 200 µL of working

reagent were gently pipetted into each well. The transfected cells were grown for a further 36-48 hours before being used for experiments, expression timeframe initially determined by Western Blot with C-terminal GluT1 Ab. (Fig 4.3)

WESTERN BLOTTING

Western Blot analyses were made using c-myc primary mouse antibody (1:700) or GLUT1 c-terminal rabbit antibody (1:5000) as described here (*66*).

IMMUNOFLUORESCENCE FOR SURFACE EXPRESSION VERIFICATION

Unless stated differently, all incubations were at room temperature (22ºC). Round glass cover slips were sterilized by washing with neat ethanol followed by irradiation under UV light for 10 minutes, cover slips were then placed one/well in a Nunc 6 well dish. HEK cells were seeded at a density of $1x10^6$ cells per well, and transfected with 4.0 µg of DNA and 10µL of Lipofectamine. After 36-48 hours post transfection, plates were washed with PBS, covered with fresh 4% paraformaldehyde, and incubated on a rocker for 20 minutes. Wells designated to have permeable cells were rinsed with PBS once and covered with 0.5% Triton for 5 minutes with agitation. Plates were washed at least 3X w/ PBS, and blocked for 30 minutes using 1% gelatin. Cells were then covered with BioMol C-myc primary antibody SA-294, at 1:350 dilution in 0.5% gelatin, incubated for 1 hour, then rinsed 4x5min with PBS. Cells were covered with goat anti-mouse antibody (1:900) in 0.5% gelatin, wrapped in aluminum foil, incubated for an hour, then rinsed in a darkened room 8x5min with PBS on a rocker. Cover slips were lightly aspirated and wet-mounted on glass slides using 20µL Vectashield and clear nail polish in a darkened

room. Cells were imaged with bright field and the FITC/GFP filter (492 nm) using a

Zeiss Axioskop 2 upright microscope.

E1 LIGAND-INHIBITED ^{3}H 2-DG TRANSPORT

Cells were seeded and transfected as described above. 24 hr post-transfection,

10µL/mL Geneticin was added to all wells. 40-48 hr post transfection, the medium was

changed to medium lacking glucose and fetal bovine serum. Cells were starved of

glucose and serum for a minimum of two hours prior to uptake, rinsed twice with 37ºC

PBS, and incubated in PBS ± CB for a minimum of 15 minutes at 37ºC. PBS was

aspirated and 400 µL of uptake solution was added to the dish. After 6 minutes of

incubation, the uptake solution was aspirated and the cells were rinsed twice with 1 mL

of ice cold stop solution. Zero-uptake was measured by adding stop solution prior to

radiolabeled uptake solution. After the second stop rinse, 500 µL of Triton lysis solution

was added to the wells which were then incubated at 37ºC for 30 minutes to ensure

complete cell lysis. Lysed cells were subjected to centrifugation for 5 minutes at 4ºC at

13,000 rpm. Aliquots (200 µL each) of supernatant were placed into duplicate vials,

suspended in scintillation fluid, and counted. Small (10 µL) aliquots of supernatant were

retained in duplicate and assayed for protein concentration using a Pierce BCA assay in a

96 well plate.

Sugar uptake was calculated as: $CMTP = \dfrac{(AvgCounts)(WellFraction)}{Totalprotein} * (\frac{RCP}{mol})$

CMTP is Counts Per Mol Total Protein, which were converted into units of moles of sugar per μg protein. AvgCounts are the average of duplicate samples for each well; well fraction is 500μL/200μL, RCP/Mol is radioactive mol ^{3}H 2-DG per μL times DPM/μL of solution, and total protein is the BCA estimated total protein content of the well.

RATIONALE FOR AND CONSTRUCTION OF MUTANT GLUT1

All point mutants were changed to alanine, and made in a GLUT1 containing the Myc epitope (EQLISEEDL) in the exofacial loop between residues 55 and 56, to verify surface expression. (The c-myc insertion primer 'CGCTATGGGGAGAGCATC *GAGCAAAAGCTTATTTCTGAAGAGGACTTG* CTGCCCACCACGCTCACC' and its complement were ordered. The insertion is italicized.) Primers were constructed such that point mutants were inserted via mismatched base pairs (Table 4.1). The entire plasmid was replicated by high-fidelity PCR (Herculase), and the product digested with Dpn1. The PCR product was

Table 4.1 Point Mutagenesis Primers

Primers	%gc	#GC	Bases	Sequence
S80A	64.5	20	31.0	GGGGGCATGATTGGC*TCC*TTCTCTGTGGGCC
Mutated :				GGGGGCATGATTGGC*GCC*TTCTCTGTGGGCC
F88A,R92A	52.4	22	42.0	CTCTGTGGGCCTTTTCGTT*AAC*CGCTTTGGC*CGG* CGGAATTC
Mutated :				CTCTGTGGGCCTTTTCGTT*GCC*CGCTTTGGC*GCG* CGGAATTC
W412A	48.7	19	39.0	GCAGGCTTCTCCAAC*TGG*ACCTCAAATTTCATTGTGGGC
Mutated :				GCAGGCTTCTCCAAC*GCG*ACCTCAAATTTCATTGTGGGC
C421A	52.6	20	38.0	GTGGGCATG*TGC*TTCCAGTATGTGGAGCAACTGTGTGG
Mutated :				GTGGGCATG*GCC*TTCCAGTATGTGGAGCAACTGTGTGG
R126A	54.1	20	37.0	GCTGATCCTGGGC*CGC*TTCATCATCGGTGTGTACTGC
Mutated :				GCTGATCCTGGGC*GCC*TTCATCATCGGTGTGTACTGC
R400A	71.9	23	32.0	CAGCCAGGGTCCA*CGT*CCAGCTGCCATTGCCG
Mutated :				CAGCCAGGGTCCA*GCC*CCAGC*C*GCCATTGCCG
GLUT141 (I404M)	66.7	20	30.0	CCACGTCCAGCTGCC*ATC*GCCGTTGCAGGC
Mutated :				CCACGTCCAGCTGCC*ATG*GCCGTTGCAGGC

[a] For R400A, a G was switched to a C as a silent mutation to reduce primer

hairpin formation.

Table 4.2 Horn Mutagenesis Primers

'Horn' Primer	Sequence
GLUT1/ GLUT5$_{388-412}$/ GLUT1 Forward	*CGGCCATCTGCCTTCATGGTGGGGGGGCAGTGTGCACT* GGACCTCAAATTTCATTGTGGGC
GLUT1/ GLUT5$_{388-412}$/ GLUT1 Reverse	*AGAGGACTGCAGGAAGATCTCAGTGATGAGCAGCGC* TGGGATGGGGCCAGGACCC

Italicized fragments are the 5' extensions corresponding to the GLUT5 insertion

sequence.

Figure 4.1. GLUT1 structural schematic to illustrate mutant loci.

Structural features of GLUT1 depicted include: the exofacial loop between the first and second transmembrane (TM) domains has an n-linked glycosylation site, while the large loop between TM6 and 7 and the and N and C termini are located within the cytosol. A.) GLUT1 point mutations analyzed. Squares indicate mutations implicated in clinical disease, with Arg126 in TM 4 and Cys421 in TM 11. The hexagon is Trp412, which when mutated decreases CB photolabeling. The circles are residues mapped by *Salas-Burgos et al* to bind CB: Phe88, Arg92 in the TM3-4 endofacial loop, and Arg400 on TM11 (*5*). B.) GLUT1 chimeras. The light gray region is Trp388-Trp412, the smallest fragment of GLUT1 found photo-crosslinked to CB after N-Bromosuccinamide digestion, and the portion of GLUT1 substituted with GLUT5 for the GLUT1/GLUT5$_{388-412}$/GLUT1 chimera. The gray circle is GLUT1$_{Ile404Met}$, the only amino acid difference between GLUT1 and GLUT4 in this highly conserved region.

Fig 4.1
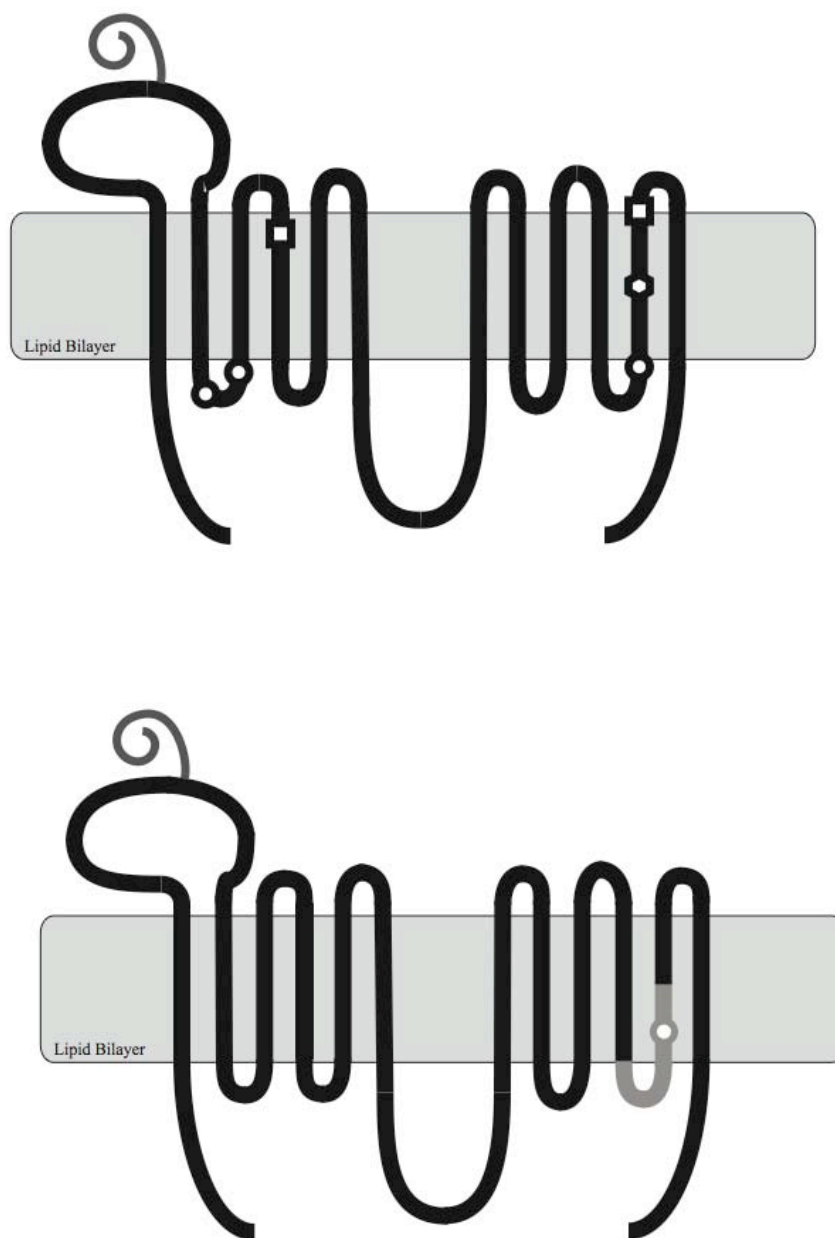
Figure 4.2. Sequence Alignment of GLUT1 and GLUT5, as prepared by Genious.

Green 'similarity' bars indicate identical amino acids. Each transmembrane domain has been boxed for ease of reference. The 388-412 region crucial to CB photolabeling has been highlighted in red.
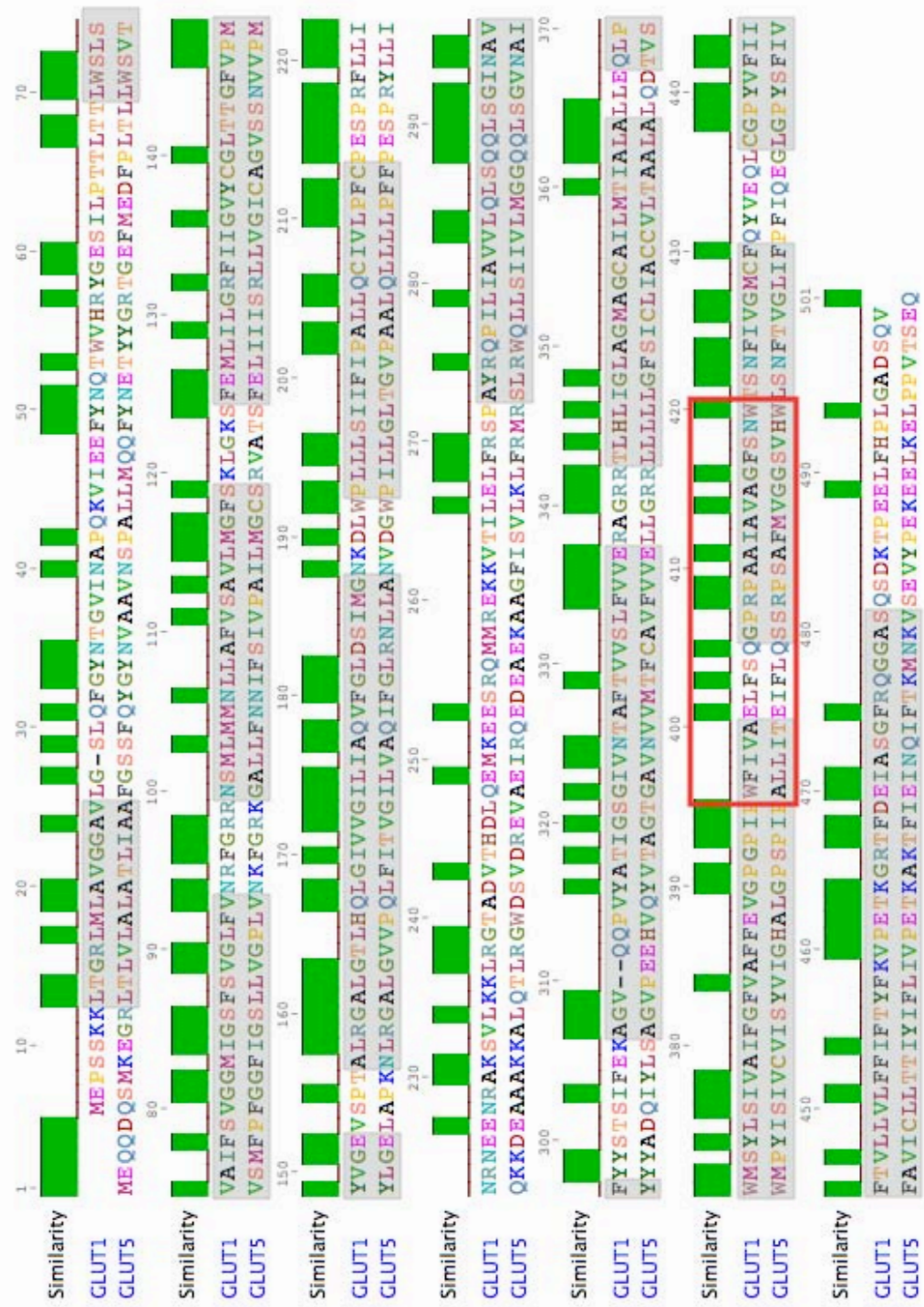
Fig 4.2

then transformed into Stratagene XL1Blue Supercompetent cells or Z-Competent cells, and amplified using plasmid extraction via Qiagen kits. The insert was verified by sequencing and placed in fresh Invitrogen pcDNA 3.1+ expression plasmid via restriction digest.

One endofacial photolabeling mutant (W412) and two exofacial (R126 and C421) point mutants that present as clinical GLUT1DS with altered CB affinity were chosen. *Salas-Burgos et al* mapped the GLUT1 sequence onto the GlpT scaffold and docked forskolin and cytochalasin B to GLUT1; S80, R400, N88&R92 were chosen from the residues that interacted at the presumed e1 interface (*5*) (Fig 4.1A).

Two chimeras were constructed for the GLUT1 region between W387 and W412 – GLUT1/GLUT4$_{388-412}$/GLUT1 and GLUT1/GLUT5$_{388-412}$/GLUT1 (Fig 4.1B). Since this region is highly conserved between GLUT1 and GLUT4, only Ile404 had to be changed to Met to produce a chimera, via the point mutation. For construction of the GLUT1/GLUT5$_{388-412}$/GLUT1 chimera we utilized 'Around the Horn' PCR. Briefly, primers were made that matched twenty-five base pairs of GLUT1 adjacent to the region of interest, with 5'extensions that matched thirty-six base pairs (half) of the desired GLUT5 sequence. These primers were phosporylated using T4 phosphorylase kinase (PNK) in T4 ligation buffer, then used with high-fidelity PCR polymerase (Herculase) to produce a linear fragment. This fragment was then circularized by T4 DNA ligase and the ligation product used to transform Z-Competent treated cells. Insertion was verified by sequencing.

RESULTS

GLUT1 Mutant Constructs

Ten constructs were made from an untagged GLUT1 sequence in Invitrogen's pcDNA3.0+ vector background. The first construct engineered was the insertion of a myc epitope sequence (EQULISEEDL) into the TM1-TM2 exofacial loop of GLUT1. After sequence validation, all subsequent constructs were made from this Myc-GLUT1 plasmid. Seven point mutants were made using mismatched primers, and one chimera engineered from 'around the Horn' PCR. A tenth construct, GLUT1-Myc-HAHis was made by inserting the myc epitope into a GLUT1 C-terminal HA-His background. All constructs displayed at least minimal overexpression of GLUT1 in HEK 293 cells at 36 hrs post transfection. To analyze mutant protein sensitivity to CB inhibition, three criteria must first be met: protein expression by Western blot, surface expression by immunofluorescence, and successful sugar transport to verify function.

GLUT1 Expression in HEK cells

IMMUNODETECTION OF OVEREXPRESSED GLUT1

C terminal antibody immunoblot analysis of transporter expression in HEK membranes indicates successful overexpression of GLUT1 and various mutants. We detect the presence of a 50-55 kDa C-terminal Ab reactive protein in the WT, GLUT1-Myc, GLUT1-Myc-HaHis dual tagged, R400A, and C421A lanes, as opposed to the untransfected lane (Fig 4.3). R126A shows intermediate expression by immunoblot

Fig 4.3
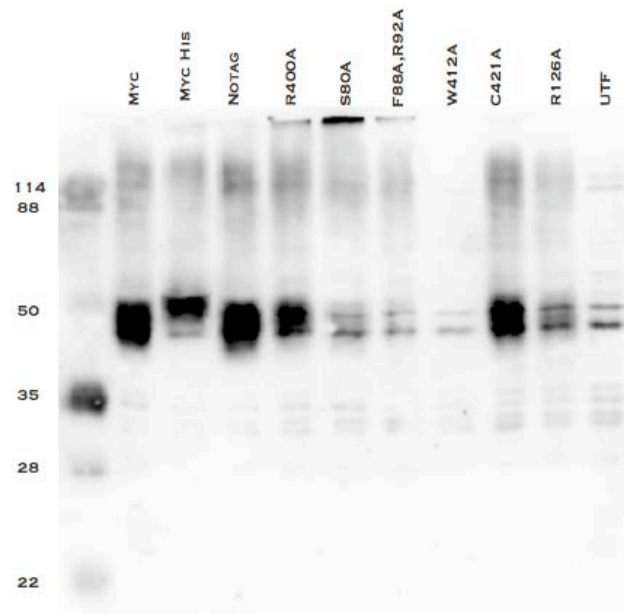
Figure 4.3 HEK293 C-AB Immunoblot Expression of GLUT1.

Western blot using GLUT1 carboxyl-terminal antibodies (C-Ab) of GLUT1 expressed in

HEK293 cells. Membranes were isolated by differential centrifugation, resolved by 10%

SDS-PAGE, and transferred to nitrocellulose for Western blotting. Each lane contains 2

μg of total membrane protein. Strongest protein expression by construct proceeds as

follows: WT (NoTag) GLUT1 > GLUT1-Myc ≥ C421A > R400 > Dual Tagged GLUT1

Myc+His > R126 > S80A ≥ F88A, R92A ≥ W412A ≥ UTF.

Figure 4.4 Expression of c-myc GLUT1 in HEK293 cells..

Cells were transfected at 24 hours after splitting, and visualized 36-48 hours after transfection. Cells were fixed with 4% paraformaldehyde, treated with $\pm$ 0.5% Triton, visualized with mouse anti-Myc and goat anti-mouse FITC conjugate antibody, and wet mounted with Vectashield. Pictures taken at room temperature, 492 nm setting, on a Zeiss Axioskop microscope. Surface untransfected (UTF) and untagged cells were indistinguishable from background fluorescence. Top row: Triton treated, untagged GLUT1 and UTF cells. For the second row and all following rows, surface fluorescence is on the left, with Triton treated, permeable membranes on the right. Second row, C-myc GLUT1. Third row, S80A GLUT1. Note aggregate formation. Fourth row, R126A GLUT1. Fifth row, R400A GLUT1. Bottom row, C421A GLUT1.

Fig 4.4
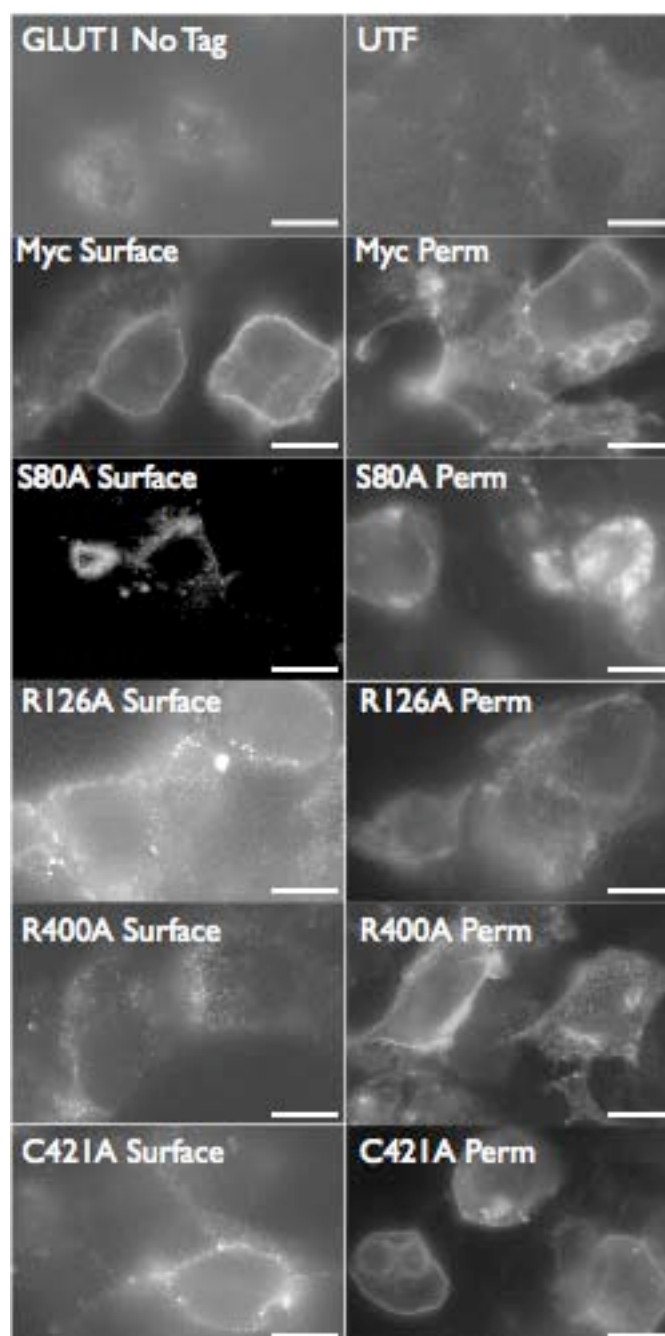
compared to WT GLUT1 and untransfected. However, expression of S80A, W412A, and F88A, R92A constructs was comparable to untransfected, with S80A showing high molecular weight aggregates (Fig. 4.3). The amount of immunoreactive protein in the WT construct-transfected HEK293 cells is comparable to that seen previously in this laboratory (*66*). This indicates strong overexpression of GLUT1-Myc, GLUT1-Myc-His, R400A, and C421A.

IMMUNOFLUORESCENCE

Anti-Myc Ab FITC-Immunofluorescence in HEK cells of non-permeabilized (-Triton X100) Myc-GLUT1-transfected HEK cells shows cell surface Myc-GLUT1 expression (Fig 4.4). Untransfected cells ± Triton treatment show fluorescence indistinguishable from background. WT GLUT1 (-Myc) transfected cells display equal fluorescence to untransfected cellls; non-permeablized cells show fluorescence indistinguishable from background. For F88A-R92A, and W412A constructs, fluorescence is indistinguishable from fixed, non-permeablized untransfected cells. S80A protein, however, displays low surface expression and appears concentrated in vesicular aggregates. R126A, R400A, and C421A mutants show surface expression as well as internal expression in HEK293 cells comparable to myc-tagged GLUT1. Therefore, we conclude that the R126A, R400A, and C421A mutants are expressed and successfully traffic to the plasma membrane.

Mutant Function Verified by ^{3}H 2 deoxy Glucose Uptake Into HEK Cells

Functional mutant protein is characterized by successful 2 deoxy glucose (2-DG)

Figure 4.5. 100μM ^{3}H 2-DG Uptake by Mutant GLUT1 into HEK293 cells.

Ordinate: Rate of 2 DG uptake expressed as a percentage of the GLUT1-Myc protein

uptake rate. Abscissa lists uptake by vector, with GLUT1/GLUT4$_{W388-W412}$/GLUT1

represented as GLUT1/4/1, and GLUT1/GLUT5$_{W388-W412}$/GLUT1 represented as

GLUT1/5/1. Uptake experiments were performed as follows: cells were seeded at

10^6/well, transfected in quadruplicate after 24 hours, and assayed 48 hours after

transfection. Briefly, cells were starved of glucose and serum for 2 hours, rinsed,

incubated for 6 minutes with 100μM ^{3}H supplemented 2-DG at 37ºC, rinsed twice with 1

mL ice cold stop solution, coated with 500μL 0.5% Triton, and incubated for 30 min at

37ºC to facilitate lysis. Zero time points had stop solution added before radiolabel.

Lysed cells were centrifuged, placed in 200μL duplicate aliquots in scintillation vials and

counted, with 10μL aliquots tested for total protein well content. Total uptake was

normalized to each day's mean c-myc tagged GLUT1 uptake. Each point represents a

mean of three experiments, n=4. Error bars were the standard deviation of the mean

divided by the number of wells, then normalized to GLUT1 Myc uptake.

Fig 4.5

uptake. 2-DG is a sugar transported by GLUT1 into the cell and then phosphorylated by

hexokinase to form 2-deoxy glucose 6-phosphate. In the absence of significant

intracellular glucose-6-phosphatase activity, the phosphorylated sugar is trapped in the

cytosol. Neither of the GLUT1 binding sites tolerate large, polar substitutions at carbon 6

(*6, 111*) thus the phosphorylated sugar is trapped in the cell and does not interfere with

sugar transport.. 2-DG therefore provides a convenient measure of sugar uptake at

physiologic temperature and is useful in characterizing successful function of mutant

GLUT1.

Fig 4.5 shows uptake catalyzed by point mutant GLUT1 as a percentage of uptake

of 2 DG catalyzed by each GLUT1 point mutant. Each mutant assay was made in

duplicate with n=4 transfected wells, and uptake was determined as a percentage of the

rate of myc tagged GLUT1 uptake assayed the same day. Constructs S80A, F88A-R92A,

and W412A when expressed in HEK cells show total uptake activity that is not

significantly different from that of untransfected cells. R400A, R126A, and C421A

mutant GLUT1 show a more intermediate phenotype, with the approximate ranking being

R126A>MYC> R400A>C421A.   Because K_{iApp} for 2-DG by native GLUT1 is 10mM

(*66*), uptake assays at 100µM 2-DG provide an estimate of the parameter V_{max}/K_m.

Uptake (V) may be described as $V = [2\text{-}DG]*(V_{max}/K_m)$ where V is the maximum rate of

2-DG uptake and K_m is that 2-DG concentration where $V = V_{max}/2$. It therefore follows

that $\pi = V_{max}/K_m = V/[2\text{-}DG]$. Our results indicate that constructs S80A, F88A-R92A,

and W412A display extremely low π values. Although the formal possibilities remain

that either K_m has increased, resulting in loss of affinity, or that hexokinase activity has

been inhibited, we conclude the reduced π values are most likely the result of a

diminished V_{max} due to decreased surface protein expression or other loss of transport

capacity.

Cytochalasin B Dose Response

An alteration in GLUT1 affinity for CB implies that a given mutation may affect the CB

binding site, and therefore pinpoint specific amino acids contributing to the endofacial

sugar binding site in the GLUT1 sequence. Therefore, CB inhibition of 2-DG uptake was

utilized to measure changes in protein-CB affinity. In the control experiment (Fig 4.6)

untransfected (UTF) cells show CB sensitive, non-GLUT1, protein mediated uptake with

an IC_{50} of 250 ± 60 nM. WT GLUT1 expressed in HEK 293 cells shows an $IC_{50} = 2.7 \pm$

0.5 µM for CB. To expedite mutant analysis, three concentrations (50nM, 500nM,

$$\frac{K_{IApp}}{K_{ICB}} = \frac{[CB]}{\left(\dfrac{(100\% - \text{Mutant\%}_{0CB})}{(100\% - \text{Mutant\%}_{XCB})} - 1 \right)}$$

5000nM) of CB were chosen to test our constructs for altered CB sensitivity. Construct

rates are compared in two ways after being expressed as a percentage of the GLUT1-

Myc uninhibited rate: first, by using a two-way ANOVA with a Bonferroni's post hoc

test for significance (Fig 4.7), and second by calculating a ratio of K_{iapp} for the

concentrations of CB tested. Ratio K_i's were calculated assuming complete inhibition at

5000nM CB, using the following equation and presented in Table 4.3.   Bonferroni

analysis facilitated comparison of data sets, with the values pertaining to Myc-GLUT1

Figure 4.6 HEK293-expressed WT GLUT1 and UTF 6 min uptake of 2DG (0 CCB) and CB dose response.

Ordinate, increasing [CB] in nM. Abscissa, the rate of 2 DG uptake per minute, measured over six minutes. The experiment was done as in Fig 4.5, with an additional 30 minute incubation ± each CB concentration after serum starving. GLUT1 (closed circles,●) IC_{50} for CB = 2.7 ± 0.5 µM. Untransfected cells (open circles,○) had an IC_{50} of 250 ± 60 nM Each point represents a mean of three experiments, n=4. Error bars were calculated as the standard deviation of the mean divided by the number of wells.

Fig 4.6
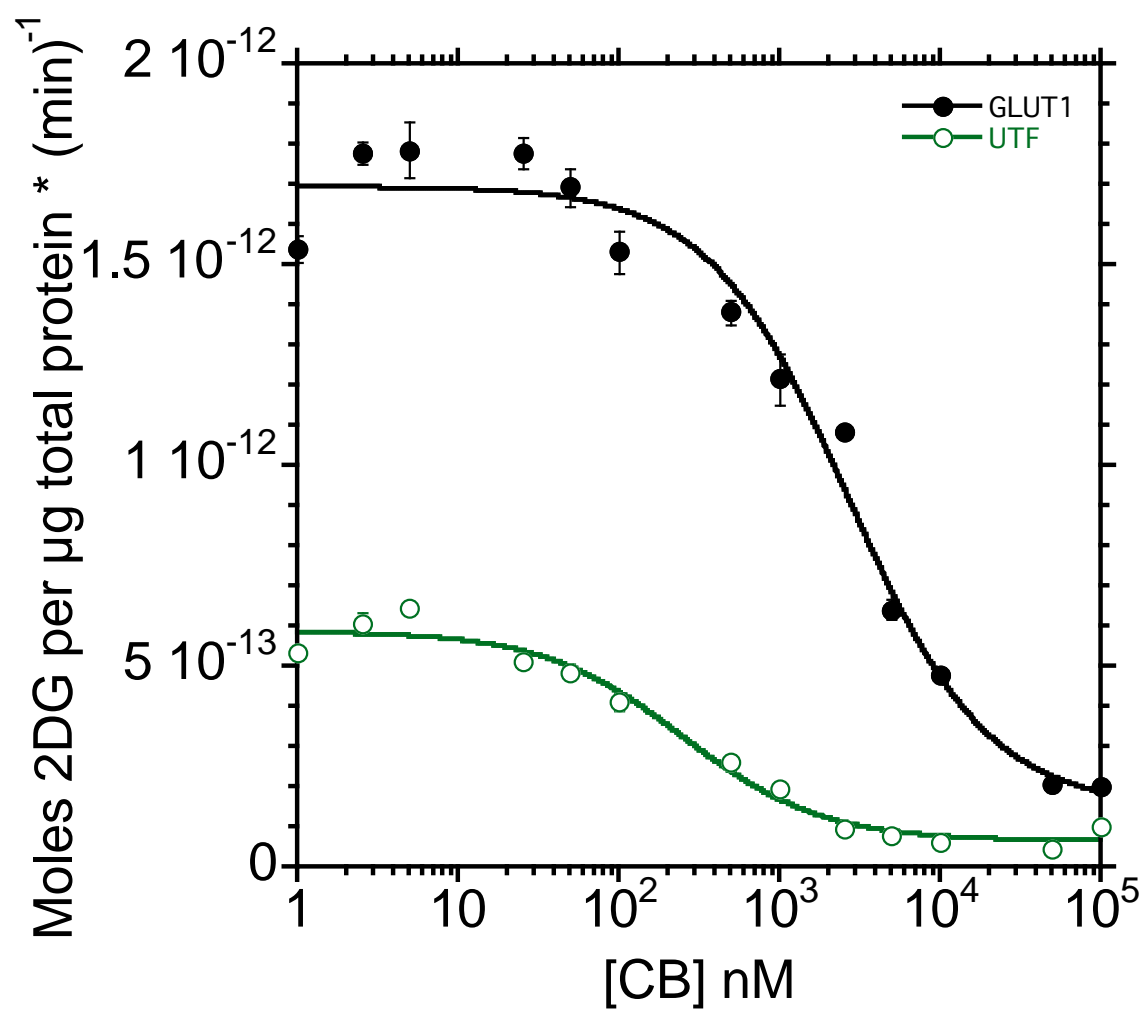
Figure 4.7 HEK-293 Mutant GLUT1 100 µM ^{3}H 2-DG Uptake sensitivity to 50, 500, and 5000 nM CB, normalized to GLUT1-Myc uptake rate.

Each point represents a mean of three experiments, n=4. Three concentration "dose responses" were carried out to characterize mutant GLUT1 sensitivity to CB. Experiments done as seen in Fig 4.6. Each value was normalized to the internal standard of that day's GLUT1-Myc uptake rate without CB. GLUT1/4/1 on the graph corresponds to GLUT1/GLUT4$_{388-412}$/GLUT1, or Ile404Met. GLUT1/5/1 on the graph corresponds to GLUT1/GLUT5$_{388-412}$/GLUT1. Statistical significance was assigned by Bonferroni analysis, with values significantly different from corresponding GLUT1-Myc CB concentrations starred. R126A uninhibited uptake is notable given weak expression by Western blot, and a modest stimulation of 2 DG transport by CB may be seen with the GLUT1/GLUT5$_{388-412}$/GLUT1 vector at 50 nM CB. Error bars were the standard deviation of the mean divided by the number of wells, then normalized to GLUT1 Myc uptake.

Fig 4.7
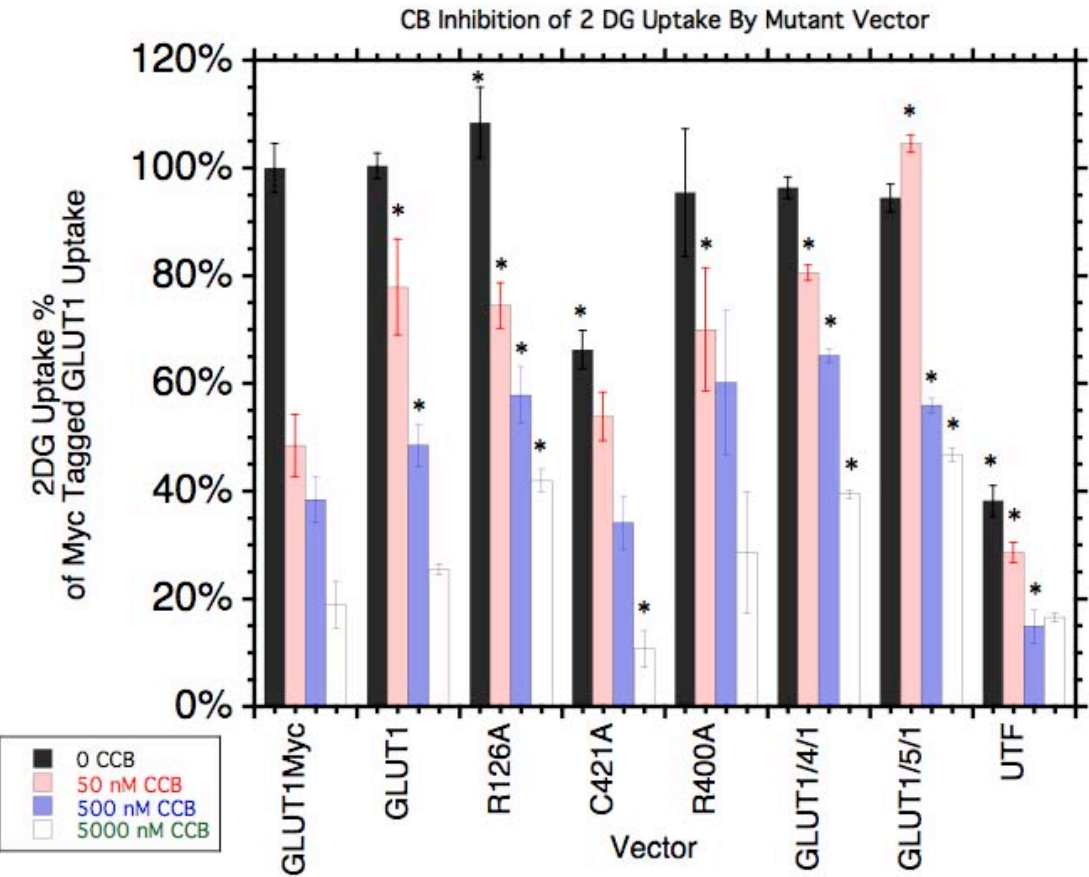
Figure 4.8 HEK-293 Mutant GLUT1 100 µM ^{3}H 2-DG Uptake sensitivity to 50, 500, and 5000 nM CB.

Ordinate: The rate of mutant uptake of 2 DG, expressed as a percentage of uninhibited uptake of that protein. Abscissa lists uptake by vector. Graph redrawn in this manner to further illustrate differences in CB inhibition by construct. Error bars were the standard deviation of the mean divided by the number of wells, then normalized to 0 CCB 6 minute uptake.

Fig 4.8

CB Inhibition of 2-DG Uptake By Vector, Normalized to 0 CB
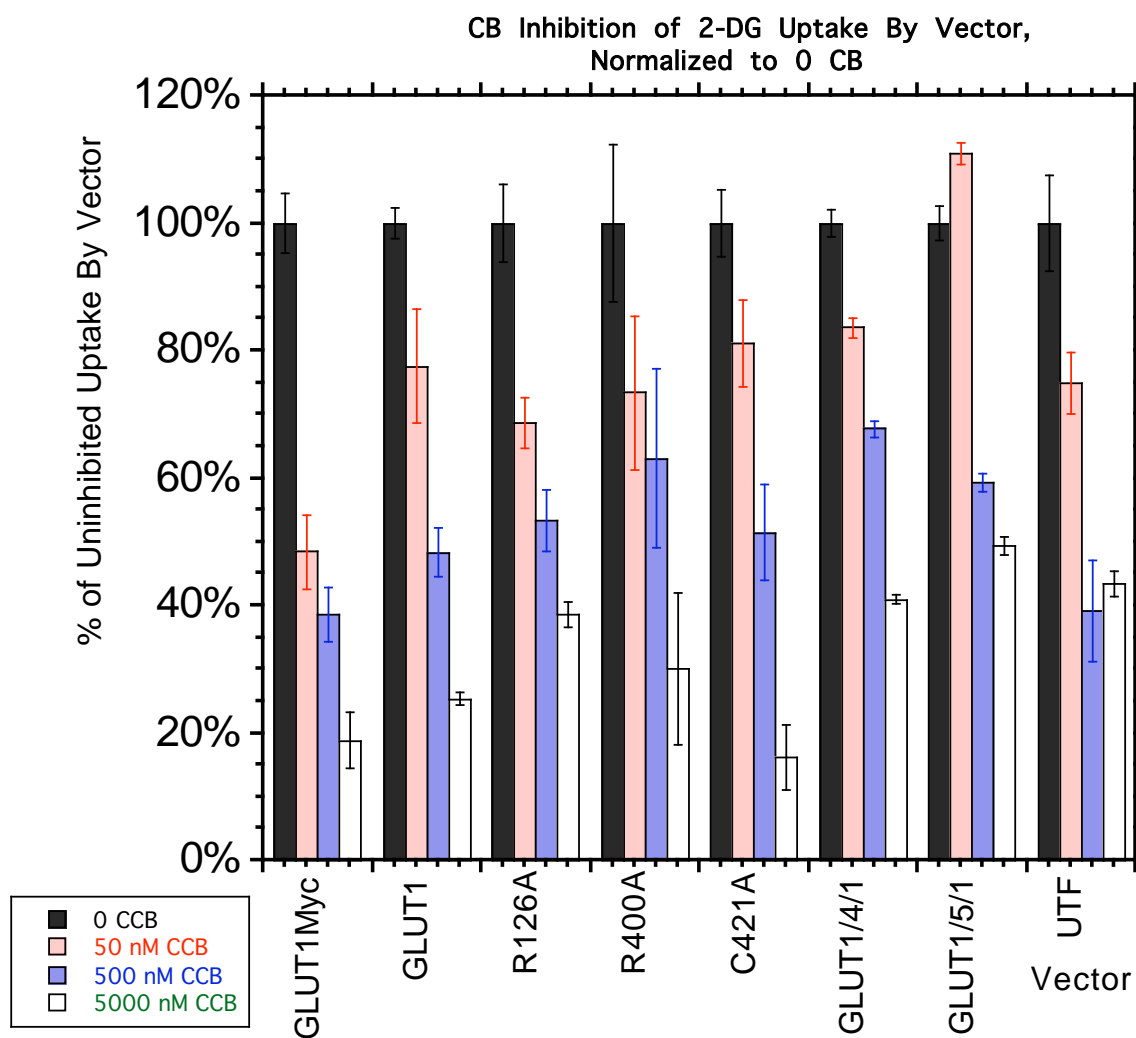
reported here.

For further visual comparison, the same uptake data was compared expressing CB-inhibited uptake as a percentage of each uninhibited construct rate. (Fig 4.8)

Chimeras of TM10-11 GLUT1/GLUT4$_{388-412}$/GLUT1 and GLUT1/GLUT5$_{388-412}$/GLUT1 were also made and tested for CB sensitivity in the same fashion. GLUT1/GLUT4$_{388-412}$/GLUT1 was significantly different at all CB concentrations from the GLUT1-Myc according to the Bonferroni analysis as well as the K$_{iapp}$ ratio approximation (Table 4.3). The apparent activation of GLUT1/GLUT5$_{388-412}$/GLUT1 mediated transport by 50 nM CB warranted further investigation. A more extensive dose response experiment was made with n=4 in quadruplicate. (Fig 4.9) The inhibition of 2-DG uptake by CB was tested for all constructs except for GLUT5, which was tested by measuring the inhibition of 100μM fructose uptake by CB, as GLUT5 does not appreciably facilitate 2-DG transport. (Fig 4.10) The data were fit using a modified Michaelis-Menton equation to provide initial estimates of IC$_{50}$ values. Calculated by GraphPad Prism with α=0.05, these were 3.07 ± 0.98 μM for GLUT1, $2.91 \pm .58$ μM for GLUT1Myc, 3.04

Figure 4.9 HEK293 Mutant GLUT1 constructs in CB Dose Response.

Ordinate, increasing [CB] concentration in nM. Abscissa, percent CB inhbition of 2 DG transport, normalized within each vector to uninhibited uptake. Closed circles (●) GLUT1 WT, Open circles (○) c-myc GLUT1, Diamonds (◆) GLUT151, and open circles (○) UTF cells; CB inhibition was measured against 100 μM 2 DG sugar uptake over 6 minutes. Closed triangles are (▲) GLUT5 CB dose response to 100μM ^{14}C fructose uptake, normalized to uninhibited uptake of fructose. Each point is a mean of three experiments, n=4 transfected wells. Method used as in Fig 4.5. Analysis made using Kaleidagraph and mutant K_I values were determined by fitting the data to a modified Michaelis-Menton equation. Overall inhibition of GLUT1 transfected protein K_i are statistically similar to GLUT1-Myc, indicating only subtle changes on CB affinity. Error bars were the standard deviation of the mean divided by the number of wells, then normalized to 0 CCB 6 min uptake.

Fig 4.9
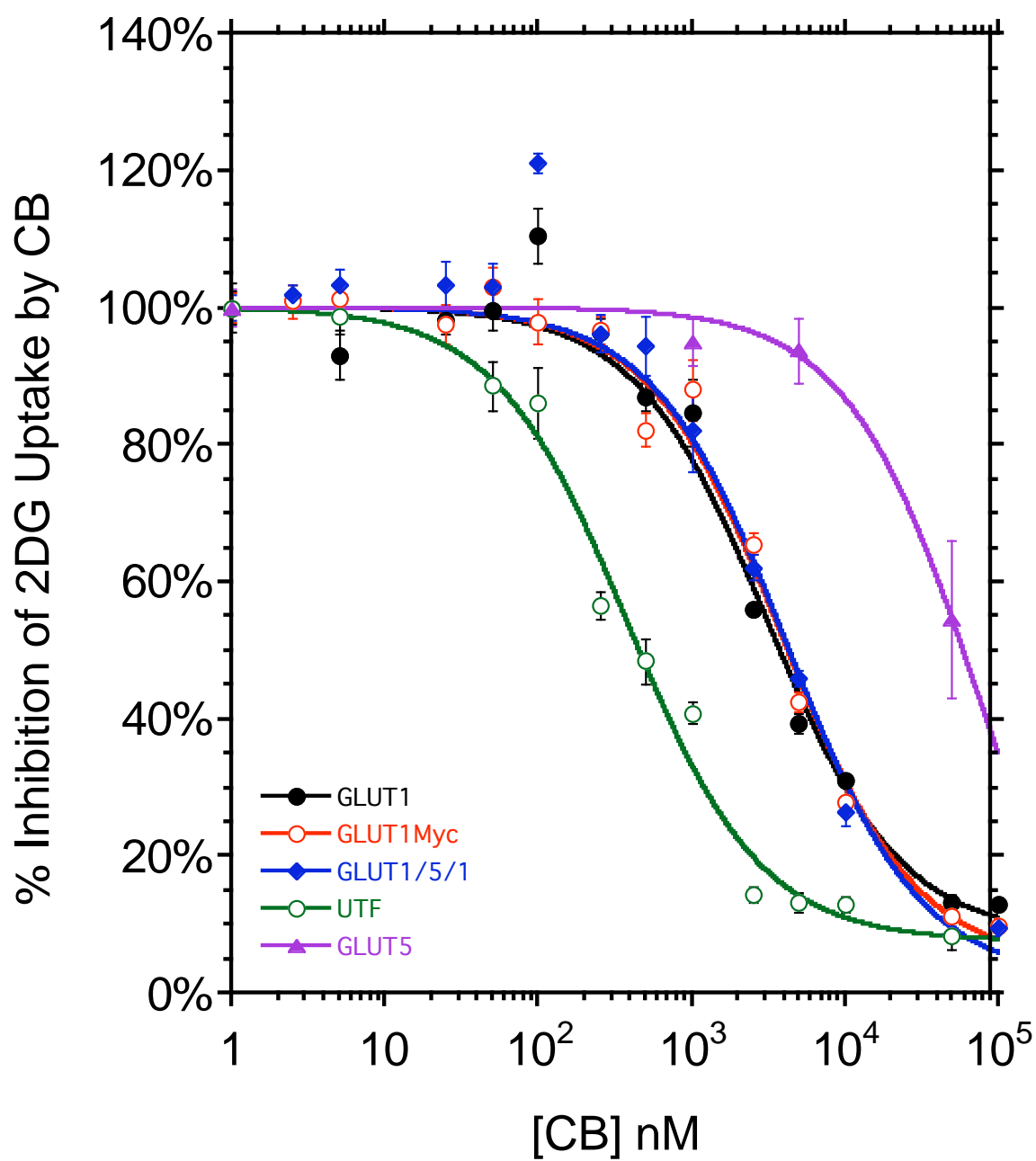
**Figure 4.10**. HEK-293 Expressed Uptake by GLUT5 of 2-DG within error of

untransfected.uptake of 100µM ^{3}H 2DG at 37ºC .

Abscissa, the rate of 2 DG uptake per minute, measured over six minutes. This

experiment performed as described in Fig 4.5, with each point the mean of three

experiments, n=4. Error bars were the standard deviation of the mean divided by the

number of wells.

Fig 4.10
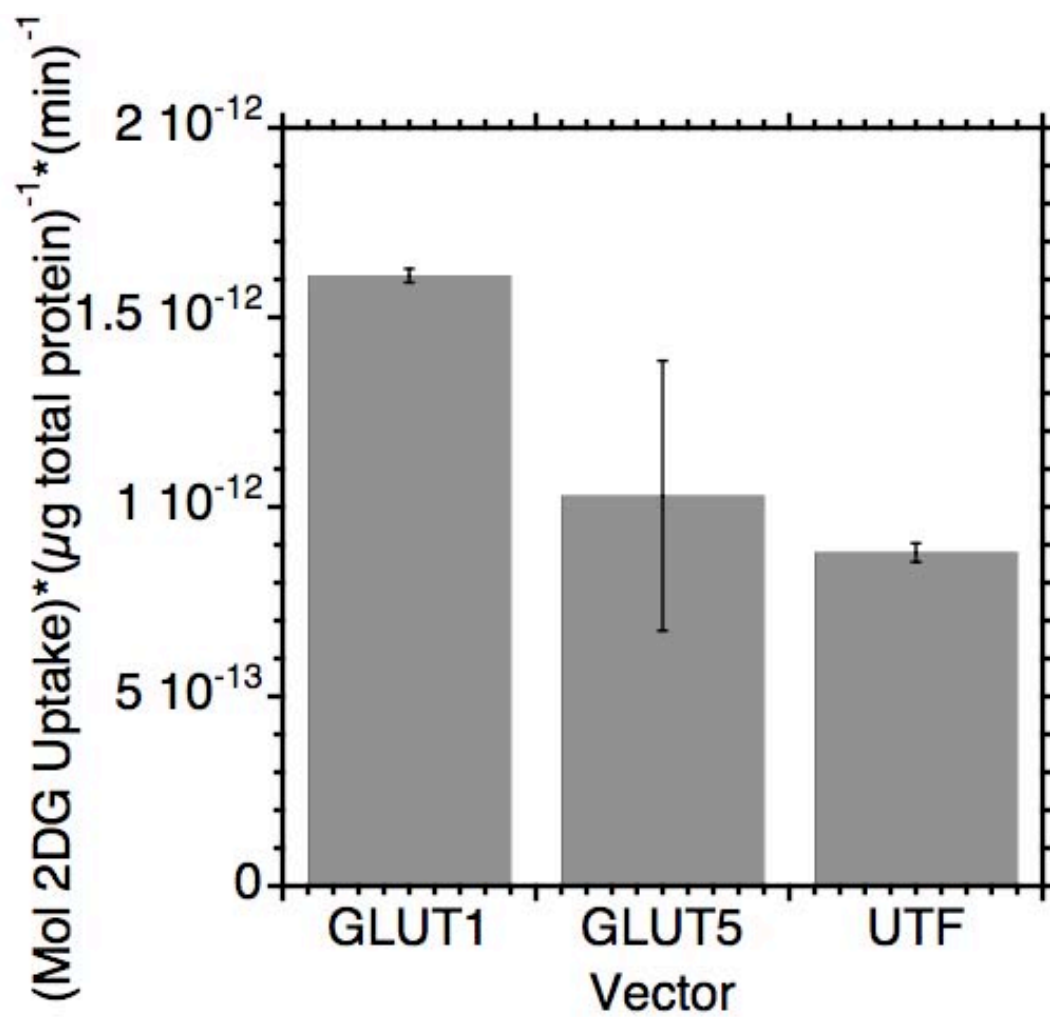
Figure 4.11 Graphical representation of cooperative inhibition of 2 DG uptake by CB shows moderate stimulation of sugar transport at low inhibitor concentration. Ordinate, increasing [CB] concentration in nM. Abscissa, percent CB inhbition of 2 DG transport, normalized within each vector to uninhibited uptake. Analysis was made using Kaleidagraph. Closed circles (●) GLUT1 WT, Open circles (○) c-myc GLUT1, Diamonds (◆) GLUT151, and open circles (○) UTF cells; CB inhibition was measured against 100 µM 2 DG sugar uptake over 6 minutes. Closed triangles are (▲) GLUT5 CB dose response to 100µM ^{14}C fructose uptake, normalized to uninhibited uptake of fructose. Each point is a mean of three experiments, n=4 transfected wells. Method used as in Fig 4.5. Analysis made using Kaleidagraph and mutant K_I values were determined by fitting the data to a multisite, oligomeric fit equation as described in Appendix 1. While an increase in first-site CB affinity was seen for GLUT1/5/1, increasing concentrations of CB display reduced second-site inhibition of 2 DG uptake. Overall inhibition of GLUT1 transfected construct K_Is remain statistically similar to GLUT1-Myc, indicating W388-W412 necessary for CB binding and photolabeling of GLUT1 but not sufficient for CB inhibition of transport.

Fig 4.11
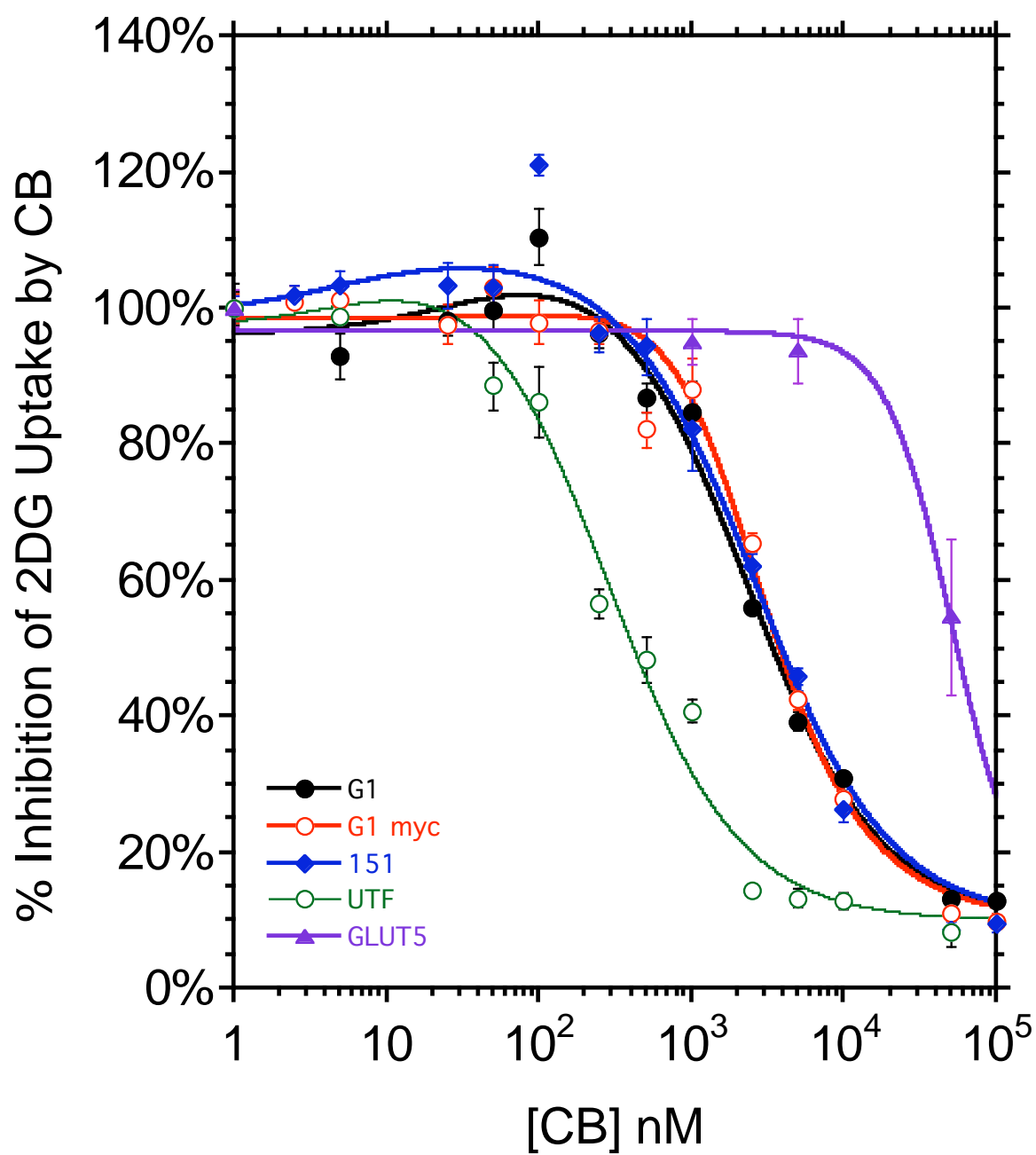
Table 4.3 Ratio K_I/K_{CB} calculations for Abbreviated Dose Responses.

[a] A K_{IApp} ratio value, based upon 2 DG uptake by vector normalized to GLUT1-Myc uptake, assuming complete inhibition of transport at 5000 nM CB. Calculated from the following eqn:

$$\frac{K_{IApp}}{K_{ICB}} = \frac{[CB]}{\left(\dfrac{(100\% - Mutant\%_{0CB})}{(100\% - Mutant\%_{XCB})} - 1 \right)}$$

This does not give us an exact value, but lets us approximate a K_I and compare between vectors in a manner alternate to the Bonferroni statistical method. Unlike the Bonferroni, this method is only really useful for comparing two concentrations – inhibition of uptake at 50nM and at 500nM vs GLUT1-Myc. [b] $\Delta G = 1.987*310*LN(1/(MeanK_{IApp}*0.000000001))/1000.$ [c] The difference between GLUT1-Myc ΔG and Mutant ΔG. [d] The ratio of calculated K_{Iapps}, to approximate similarity between constructs. Ratio values less than GLUT1Myc indicate proteins more sensitive to CB inhibition of 2 DG uptake, while larger values indicate less overall sensitivity. [e] Because of the stimulation of 2 DG transport by 50nM CB for GLUT1/GLUT5$_{388-412}$/GLUT1, we cannot use this method to approximate K_I.

Table 4.3

Vector	K_I/K_{50} 50nM[a]	K_I/K_{500} 500nM[a]	Mean K_I/K_{CB}	ΔG^o (kcal)[b]	$\Delta\Delta G^o$ vs. Myc[c]	$K_{I\,500}/K_{I\,50}$[d]
GLUT1-Myc	28.7	158.6	93.7	9.97	0.00	5.53
WT GLUT1	116.4	222.8	169.6	9.60	0.37	1.91
R126A	47.9	157.3	102.6	9.91	-0.59	3.28
R400A	81.6	1603.3	842.4	8.62	1.35	19.66
C421A	173.5	364.4	269.0	9.32	0.65	2.10
GLUT1/4/1	130.0	157.3	102.6	9.91	-0.59	3.28
GLUT1/5/1[e]	-285.1	95.0	N.D.	N.D.	N.D.	N.D.
UTF	71.2	38.0	54.6	10.30	-1.69	0.53

± 0.83 µM for GLUT1/GLUT5$_{388-412}$/GLUT1 , and 0.42 ± 0.05 µM for untransfected. These IC$_{50}$ values failed to be significantly different than that of GLUT1-Myc uptake by a Tukey's multiple comparison test, arguing that the GLUT1/GLUT5$_{388-412}$/GLUT1 chimeric insertion did not effect the CB binding site.

A multisite fit modeled after CB binding competition was also utilized to analyze the data (see Chapter 3 of this work, Appendix 4.1, and Fig 4.11). Using this method we were able to quantify the concentration of CB at which stimulation of 2-DG transport occurred: 83 ± 118 nM for WT GLUT1, and 10 ± 39 nM CB for GLUT1/GLUT5$_{388-412}$/GLUT1. When tested by one-way ANOVA with Tukey post hoc (α=0.05), these numbers are significantly different than results obtained with UTF and GLUT1-Myc constructs.

DISCUSSION

Cytochalasin B inhibition of and binding to erythrocyte GLUT1 is more complex than expected for a simple, alternating conformer carrier (*201*). *Carruthers et al* refuted the simple carrier model of GLUT1 sugar transport by analysis of ligand modulation of carrier function. (*97*). According to the simple carrier model, if GLUT1 behaves as a simple uniporter, high concentrations of e2 inhibitor should block e1 inhibitor binding by trapping all subunits in e2 or exofacial conformation. This was not observed. Rather, the occupancy of the e2 site by maltose allosterically modulates the affinity of the e1 site for cytochalasin B. *Hamill et al* went on to show that low concentrations of maltose

stimulate 3-O-MG uptake (*7*), while *Cloherty et al* found that low concentrations of

cytochalasin B (5nM) also stimulate 3MG uptake (*16*). The simplest model accounting

for inhibitor data is an obligate, functionally antiparallel tetrameric subunit arrangement

in which two GLUT1 subunits each present a sugar uptake (e2) site and two subunits

present sugar export (e1) sites (*16*). *Robichaud et al* analyzed subunit/subunit

interactions from binding CB and other CB derivative ligands to determine that substrate

interaction with the tetramer is highly cooperative (*202*). This complex behavior

underscores the importance of the e1 sugar binding site to protein function.

The location of the CB binding site to GLUT1 is presently unknown, though two

endofacial locations have been proposed. The first site was proposed by following

analysis of limited proteolytic digests of GLUT1. CB may be covalently cross-linked to

GLUT1 by UV irradiation, and this in combination with N-bromosuccinamide induced

cleavage at tryptophan residues, indicates that the smallest ^{3}H-CB labeled GLUT1

fragment obtained is a peptide comprising W388 through W412 (*13*). This cytoplasmic

domain connects TMs 10 and 11 of the transporter. Mutation of either W388 or W412 to

alanine in *X. laevis* oocytes decreases GLUT1 photolabeling by CB significantly, and

mutation of both residues eliminates CB binding. (*116, 117*). These data argue that the

W388 to W412 region plays a crucial role in CB binding.

The second CB binding site was proposed through docking of the ligand to a

theoretical crystal structure. *Salas-Burgos et al* homology modeled the GLUT1 sequence

onto the protein backbone of GlpT, and computationally docked CB to a binding site in

an endofacial pocket outside the presumed e1 cavity (*5*). According to this *in silico*

analysis, CB interacts with L85, N88, R89, R92, K225, Q250, M251, and R400 in largely polar pocket. This site is 3Å distant from the TM10-11 binding site proposed by *Holman and Rees* (*13*), but is plausibly close enough to the glucose-binding cavity to interfere with glucose docking (*5*).

Other data in the literature suggests further residues are involved in CB binding to GLUT1. Analysis of clinical missense GLUT1 mutations reveals sites implicated in the CB/GLUT1 interaction (*42, 44*). R126 is the most common locus for clinical GLUT1DS, presenting in the literature as R126H, L, C, K, & E (*193*). C421 forms part of the putative intramolecular disulfide bridge thought to stabilize tetrameric subunit-subunit interactions of GLUT1(*65*), and mutation to alanine is expected to abrogate cooperative CB binding (*202*). We discuss each construct analysed in turn.

GLUT1-Myc

The presence of the myc epitope tag on GLUT1 does affect CB affinity as compared to WT GLUT1. Comparison of GLUT1-Myc 2 DG uptake to WT GLUT1 shows significant effect of the epitope tag on CB binding at 500 and 5000 nm CB (Fig 4.7). We conclude this effect may be due to either 1) the polar myc epitope on the exofacial surface of the protein promotes a conformational change altering distal ligand binding, or 2) the myc tag alters subunit-subunit communication and low-concentration CB binding cooperativity. With this in mind, the ability of each point mutant to transport 2 DG in the presence of CB was compared to GLUT1-Myc rather than WT GLUT1.

R126A GLUT1

The R126 locus is the most common missense mutation resulting in GLUT1 DS, and displays altered CB affinity. The R126A construct 2 DG uptake rate shows mild stimulation over GLUT1-Myc (108 ± 6 %), as well as less CB mediated inhibition of 2 DG uptake at all concentrations tested. In collaboration with Dr. Mary Jo Ondrenchen, the reported e1-facing GlpT homology-threaded structure of GLUT1 was docked using THEMATICS with CB (personal communication, 2007). The modeling program predicted CB interaction with GLUT1 at Y28, R126, and C133. In this model, R126 rests in a highly conserved, large polar area of the sequence near the equator of GLUT1. It is possible CB binding fixes a GLUT1 subunit in an e1 state that is kinetically indistinguishable from direct competition at the same site. Alternately, R126 may function as part of a glucose (or CB) sensing area of the protein, or may be a structural lynchpin of successful sugar transport. Given the proximity of the R126 residue to the exofacial side of the membrane, it is unlikely that it participates directly in CB binding to the endofacial sugar binding site. We conclude that mutations at this locus have distal effects upon CB binding to GLUT1.

C421A GLUT1

It is likely that C421A GLUT1 protein does not form correct oligomeric structures in the lipid bilayer, thereby displaying reduced sugar transport. GLUT1 possesses an internal disulfide bond between residues C347 and C421 on the exofacial side of the protein. This bond is known to stabilize GLUT1 tertiary structure so that oligomers may be formed (*65*). Mutation of C421 to alanine shows significantly reduced transport

capacity for 2 DG. C421A GLUT1 expression is comparable to WT GLUT1, and C412A GLUT1 successfully traffics to the plasma membrane. When considering the CB sensitivity of C421A GLUT1, CB inhibition of 2 DG glucose uptake is significantly reduced compared to inhibition of GLUT1-Myc only at 5 μM CB. The net effects of the C421A mutation therefore likely reflect perturbations in the quaternary associations of protein subunits, making it unlikely that C421A is within the e1 sugar binding site.

R400A GLUT1

The R400A GLUT1 protein behaves similarly to GLUT1-Myc tagged protein. This model showed CB interacting directly with the R400 residue of GLUT1 by *Salas-Burgos et al* in a theoretical e1 crystal structure (*5*). Although R400A GLUT1 protein has somewhat less overall expression by Western blot (Fig 4.3), it does express at the plasma membrane (Fig 4.4). Uninhibited 2 DG uptake, 500nM CB & 5000 nM CB inhibited uptake of 2 DG are similar to GLUT1-Myc, with the 50 nM CB data point the only significant alteration in affinity. We conclude that while R400A might be involved in CB binding, this amino acid substitution alone is not enough to abrogate CB inhibition of sugar transport.

GLUT1/GLUT4$_{388-412}$/GLUT1 CHIMERA, A.K.A. I404M

The point mutation I404M, or the GLUT1/GLUT4$_{388-412}$/GLUT1 chimera, is less sensitive to CB than GLUT1-Myc protein. This change was suggested because indinavir competitively inhibits CB binding to and sugar transport by GLUT4, with half maximal inhibition at 10^{-6}M. Indinavir, however, inhibits GLUT1 with half-maximal effects at 10^{-3}M, and does not compete with CB for binding to GLUT1 (*203*). The GLUT1 W388-

W412 region is highly conserved between GLUT1 and GLUT4, with I404 in GLUT1 substituted by a methionine in GLUT4. The GLUT1/GLUT4$_{388-412}$/GLUT1 chimera showed significantly more transport of 2 DG in the presence of CB, making it likely that the I404 residue is necessary for CB affinity for GLUT1.

GLUT1/GLUT5$_{388-412}$/GLUT1 CHIMERA

GLUT5, a group 2 transporter, is highly insensitive to CB (*2*). GLUT5 TM10-11 region shares 58% similarity with GLUT1, and lacks the photolabeling-critical residue W388. The GLUT1/GLUT5$_{388-412}$/GLUT1 chimera transports 2 DG with less CB inhibition at 500 and 5000nM CB. Moreover, the chimera showed a statistically significant stimulation of sugar transport at 50 nM CB, prompting us to undertake a more extensive dose response analysis. While the stimulation at 50 nM for the GLUT1/GLUT5$_{388-412}$/GLUT1 chimera was confirmed, the IC$_{50}$ determined for CB inhibition of GLUT1/GLUT5$_{388-412}$/GLUT1 is not significantly different from that for inhibition of WT or myc-tagged protein. A multisite analysis of CB inhibition based upon CB binding kinetics was developed, and from this KI$_{app}$ values were calculated for the first CB binding site on the tetramer in the presence of 2 DG. While GLUT1-Myc does not display stimulation of 2 DG uptake by 50 nM CB, both WT GLUT1 and GLUT1/GLUT5$_{388-412}$/GLUT1 do. Interestingly, the first site KI$_{app}$ for the chimera (10 ± 39 nM) was almost eightfold less than that of WT GLUT1 (83 ± 118 nM). The multisite fit argues that while the chimera's first site affinity for CB has increased, after a threshold the overall sensitivity of the protein to CB inhibition of sugar transport has decreased, likely from a decrease in affinity or cooperativity at the second CB or e1 binding site on

the tetramer. It is also possible that the W388-412 photolabeling region comprises that part of the CB binding pocket most important for initial binding of ligand, while another section of GLUT1 interacts with CB to functionally inhibit sugar transport.

CONCLUSIONS AND FUTURE IDEAS

Overall, we conclude: 1) CB inhibition of wild-type and myc-tagged GLUT1 constructs is considerably less potent ($K_{iapp} \approx 2\mu M$) than inhibition of erythrocyte sugar transport (K_{iapp}=460 nM, (*104*)). 2) R126A and C421A show altered CB affinity, but are not likely part of the e1 sugar binding site. 3) R400A and GLUT1/GLUT4$_{388-412}$/GLUT1 are implicated in CB binding, but do not confer CB insensitivity to the protein. 4) The GLUT1/GLUT5$_{388-412}$/GLUT1 chimera sequence comprises part of the binding pocket for CB but may not be sufficient for CB inhibition of 2 DG transport. 5) W388 is necessary for photolabeling of GLUT1 by CB but not for CB mediated inhibition of sugar uptake.

Examining the GLUT1/GLUT5 sequence alignment suggests further nonconserved areas which may implicate the CB binding site, and in turn, the endofacial sugar binding site. In the *Salas-Burgos* threaded GLUT1 structure, CB interacts with the sugar porter motif RFGRR at residues 88-93 (*5*). While attractive, swapping in this GLUT5 sequence into GLUT1 is unlikely to result in altered affinity for CB because the equivalent GLUT5 sequence (KFGRK) has a similar charge. Another docking site (Q250, M251) might produce a stronger effect upon exchanging residues 248-259 of GLUT1 for 254-265 of GLUT5, because the GLUT1 and GLUT5 sequence in this region is dissimilar in the arrangement of polar charges. Lastly, exchanging a region near R126 (121-139) in the GLUT1/GLUT5 alignment might also perturb binding and determine

whether CB inhibition of glucose transport is directly competitive for the e1 site. GLUT5 insensitivity to CB may suggest further loci for the endofacial sugar binding site.

Our results demonstrate that the GLUT1 residues W388 to W412 may form the site of CB-GLUT1 covalent association upon UV irradiation but that this region is not the only determinant of GLUT1 affinity for CB.

APPENDIX 4.1

Tetrameric Analysis of GLUT1 Inhibition.

If we assume a tetramer of GLUT1 subunits, seven configurations of oligomeric subunits may successfully bind sugar in the presence of an e1 inhibitor such as CB (Fig 4.12). Each GLUT1 tetramer is thought to exist in the membrane as a dimer of dimers; when an inhibitor is bound to a dimer it may not transport sugar. Its partner dimer in the tetramer, however, is unconstrained. The total rate of sugar entry into HEK cells is the

$$V_{total} = [S] * \frac{8\left(V_1 + V_2 \frac{[2\,DG]}{\beta K_{m(2\,DG)}} + V_3 \frac{[2\,DG][CB]}{\beta K_{m(2\,DG)} K_{m(CB)}} + V_4 \frac{[CB]}{\gamma K_{m(CB)}}\right)}{K_{m(2\,DG)}\left(4 + \frac{[CB]}{K_{m(CB)}}\left(8 + \frac{4\,[CB]}{\alpha K_{m(CB)}}\right)\right)}$$

sum of four transport-capable conformations. This may be mathematically represented using the following equation, derived from the two-site carrier model for transport(*92*) as well as two-site ligand competition binding(*202*).

α, β, and γ are cooperativity factors used to measure the interactions between sites. Positive cooperativity has a value less than one, while negative has a value assumed greater than one. α measures CB cooperativity for CB binding at the second site. β values are the 2 DG cooperativity for 2 DG at the second site. γ represents the cooperativity effects of CB on the other site for 2 DG binding, and vice versa. When modeling the fit in Kaleidagraph, we made the following assumptions: that v_3 and v_4 were functionally equivalent rates retaining unique (calculated) cooperativity values, that K_{mapp} for 2 DG was 600 μM, S was 100 μM, K_d for CB was the same as K_i for CB, α=5, β=0.5, and γ=1.

Figure 4.12 Ligand Binding Conformations on Tetrameric GLUT1.

The seven possible binding conformations in conditions of unidirectional sugar uptake. S = Sugar. CB = inhibitor, in this case cytochalasin B. Each GLUT1 tetramer is shown as a dimer of dimers. Transport through the tetramer complex may only occur when a bound S has no CB in the same dimer.

Fig 4.12

Transporting Conformations

$= v_1$

$= v_2$

$= v_3$

$= v_4$
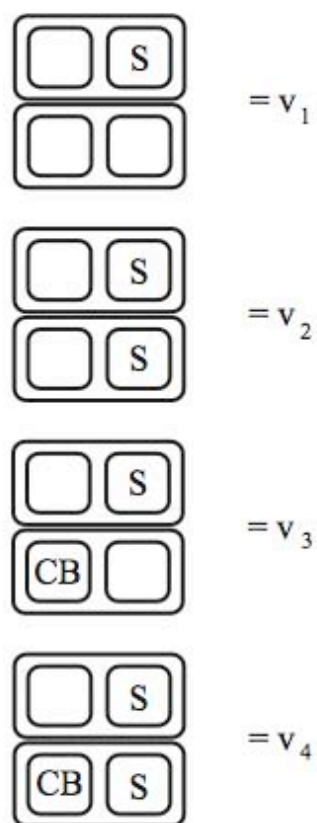
Inhibited Conformations

$\neq v$

$\neq v$

$\neq v$
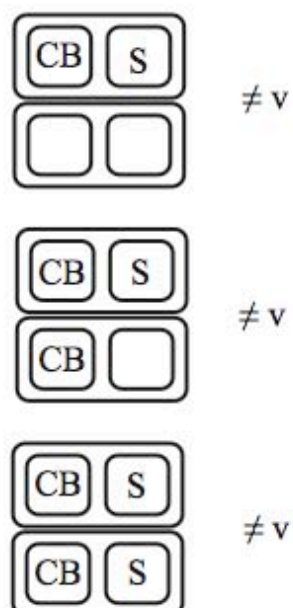
CHAPTER V

CONCLUSIONS AND FUTURE DIRECTIONS

CONCLUSIONS AND FUTURE DIRECTIONS

Nutrient importers such as GLUT1 are vital for cellular growth and life. In this thesis we have discussed the effects of cellular context upon GLUT1 function, the structural requirements for ligand binding to the endofacial sugar binding site, and which regions of GLUT1 primary amino acid sequence comprise the endofacial sugar binding site. Revisiting these conclusions from the previous chapters illuminates future directions of study.

GLUT1 in Cellular Context

GLUT1 may be regulated by bilayer thickness or bilayer physical state. *Connolly et al* reconstituted erythrocyte sugar transporters in lipid vesicles with increasing amounts of cholesterol, and discovered that glucose transport behavior was abruptly stimulated when the membrane contained 15 mole % cholesterol (*204*). This stimulation was reversible at 17.5 mole % cholesterol, with a modest increase in activity again at 30-40% mol cholesterol. Membrane phase transitions from 0ºC – 65ºC in synthetic lecithin bilayers also affected GLUT1 transport rates (*205*). These in vitro findings concerning GLUT1 behavior and membrane composition demonstrate that GLUT1 function is affected by cellular context and lipid composition.

Erythrocytes are a readily available source of wild type GLUT1, but to facilitate mutational analysis of the protein we explored an alternate expression system. RE700A yeast devoid of endogenous glucose transporters were successfully transformed with GLUT1, GLUT1 HA-HIS$_6$, and the transport-incompetent mutant GLUT1$_{338-A3}$. RE700a transformed with wild-type GLUT1 and GLUT1HA-HIS showed GLUT1 specific

behaviors such as growth on yeast medium containing glucose, specific inhibition of

transport by CB, and uptake of nonmetabolizeable 3-OMG. Since these phenotypes were

reversed by 5-fluoro-orotic acid (FOA), yeast plasmid expression of GLUT1 was

confirmed, making available another expression system for mutant GLUT1.

However, we soon learned that GLUT1 functions differently in each cellular

context. Erythrocyte GLUT1 displays transport asymmetry (V_{max} and K_m for net sugar

exit are greater than the equivalent parameters for uptake(*63*)), intracellular sugar can

increase the rate of sugar uptake (trans acceleration, (*157*)), and uptake is inhibited by

extracellular reductant(*65*). Compared to erythrocytes, RE700A-GLUT1 is not inhibited

by extracellular reductant(*65*), nor does it show trans-acceleration. Oocyte expression of

GLUT1 is not inhibited by reductant (*65*) but may show trans-acceleration. HEK-293

expression of GLUT1 shows transacceleration but competition with other sugars that

differs from that competition observed in red cells. Thus GLUT1 behavior varies by

expression system.

These findings underscore the importance of the model system in experimental

design and expression of mutant proteins, and illustrate the following caveats. 1.)

Membrane physical state and composition strongly affect function. The RE700A plasma

membrane may be significantly different than that of mammalian cells thereby altering

GLUT1 function. 2.) GLUT1 glycosylation may affect function. For example, *S.*

cerevisiae has N-linked glycosylation machinery resulting in mammalian-like

glycosylation (*206*), but the few sugars added are relatively uniform as compared to the

typical mammalian heterogeneity. This may result in proteins with altered structural and

functional properties. 3.) Protein density vs. ease of culture and purification may limit

biophysical analysis. Thus, it is important that the context of expression should be

considered in any course of study.

EXTENDING THE YEAST EXPRESSION SYSTEM

In spite of these reservations, questions remain that may be addressed by a

functional yeast GLUT1 expression system. GLUT1 immunostaining on a red blood cell

is distinctly punctate(*131*), arguing for heterologous associations on the bilayer surface.

TAT2p, a tryptophan permease native to yeast, is known to associate with detergent-

resistant lipid microdomains (*206*). Confocal analysis of GLUT-expressing yeast cells

and spheroplasts may demonstrate GLUT1 inclusion or exclusion from detergent resistant

lipid microdomains and, given the relative ease of genetic manipulation in S. cerevisiae,

may offer a powerful model for genetic screening of determinants of GLUT1 lateral

segregation in the plane of the membrane bilayer.

Other attractions of a yeast expression system include plate based screening of

new GLUT1 inhibitors. Furthermore, yeast's remarkable facility with homologous

recombination and second-site mutagenesis could be combined with small molecule

growth screens to pinpoint ligand binding sites in the GLUT1 sequence.

Affinity and Cooperativity Determinants

Many natural compounds inhibit GLUT1 transport. Methylxanthines and ATP act

as mixed inhibitors of sugar exit, reducing V_{max} and increasing K_m, but are thought to act

at areas distinct from sugar binding sites (*98, 184, 185*). Androgens and catechins as well

as tyrosine kinase inhibitors are competitive for sugar import, with reduced V_{max} for exit

and increased K_m for uptake (*106, 186*). Maltose and phloretin inhibit GLUT1 by interacting with the exofacial site, increasing K_m for sugar uptake (*97, 105*). Forskolin (FSK) and cytochalasins reduce V_{max} for net entry, indicating noncompetitive inhibition of uptake and increase K_m of exit, implying direct interaction with the endofacial e1 binding site (*97, 107, 194, 202*). Understanding the structural basis of GLUT1 inhibition may elucidate functional ligand binding domains of GLUT1.

Comparative analysis of the ability of cytochalasin and forskolin derivatives to displace cytochalasin B (CB) reveal some determinants of binding at the endofacial sugar binding site. We shall discuss cytochalasin binding first. All of the cytochalasins share a common rigid bicyclic isoindoline moiety plus a macrocyclic ring. Dehydration of the macrocycle hydroxyl to form cytochalasin A decreases affinity by 6-fold. Shortening of the macrocycle (e.g. comparing CB to cytochalasin C, H or J) reduces affinity by 5-8 fold. Comparison of cytochalasins C and D, indicates that methyl substitution at position 5 of the isoindoline reduces affinity by 55 fold. This indicates that the cytochalasin binding pocket may tolerate changes at one end of the molecule or the other, but not both. CB may be thought of as an 'open book' structure, with two planes meeting along a more rigid, central 'spine'. Altering the planar angle or the size of the 'pages' severely limits ligand binding.

We tested the GLUT1 binding capabilities of an extensive library of forskolin shapes to characterize its binding pocket. Forskolins with acetyl groups at 6 and 7 showed the greatest affinity for GLUT1; replacement of both acetyls with hydroxyls results in a complete loss of binding affinity. Substitution of only the 6-acetyl with a

hydroxyl results in the parent molecule and a 500-fold loss of affinity as compared to 1,6 FSK. Acetylation of the parent at position 1 increases affinity tenfold, while removing a hydroxyl group at positions 1 and 9 restores affinity fifty and thirty-fold, respectively. Extensive, even bulky, substitution at the seven acetyl position is tolerated within the binding pocket. Forskolin is planar compared to cytochalasin B, and its determinants of binding imply that the entire molecule is engulfed within GLUT1.

COOPERATIVE EFFECTS OF LIGAND BINDING

Erythrocyte inhibitor studies with GLUT1 support an oligomeric model. Low concentrations of extracellular inhibitor, such as maltose, or intracellular inhibitors like cytochalasin B or forskolin modestly stimulate sugar transport (*7*). The simplest explanation for this remains a homo-oligomer of GLUT1, most likely a tetramer or dimer of dimers, in which at any instant two subunits adopt an e1 conformation and two subunits adopt the e2 state. When one inhibitor such as CB binds, a conformational change occurs resulting in increased activity in the opposite dimer (*7, 16*). Increased concentrations of ligand result in occupancy of the second site and cessation of substrate transport. The intermediate effects of ligand binding upon transport suggest communication between binding sites, supporting the oligomeric model.

Although previous work examined inhibition of erythrocyte sugar uptake by cytochalasin B and forskolins (*107, 121, 182, 188*), this present study differs in its analysis of transport inhibition. Because of our observed cooperative interactions, a Michaelis based kinetics analysis of inhibition is of less utility. Unlike previous work,

we allow for two interacting binding sites and measure the cooperativity of these sites across multiple log units of inhibitor concentration.

In competition experiments such as the ones made here, we find hetero- and homo- cooperative interactions in the nonlinear, non-Michaelis shapes of the [inhibitor] vs [CB bound]/[CB free] curves. We model these interactions mathematically as the cooperativity factors α (homo- or CB.CB interactions), β (hetero- or CB.I interactions) and γ (homo- or I.I interactions). Values less than one represent positive cooperativity with apparent increases in second-site affinity for ligand. If we consider a competition experiment between FSK and CB, CB displays positive homo cooperativity, with $\alpha<1$. CB and FSK show hetero-cooperativity for one another, each with a β cooperativity factor of 0.44 ± 0.05. Functionally, this implies that the presence of a FSK in the first site increases the apparent affinity of the second site for CB, and vice versa. The γ value represents inhibitor cooperativity for itself; in this example, FSK is not significantly different than 1. This indicates that a given FSK binding event does not affect the affinity of the remaining binding site. Each derivative displays unique values for β and γ in competition with CB. The lack of independent binding interactions for some ligands suggest that subunit surfaces are in direct contact to facilitate conformational change and hetero-cooperativity, or that the ligands themselves interact due to the proximity of their binding sites.

EXTENDING AFFINITY/COOPERATIVITY DETERMINANTS

GLUT1 is known to homooligomerize *in vivo*, *in vitro* and in culture; hetero oligomers of GLUTs or GLUT chimeras could display modified cooperative behavior.

GLUT1 normally does not oligomerize with GLUT3 (personal communication, Kara Levine, and (*207*)) or GLUT4 (*65*). *Levine et al* have created a series of GLUT1-GLUT3 chimeras to test oligomeric association in the membrane, progressively replacing each GLUT1 transmembrane helix with the equivalent GLUT3 transmembrane helix. Limited proteolysis with N-bromosuccinamide combined with ^{3}H-CB photolabeling argues for CB association with TM's 10 and 11. Testing GLUT1-GLUT3 chimeras in combination with inhibitor modulation of cytochalasin B or forskolin binding assays may reveal 'GLUT1 cooperativity TMs' and could localize the cytochalasin B or endofacial sugar binding site within the protein sequence.

GLUT1 conformational changes induced by e1 ligand binding may also be investigated by thiol crosslinking combined with mass spectrometric analysis or immunofluorescence. *Blodgett et al*. utilized mass spectrometric analysis of GLUT1 to determine that upon trypsinized GLUT1 interaction with 10 µM CB, full-length TM8 is released into the aqueous fraction of peptides (*208*). Cysteine scanning mutagenesis and thiol-reactive crosslinkers may illuminate the TM domains or loops required for e1 ligand binding. Using short sulfhydryl crosslinkers such as bis-maleimidoethane between TM's 10 and 11 in a cys-less GLUT1 background, might mimic or prevent cytochalasin B displacement of TM8. Since *Mueckler et al* have confirmed the aqueous access of TM8 in Xenopus oocytes (*80*), surface immunofluorescence microscopy using endofacial loop 8-9 antibody ± sulfhydryl crosslinking might determine if TM8 is displaced specifically to the exofacial side of the membrane. A similar phenomenon is thought to occur in the

transport cycle of the anion transport protein AE1 (*209*). This analysis provides an opportunity to confirm tertiary conformational changes as a result of e1 site occupation.

Mutational & Chimeric Localization of the e1 Site

An integral membrane protein such as GLUT1 is refractory to crystallization, so the location of the endofacial sugar binding site within the primary sequence remains unknown. Cytochalasin B reduces the V_{max} for sugar entry and increases K_m for sugar exit and is thus thought to act directly upon the e1 sugar binding site (*102*). HEK293 expressed mutant GLUT1 combined with CB inhibition of 2-DG uptake provides a metric for GLUT1 mutant involvement in CB binding. Three point mutants (R126A, C421A, and R400A) and two chimeras (GLUT141, GLUT151) were successfully expressed and analyzed via this technique to pinpoint the CB, and therefore endofacial glucose binding site.

GLUT1 R126A expresses at the membrane, but R126 is thought to be exofacial and therefore not part of the e1 sugar binding site. Arg 126 is the most common missense mutant locus in clinical cases of GLUT1DS, with R126L presenting the most severe phenotype (*193*). Computer modeling has successfully docked CB to R126 in an exofacial vestibule (Ondrenchen, personal communication). We find GLUT1 R126A moderately increases in 2DG uptake over myc tagged GLUT1 ($108.4 \pm 6.5\%$), and significantly increases resistance to CB inhibition of 2DG uptake. It is possible CB binds exofacially, fixing a GLUT1 subunit in the e1 orientation. However, this would enhance, rather than competitively inhibit sugar binding at the endofacial site. Thus an exofacial cytochalasin B binding site and the endofacial sugar binding site must be

mutally exclusive. Alternately, R126 may function as part of a glucose (or CB) sensing area of the protein which does not directly participate in transport inhibition. Since our assays measure inhibition and not binding, alteration of a second, lower affinity site not directly involved with the e1 sugar binding site would go undetected.

Mutating GLUT1 at C421A removes one-half of the proposed intra subunit sulfhydryl stabilizing tetrameric association of GLUT1, and may disrupt cooperative action of CB on GLUT1. CB is known to bind to GLUT1 in a highly cooperative manner (*202*); the observed profile of CB inhibition of GLUT1 C421A might illuminate cooperative inhibition effects upon transport. GLUT1 C421A has reduced transport capacity: it shows 66.3±3.5% of uninhibited myc tagged GLUT1 sugar transport. CB inhibition of 2 DG uptake for GLUT1 C421A was only statistically greater than myc tagged GLUT1 at 5000nM, showing less total uptake. It is possible that CB binds each GLUT1 C421A dimer independently at lower affinity, due to lack of intra-subunit communications, but a direct effect of C421A upon CB binding or the e1 site is unlikely.

A theoretical crystal structure suggests R400 as a likely participant in the e1 site. *Salas-Burgos et a*l docked phloretin, cytochalasin B, and forskolin to a highly polar endofacial binding site in homology-modeled GLUT1 (*5*). The R400 site on threaded GLUT1 is the sole amino acid that interacts with all three inhibitors in the model structure. The overall sugar transport capacity of GLUT1 R400A is 95.4 ± 11.8% of myc tagged GLUT1, has somewhat reduced protein expression levels, and both the uninhibited and the 50nM concentration of CB show significantly different values than myc tagged GLUT1 at the same site. Mutation of R400A appears to alter ligand affinity,

supporting its role in the e1 site, but this point mutation alone does not prevent CB binding or concomitant inhibition of sugar uptake.

A point mutation may be insufficient to abrogate CB binding to the e1 site, so we examined a larger section by swapping chimeric regions from homologous GLUTs to find residues that interacted with the e1 site. Photolabeling by ^{3}H-CB followed by N-bromosuccinaminde digestion reveals the smallest CB interacting fragment is W388 to W412(*13*). This GLUT1 sequence was exchanged with sequences from GLUT4 and GLUT5, both known to have altered e1 inhibitor affinities.

Ironically, GLUT4 differs from GLUT1 in the 388-412 region by only one amino acid, I404M. The rationale for GLUT4 selection was that *Mueckler et al* found GLUT4 sugar efflux was inhibited by indinavir, a drug used in Highly Active Antiretroviral Therapy (HAART) Human Immunodeficiency 1 (HIV-1) antiretroviral cocktails (*210*). Indinavir acutely and reversibly inhibits GLUT4 with high affinity (26 µM), but does not inhibit GLUT1 uptake of substrate even at 1mM. Furthermore, addition of increasing concentrations of CB to GLUT4 uptake of 2-DG in oocytes showed competitive inhibition vs indinavir at the e1 site(*203*). GLUT1 I404M was constructed as a GLUT1/GLUT4$_{388-412}$/GLUT1 chimera and tested for 2DOG uptake and CB sensitivity. GLUT1/GLUT4$_{388-412}$/GLUT1showed uptake 96.3±2.1% of myc tagged GLUT1, and its 2 DG uptake was statistically less sensitive to CB inhibition at all concentrations tested. Similar to GLUT1 R400A, the GLUT1/GLUT4$_{388-412}$/GLUT1mutation is insufficient to eliminate CB binding, though its alteration of affinity supports its involvement in the e1 binding site. Furthermore, WT GLUT1 and GLUT1/GLUT4$_{388-412}$/GLUT1 2-DG uptake

Figure 5.1 Mutant GLUT1 sensitivity to Indinavir inhibition, assayed by 6 minute, 2-DG uptake.

Ordinate: Rate of 2 DG uptake expressed as a percentage of the GLUT1-Myc protein uptake rate. Abscissa lists uptake by vector, with GLUT1/GLUT4$_{W388-W412}$/GLUT1 represented as I404M Myc. Uptake experiments were performed as follows: cells were seeded at 10^6/well, transfected in quadruplicate after 24 hours, and assayed 48 hours after transfection. Cells were starved of glucose and serum for 2 hours, rinsed, incubated for 30 minutes ± indinavir, incubated for 6 minutes with 100µM ^{3}H supplemented 2-DG at 37ºC, rinsed twice with 1 mL ice cold stop solution, coated with 500µL 0.5% Triton, and incubated for 30 min at 37ºC to facilitate lysis. Zero time points had stop solution added before radiolabel. Lysed cells were centrifuged, placed in 200µL duplicate aliquots in scintillation vials and counted, with 10µL aliquots tested for total protein well content. Total uptake was normalized to each day's mean c-myc tagged GLUT1 uptake. Each point represents a mean of three experiments, n=4.

Fig 5.1

Indinavir Inhibition of 2 DG Uptake in HEK Cells by Vector
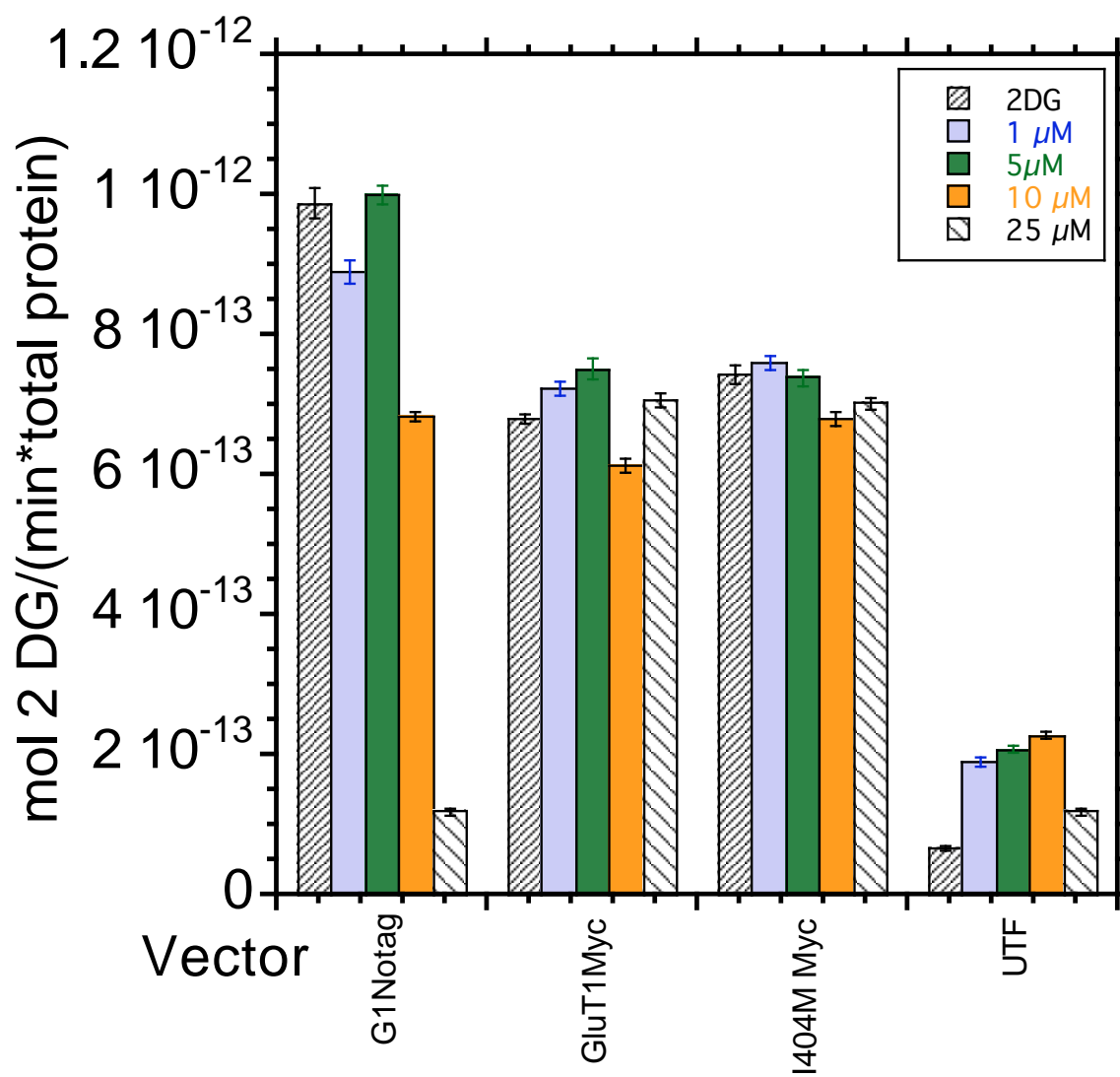
assays were performed to ascertain if I404M confers indinavir sensitivity upon GLUT1, but indinavir remained without significant effect on substrate uptake. (Fig 5.1)

GLUT5 was chosen for chimeric e1 binding site analysis because cytochalasin B is largely without effect upon substrate transport by Group 2 sugar porters (*2, 197, 211*). GLUT5 shares approximately 58% sequence similarity at region W388-W412 with GLUT1, with the notable substitution of alanine for tryptophan at position 388. A GLUT1/GLUT5$_{388-412}$/GLUT1 chimera was constructed for this region and assayed for CB sensitivity. The uninhibited transport capability of the GLUT1/GLUT5$_{388-412}$/GLUT1 construct is very similar to GLUT1 Myc at $94.4 \pm 2.5\%$. However, all concentrations of CB were significantly less effective at inhibiting 2 DG uptake, with 50 nM CB actually stimulating 2 DG uptake. A more extensive dose response was made for GLUT1NT, Myc-GLUT1, GLUT1/GLUT5$_{388-412}$/GLUT1, GLUT5, and untransfected HEK cells. By traditional Michaelis-Menton analysis, the IC$_{50}$ for CB inhibition of GLUT1/GLUT5$_{388-412}$/GLUT1 uptake was not statistically significant from that of the dose response pertaining to the WT or myc-GLUT constructs. However, utilizing a multisite analysis derived from the work in Chapter 3, nM first-site K$_{Iapp}$ constants were obtained for the stimulation of uptake by both GLUT1/GLUT5$_{388-412}$/GLUT1 (10 ± 39 nM) and WT GLUT1 (83 ± 118 nM). We conclude the chimera has increased first-site affinity for CB, the potential for negative second-site cooperativity, and overall decreased inhibition of 2 DG transport by CB.

This suggests four possibilities: 1) while CB photo-crosslinks to the W388 and W412 amino acids, the photoreactive moieties of CB are not involved in transport

inhibition, 2) the W388-W412 region is not necessary for affinity of CB binding but is required for CB inhibition of uptake, 3) it is possible the W388-W412 sequence comprises a cooperativity sensor area, resulting in altered subunit communication, or 4) the W388-W412 region of GLUT1 is not the major determinant of ligand binding at the e1 sugar binding site.

Further GLUT1-GLUT5 chimeras should be constructed to test these hypotheses. Nonconserved areas of interest include region 334-351 on GLUT1, near the endofacial loop between TMs 7 and 8, and 121-138 on TM 4, thought to line the vestibule of the e1 cavity (*81*). Also, the Salas-Burgos model indicates that CB interacts with the sugar porter motif RFGRR at residues 88-93. An equivalent GLUT5 substitution is unlikely to show altered affinity for CB because that sequence (KFGRK) has a similar charge. Another docking site (Q250, M251) might produce a stronger effect upon exchanging residues 248-259 of GLUT1 for 254-265 of GLUT5, because the GLUT1 and GLUT5 sequence in this region is dissimilar in arrangement of polar charges.

A COOPERATIVITY REGION IN GLUT1

The existing GLUT1/GLUT5$_{388-412}$/GLUT1 chimera may possess altered cooperativity and subunit communication patterns. We know that CB is a highly cooperative inhibitor of GLUT1, it is possible that changes resulting from the chimeric substitution would be masked by this ligand. To test the hypothesis that the GLUT1/GLUT5$_{388-412}$/GLUT1 amino acid region is involved in ligand binding cooperativity, inhibition of 2 DG transport by a noncooperative e1 ligand such as forskolin should be attempted. If the forskolin mediated inhibition pattern of the chimera

matches that of untagged GLUT1, the W388-W412 region is not explicitly involved in subunit-subunit communication.

HELIX MAPPING OF THE CB BINDING SITE

Dezutter et al have constructed a series of factor Xa protease site mutants in the exofacial loops between TM's 7&8, 9&10, and 11&12 (in progress). A combined approach of photolabeling GLUT1 with CB or IAPS-FSK (both thought to bind between W388-W412) followed by factor Xa proteolysis and analysis by gel electrophoresis should confirm which TM helixes interact with CB.

Final Conclusion

This thesis has strengthened the GLUT1 structure-function relationship by analyzing the effect that the model system has upon protein function, by utilizing ligand binding to deduce multisite interactions, and by investigating the effects of directed mutagenesis on binding of a classic GLUT1 e1 inhibitor. The main discoveries include: 1) A ubiquitous polypeptide of identical sequence has markedly different functional characteristics when expressed in erythrocytes, yeast, Xenopus oocytes, and mammalian tissue culture cells. 2) For some ligands, especially cytochalasin B, inhibition of the GLUT1 tetramer is a cooperative phenomenon involving subunit communication. 3) We have shown that non conserved regions of W388-W412 region of GLUT1 are not the primary determinats of CB binding affinity.

We discussed future directions for investigative analaysis of GLUT1 and how we may further extend and enhance our understanding of how glucose carrier structure and

function are related. Integral membrane proteins like GLUT1 comprise one-fifth of the proteins coded for in the human genome, each one fulfilling a vital cellular role in regulating cell and tissue mircroenvironment and nutrient homeostasis. Erroneous expression of these proteins results in perturbed metabolic syndromes that possess many ramifications for cell-cell interactions, organ and tissue integrity, as well as overall viability of the organism. Diseases such as GLUT1DS or diabetes mellitus illustrate well how integral membrane protein systems establish and sustain tissue homeostasis. Comprehensive understanding of the interrelationship between structure and function may prove the first step in providing treatments for these chronic metabolic disease states. This thesis offers new methods and perspectives broadly useful when designing future structure-function studies.

BIBLIOGRAPHY

1. Joost, H. G., Bell, G. I., Best, J. D., Birnbaum, M. J., Charron, M. J., Chen, Y. T., Doege, H., James, D. E., Lodish, H. F., Moley, K. H., Moley, J. F., Mueckler, M., Rogers, S., Schurmann, A., Seino, S., and Thorens, B. (2002) Nomenclature of the GLUT/SLC2A family of sugar/polyol transport facilitators, *Am J Physiol Endocrinol Metab 282*, E974-976.

2. Manolescu, A. R., Witkowska, K., Kinnaird, A., Cessford, T., and Cheeseman, C. (2007) Facilitated hexose transporters: new perspectives on form and function, *Physiology (Bethesda) 22*, 234-240.

3. Li, S., Sanna, S., Maschio, A., Busonero, F., Usala, G., Mulas, A., Lai, S., Dei, M., Orru, M., Albai, G., Bandinelli, S., Schlessinger, D., Lakatta, E., Scuteri, A., Najjar, S. S., Guralnik, J., Naitza, S., Crisponi, L., Cao, A., Abecasis, G., Ferrucci, L., Uda, M., Chen, W. M., and Nagaraja, R. (2007) The GLUT9 gene is associated with serum uric acid levels in Sardinia and Chianti cohorts, *PLoS Genet 3*, e194.

4. Lemieux, M. J., Huang, Y., and Wang da, N. (2005) Crystal structure and mechanism of GlpT, the glycerol-3-phosphate transporter from E. coli, *J Electron Microsc (Tokyo) 54 Suppl 1*, i43-46.

5. Salas-Burgos, A., Iserovich, P., Zuniga, F., Vera, J. C., and Fischbarg, J. (2004) Predicting the three-dimensional structure of the human facilitative glucose transporter glut1 by a novel evolutionary homology strategy: insights on the molecular mechanism of substrate migration, and binding sites for glucose and inhibitory molecules, *Biophys J 87*, 2990-2999.

6. Barnett, J. E., Holman, G. D., and Munday, K. A. (1973) Structural requirements for binding to the sugar-transport system of the human erythrocyte, *Biochem J 131*, 211-221.

7. Hamill, S., Cloherty, E. K., and Carruthers, A. (1999) The human erythrocyte sugar transporter presents two sugar import sites, *Biochemistry 38*, 16974-16983.

8. Hresko, R. C., Kruse, M., Strube, M., and Mueckler, M. (1994) Topology of the Glut 1 glucose transporter deduced from glycosylation scanning mutagenesis, *J Biol Chem 269*, 20482-20488.

9. Cloherty, E. K., Heard, K. S., and Carruthers, A. (1996) Human erythrocyte sugar transport is incompatible with available carrier models, *Biochemistry 35*, 10411-10421.

10. Ringler, P., Borgnia, M. J., Stahlberg, H., Maloney, P. C., Agre, P., and Engel, A. (1999) Structure of the water channel AqpZ from Escherichia coli revealed by electron crystallography, *J Mol Biol 291*, 1181-1190.

11. Graybill, C., van Hoek, A. N., Desai, D., Carruthers, A. M., and Carruthers, A. (2006) Ultrastructure of human erythrocyte GLUT1, *Biochemistry 45*, 8096-8107.

12. Carruthers, A., and Zottola, R. J. (1996) Erythrocyte sugar transport, in *Handbook of Biological Physics. "Transport Processes in Eukaryotic and Prokaryotic Organisms"* . (W.N. Konings, H. R. K. J. S. L., Ed.), pp pp 311-342., Elsevier.

13. Holman, G. D., and Rees, W. D. (1987) Photolabelling of the hexose transporter at external and internal sites: fragmentation patterns and evidence for a conformational change, *Biochim Biophys Acta 897*, 395-405.

14. Long, S. B., Campbell, E. B., and Mackinnon, R. (2005) Crystal structure of a mammalian voltage-dependent Shaker family K+ channel, *Science 309*, 897-903.

15. Oldham, M. L., Khare, D., Quiocho, F. A., Davidson, A. L., and Chen, J. (2007) Crystal structure of a catalytic intermediate of the maltose transporter, *Nature 450*, 515-521.

16. Cloherty, E. K., Levine, K. B., and Carruthers, A. (2001) The red blood cell glucose transporter presents multiple, nucleotide-sensitive sugar exit sites, *Biochemistry 40*, 15549-15561.

17. Lemieux, M. J., Song, J., Kim, M. J., Huang, Y., Villa, A., Auer, M., Li, X. D., and Wang, D. N. (2003) Three-dimensional crystallization of the Escherichia coli glycerol-3-phosphate transporter: a member of the major facilitator superfamily, *Protein Sci 12*, 2748-2756.

18. Widdas, W. F. (1954) Facilitated transfer of hexoses across the human erythrocyte membrane, *J. Physiol. (Lond.) 125*, 163-180.

19. Seidner, G., Alvarez, M. G., Yeh, J. I., O'Driscoll, K. R., Klepper, J., Stump, T. S., Wang, D., Spinner, N. B., Birnbaum, M. J., and De Vivo, D. C. (1998) GLUT-1 deficiency syndrome caused by haploinsufficiency of the blood- brain barrier hexose carrier, *Nat Genet 18*, 188-191.

20. Alberts, B. (2002) *Molecular biology of the cell*, 4th ed., Garland Science, New York.

21. Doyle, D. A., Morais Cabral, J., Pfuetzner, R. A., Kuo, A., Gulbis, J. M., Cohen, S. L., Chait, B. T., and MacKinnon, R. (1998) The structure of the potassium channel: molecular basis of K+ conduction and selectivity, *Science 280*, 69-77.

22. Fu, D., Libson, A., Miercke, L. J., Weitzman, C., Nollert, P., Krucinski, J., and Stroud, R. M. (2000) Structure of a glycerol-conducting channel and the basis for its selectivity, *Science 290*, 481-486.

23. Verkman, A. (2002) Role of aquaporins in endothelial water transport, *J Anat 200*, 528.

24. Stein, W. D. (1986) *Transport and diffusion across cell membranes*, Academic Press, New York.

25. Wu, S. L., Choudhary, G., Ramstrom, M., Bergquist, J., and Hancock, W. S. (2003) Evaluation of shotgun sequencing for proteomic analysis of human plasma using HPLC coupled with either ion trap or Fourier transform mass spectrometry, *J Proteome Res 2*, 383-393.

26. Saier, M. H. J. (2008) Explore Transport Protein Diseases, http://www.tcdb.org/disease_explore.php.

27.   Skach, W. R. (2006) CFTR: new members join the fold, *Cell 127*, 673-675.
28.   Warburg, O. (1956) On the origin of cancer cells, *Science 123*, 309-314.
29.   Schwartz, M. K. (1992) Enzymes as prognostic markers and therapeutic indicators in patients with cancer, *Clin Chim Acta 206*, 77-82.
30.   Macheda, M. L., Rogers, S., and Best, J. D. (2005) Molecular and cellular regulation of glucose transporter (GLUT) proteins in cancer, *J Cell Physiol 202*, 654-662.
31.   Helmlinger, G., Yuan, F., Dellian, M., and Jain, R. K. (1997) Interstitial pH and pO2 gradients in solid tumors in vivo: high-resolution measurements reveal a lack of correlation, *Nat Med 3*, 177-182.
32.   Martin, B. M. (1994) *Tissue culture techniques : an introduction*, Birkhäuser, Boston.
33.   Neeman, M., and Degani, H. (1989) Metabolic studies of estrogen- and tamoxifen-treated human breast cancer cells by nuclear magnetic resonance spectroscopy, *Cancer Res 49*, 589-594.
34.   Xu, J., Peng, H., and Zhang, J. T. (2007) Human multidrug transporter ABCG2, a target for sensitizing drug resistance in cancer chemotherapy, *Curr Med Chem 14*, 689-701.
35.   Klienfeld, N. (2006) Diabetes and Its Awful Toll Quietly Emerge as a Crisis, p http://query.nytimes.com/gst/fullpage.html?sec=health&res=9907E9902DA9901F9930F9993AA35752C35750A39609C35758B35763, New York Times, New York City.
36.   WHO. (2008) http://www.who.int/diabetes/en/, (Organization, W. H., Ed.).
37.   Wood, I. S., and Trayhurn, P. (2003) Glucose transporters (GLUT and SGLT): expanded families of sugar transport proteins, *Br J Nutr 89*, 3-9.
38.   Uldry, M., and Thorens, B. (2004) The SLC2 family of facilitated hexose and polyol transporters, *Pflugers Arch 447*, 480-489.
39.   Tefft, R. E., Jr., Carruthers, A., and Melchior, D. L. (1986) Reconstituted human erythrocyte sugar transporter activity is determined by bilayer lipid head groups, *Biochemistry 25*, 3709-3718.
40.   Mueckler, M., Caruso, C., Baldwin, S. A., Panico, M., Blench, I., Morris, H. R., Allard, W. J., Lienhard, G. E., and Lodish, H. F. (1985) Sequence and structure of a human glucose transporter, *Science 229*, 941-945.
41.   Simpson, I. A., Carruthers, A., and Vannucci, S. J. (2007) Supply and demand in cerebral energy metabolism: the role of nutrient transporters, *J Cereb Blood Flow Metab 27*, 1766-1791.
42.   Klepper, J., and Leiendecker, B. (2007) GLUT1 deficiency syndrome--2007 update, *Dev Med Child Neurol 49*, 707-716.
43.   Pascual, J. M., Wang, D., Lecumberri, B., Yang, H., Mao, X., Yang, R., and De Vivo, D. C. (2004) GLUT1 deficiency and other glucose transporter diseases, *Eur J Endocrinol 150*, 627-633.
44.   Wang, D., Kranz-Eble, P., and De Vivo, D. C. (2000) Mutational analysis of GLUT1 (SLC2A1) in Glut-1 deficiency syndrome, *Hum Mutat 16*, 224-231.

45. Guo, X., Geng, M., and Du, G. (2005) Glucose transporter 1, distribution in the brain and in neural disorders: its relationship with transport of neuroactive drugs through the blood-brain barrier, *Biochem Genet 43*, 175-187.

46. Saier, M. H., Jr., Beatty, J. T., Goffeau, A., Harley, K. T., Heijne, W. H., Huang, S. C., Jack, D. L., Jahn, P. S., Lew, K., Liu, J., Pao, S. S., Paulsen, I. T., Tseng, T. T., and Virk, P. S. (1999) The major facilitator superfamily, *J Mol Microbiol Biotechnol 1*, 257-279.

47. Abramson, J., Smirnova, I., Kasho, V., Verner, G., Kaback, H. R., and Iwata, S. (2003) Structure and mechanism of the lactose permease of Escherichia coli, *Science 301*, 610-615.

48. Hirai, T., Heymann, J. A., Shi, D., Sarker, R., Maloney, P. C., and Subramaniam, S. (2002) Three-dimensional structure of a bacterial oxalate transporter, *Nat Struct Biol 9*, 597-600.

49. Fischbarg, J., Cheung, M., Czegledy, F., Li, J., Iserovich, P., Kuang, K., Hubbard, J., Garner, M., Rosen, O. M., Golde, D. W., and et al. (1993) Evidence that facilitative glucose transporters may fold as beta-barrels, *Proc Natl Acad Sci U S A 90*, 11658-11662.

50. Law, C. J., Yang, Q., Soudant, C., Maloney, P. C., and Wang, D. N. (2007) Kinetic evidence is consistent with the rocker-switch mechanism of membrane transport by GlpT, *Biochemistry 46*, 12190-12197.

51. Jardetzky, O. (1966) Simple allosteric model for membrane pumps, *Nature 211*, 969-970.

52. Singer, S. J. (1974) The molecular organization of membranes, *Annu Rev Biochem 43*, 805-833.

53. Voet D, V. J. (1995) *Biochemistry*, 2nd ed., Wiley.

54. Mueckler, M. (1994) Facilitative glucose transporters, *Eur J Biochem 219*, 713-725.

55. Cheeseman, C. I. (1993) GLUT2 is the transporter for fructose across the rat intestinal basolateral membrane, *Gastroenterology 105*, 1050-1056.

56. Cheeseman, C. I. (2008) GLUT7 a class II high affinity intestinal glucose/ fructose facilitated hexose transporter, *Am J Physiol Endocrinol Metab*.

57. Stark, K., Reinhard, W., Neureuther, K., Wiedmann, S., Sedlacek, K., Baessler, A., Fischer, M., Weber, S., Kaess, B., Erdmann, J., Schunkert, H., and Hengstenberg, C. (2008) Association of common polymorphisms in GLUT9 gene with gout but not with coronary artery disease in a large case-control study, *PLoS ONE 3*, e1948.

58. Takanaga, H., Chaudhuri, B., and Frommer, W. B. (2008) GLUT1 and GLUT9 as major contributors to glucose influx in HepG2 cells identified by a high sensitivity intramolecular FRET glucose sensor, *Biochim Biophys Acta 1778*, 1091-1099.

59. Augustin, R., Carayannopoulos, M. O., Dowd, L. O., Phay, J. E., Moley, J. F., and Moley, K. H. (2004) Identification and characterization of human glucose transporter-like protein-9 (GLUT9): alternative splicing alters trafficking, *J Biol Chem 279*, 16229-16236.

60. Scheepers, A., Schmidt, S., Manolescu, A., Cheeseman, C. I., Bell, A., Zahn, C., Joost, H. G., and Schurmann, A. (2005) Characterization of the human SLC2A11 (GLUT11) gene: alternative promoter usage, function, expression, and subcellular distribution of three isoforms, and lack of mouse orthologue, *Mol Membr Biol 22*, 339-351.

61. Bourgeois, F., Coady, M. J., and Lapointe, J. Y. (2005) Determination of transport stoichiometry for two cation-coupled myo-inositol cotransporters: SMIT2 and HMIT, *J Physiol 563*, 333-343.

62. Widdas, W. F. (1952) Inability of diffusion to account for placental glucose transfer in the sheep and consideration of the kinetics of a possible carrier transfer, *J. Physiol. (London) 118*, 23–39.

63. Carruthers, A. (1990) Facilitated diffusion of glucose, *Physiol. Rev. 70*, 1135-1176.

64. Wellner, M., Monden, I., and Keller, K. (1992) The differential role of Cys-421 and Cys-429 of the Glut1 glucose transporter in transport inhibition by p-chloromercuribenzenesulfonic acid (pCMBS) or cytochalasin B (CB), *FEBS Lett 309*, 293-296.

65. Zottola, R. J., Cloherty, E. K., Coderre, P. E., Hansen, A., Hebert, D. N., and Carruthers, A. (1995) Glucose transporter function is controlled by transporter oligomeric structure. A single, intramolecular disulfide promotes GLUT1 tetramerization, *Biochemistry 34*, 9734-9747.

66. Levine, K. B., Robichaud, T. K., Hamill, S., Sultzman, L. A., and Carruthers, A. (2005) Properties of the human erythrocyte glucose transport protein are determined by cellular context, *Biochemistry 44*, 5606-5616.

67. Gould, G. W., Thomas, H. M., Jess, T. J., and Bell, G. I. (1991) Expression of human glucose transporters in Xenopus oocytes: kinetic characterization and substrate specificities of the erythrocyte, liver, and brain isoforms, *Biochemistry 30*, 5139-5145.

68. Paulsen, I. T., Sliwinski, M. K., Nelissen, B., Goffeau, A., and Saier, M. H., Jr. (1998) Unified inventory of established and putative transporters encoded within the complete genome of Saccharomyces cerevisiae, *FEBS Lett 430*, 116-125.

69. Bisson, L. F., Coons, D. M., Kruckeberg, A. L., and Lewis, D. A. (1993) Yeast sugar transporters. [Review], *Critical Reviews in Biochemistry & Molecular Biology 28*, 259-308.

70. Kruckeberg, A. L., and Bisson, L. F. (1990) The HXT2 gene of Saccharomyces cerevisiae is required for high- affinity glucose transport, *Mol Cell Biol 10*, 5903-5913.

71. Kyte, J., and Doolittle, R. F. (1982) A simple method for displaying the hydropathic nature of a protein, *J. Mol. Biol. 157*, 105-132.

72. Hirai, T., Heymann, J. A., Maloney, P. C., and Subramaniam, S. (2003) Structural model for 12-helix transporters belonging to the major facilitator superfamily, *J Bacteriol 185*, 1712-1718.

73. Hruz, P. W., and Mueckler, M. M. (2001) Structural analysis of the GLUT1 facilitative glucose transporter (review), *Mol Membr Biol 18*, 183-193.

74.   Liu, Q., Vera, J. C., Peng, H., and Golde, D. W. (2001) The predicted atp-binding domains in the hexose transporter glut1 critically affect transporter activity, *Biochemistry 40*, 7874-7881.

75.   Jung, E. K. Y., Chin, J. J., and Jung, C. Y. (1986) Structural basis of human erythrocyte glucose transporter function in reconstituted system. Hydrogen exchange, *J. Biol. Chem. 261*, 9155-9160.

76.   Cairns, M. T., Alvarez, J., Panico, M., Gibbs, A. F., Morris, H. R., Chapman, D., and Baldwin, S. A. (1987) Investigation of the structure and function of the human erythrocyte glucose transporter by proteolytic dissection., *Biochim. Biophys. Acta 905*, 295-310.

77.   Chin, J. J., Jung, E. K. Y., Chen, V., and Jung, C. Y. (1987) Structural basis of human erythrocyte glucose transporter function in proteoliposome vesicles: Circular dichroism measurements, *Proc. Natl. Acad. Sci. U.S.A. 84*, 4113-4116.

78.   Song, X. M., Hresko, R. C., and Mueckler, M. (2008) Identification of amino acid residues within the C terminus of the Glut4 glucose transporter that are essential for insulin-stimulated redistribution to the plasma membrane, *J Biol Chem 283*, 12571-12585.

79.   Mueckler, M., and Makepeace, C. (2006) Transmembrane segment 12 of the Glut1 glucose transporter is an outer helix and is not directly involved in the transport mechanism, *J Biol Chem 281*, 36993-36998.

80.   Mueckler, M., and Makepeace, C. (2004) Analysis of transmembrane segment 8 of the GLUT1 glucose transporter by cysteine-scanning mutagenesis and substituted cysteine accessibility, *J Biol Chem 279*, 10494-10499.

81.   Alisio, A., and Mueckler, M. (2004) Relative proximity and orientation of helices 4 and 8 of the GLUT1 glucose transporter, *J Biol Chem 279*, 26540-26545.

82.   Hruz, P. W., and Mueckler, M. M. (1999) Cysteine-scanning mutagenesis of transmembrane segment 7 of the GLUT1 glucose transporter, *J Biol Chem 274*, 36176-36180.

83.   Mueckler, M., and Makepeace, C. (2002) Analysis of transmembrane segment 10 of the Glut1 glucose transporter by cysteine-scanning mutagenesis and substituted cysteine accessibility, *J Biol Chem 277*, 3498-3503.

84.   Mueckler, M., and Makepeace, C. (2008) Transmembrane segment 6 of the glut1 glucose transporter is an outer helix and contains amino acid side chains essential for transport activity, *J Biol Chem 283*, 11550-11555.

85.   Appleman, J. R., and Lienhard, G. E. (1989) Kinetics of the purified glucose transporter. Direct measurement of the rates of interconversion of transporter conformers, *Biochemistry 28*, 8221-8227.

86.   Baldwin, S. A., Baldwin, J. M., and Lienhard, G. E. (1982) The monosaccharide transporter of the human erythrocyte. Characterization of an improved preparation., *Biochemistry 21*, 3836–3842.

87.   Hebert, D. N., and Carruthers, A. (1992) Glucose transporter oligomeric structure determines transporter function. Reversible redox-dependent interconversions of tetrameric and dimeric GLUT1, *J Biol Chem 267*, 23829-23838.

88. Cloherty, E. K., Levine, K. B., Graybill, C., and Carruthers, A. (2002) Cooperative nucleotide binding to the human erythrocyte sugar transporter, *Biochemistry 41*, 12639-12651.

89. Levine, K. B., Cloherty, E. K., Hamill, S., and Carruthers, A. (2002) Molecular determinants of sugar transport regulation by ATP, *Biochemistry 41*, 12629-12638.

90. Lacko, L., Wittke, B., and Geck, P. (1973) The temperature dependence of the exchange transport of glucose in human erythocytes, *J. Cell Physiol. 82*, 213-318.

91. Lowe, A. G., and Walmsley, A. R. (1986) The kinetics of glucose transport in human red blood cells, *Biochim. Biophys. Acta 857*, 146-154.

92. Carruthers, A. (1991) Mechanisms for the facilitated diffusion of substrates across cell membranes, *Biochemistry 30*, 3898-3906.

93. Heard, K. S., Fidyk, N., and Carruthers, A. (2000) ATP-dependent substrate occlusion by the human erythrocyte sugar transporter, *Biochemistry 39*, 3005-3014.

94. Naftalin, R. J., and Holman, G. D. (1977) Transport of sugars in human red cells, in *Membrane transport in red cells* (Ellory, J. C., and Lew, V. L., Eds.), pp 257-300, Academic Press, New York.

95. Cloherty, E. K., Sultzman, L. A., Zottola, R. J., and Carruthers, A. (1995) Net Sugar Transport is a Multi-Step Process. Evidence for cytosolic sugar binding sites in erythrocytes, *Biochemistry 34*, 15395–15406.

96. Blodgett, D. M., and Carruthers, A. (2005) Quench-flow analysis reveals multiple phases of GluT1-mediated sugar transport, *Biochemistry 44*, 2650-2660.

97. Carruthers, A., and Helgerson, A. L. (1991) Inhibitions of sugar transport produced by ligands binding at opposite sides of the membrane. Evidence for simultaneous occupation of the carrier by maltose and cytochalasin B, *Biochemistry 30*, 3907-3915.

98. Cloherty, E. K., Diamond, D. L., Heard, K. S., and Carruthers, A. (1996) Regulation of GLUT1-mediated sugar transport by an antiport/uniport switch mechanism, *Biochemistry 35*, 13231-13239.

99. Levine, K. B., Cloherty, E. K., Fidyk, N. J., and Carruthers, A. (1998) Structural and physiologic determinants of human erythrocyte sugar transport regulation by adenosine triphosphate, *Biochemistry 37*, 12221-12232.

100. Vera, J. C., Rivas, C. I., Fischbarg, J., and Golde, D. W. (1993) Mammalian facilitative hexose transporters mediate the transport of dehydroascorbic acid, *Nature 364*, 79-82.

101. Baker, G. F., and Naftalin, R. J. (1979) Evidence of multiple operational affinities for D-glucose inside the human erythrocyte membrane., *Biochim. Biophys. Acta 550*, 474-484.

102. Lin, S., and Spudich, J. A. (1974) Biochemical studies on the mechanism of action of cytochalasin B. Cytochalasin B binding to red cell membranes in relation to glucose transport, *J. Biol. Chem. 249*, 5778-5783.

103. Jung, C. Y., and Rampal, A. L. (1977) Cytochalasin B binding sites and glucose transport carrier in human erythrocyte ghosts, *J Biol Chem 252*, 5456-5463.

104. Afzal, I., Cunningham, P., and Naftalin, R. J. (2002) Interactions of ATP, oestradiol, genistein and the anti-oestrogens, faslodex (ICI 182780) and tamoxifen, with the human erythrocyte glucose transporter, GLUT1, *Biochem J 365*, 707-719.

105. LeFevre, P. G., and Marshall, J. K. (1959) The attachment of phloretin and analogues to human erythrocytes in connection with inhibition of sugar transport, *J. Biol. Chem. 234*, 3022–3027.

106. Naftalin, R. J., Afzal, I., Cunningham, P., Halai, M., Ross, C., Salleh, N., and Milligan, S. R. (2003) Interactions of androgens, green tea catechins and the antiandrogen flutamide with the external glucose-binding site of the human erythrocyte glucose transporter GLUT1, *Br J Pharmacol 140*, 487-499.

107. Sergeant, S., and Kim, H. D. (1985) Inhibition of 3-O-methylglucose transport in human erythrocytes by forskolin, *J. Biol. Chem. 260*, 14677-14682.

108. Strobel, P., Allard, C., Perez-Acle, T., Calderon, R., Aldunate, R., and Leighton, F. (2005) Myricetin, quercetin and catechin-gallate inhibit glucose uptake in isolated rat adipocytes, *Biochem J 386*, 471-478.

109. Holman, G. D., Kozka, I. J., Clark, A. E., Flower, C. J., Saltis, J., Habberfield, A. D., Simpson, I. A., and Cushman, S. W. (1990) Cell surface labeling of glucose transporter isoform GLUT4 by bis- mannose photolabel. Correlation with stimulation of glucose transport in rat adipose cells by insulin and phorbol ester, *J Biol Chem 265*, 18172-18179.

110. Naftalin, R. J., Cunningham, P., and Afzal-Ahmed, I. (2004) Piracetam and TRH analogues antagonise inhibition by barbiturates, diazepam, melatonin and galanin of human erythrocyte D-glucose transport, *Br J Pharmacol 142*, 594-608.

111. Barnett, J. E. G., Holman, G. D., and Munday, K. A. (1973) An explanation of the asymmetric binding of sugars to the human erythrocyte sugar transport system, *Biochem. J. 135*, 539-541.

112. Cunningham, P., Afzal-Ahmed, I., and Naftalin, R. J. (2006) Docking studies show that D-glucose and quercetin slide through the transporter GLUT1, *J Biol Chem 281*, 5797-5803.

113. Jung, C. Y., and Rampal, A. L. (1977) Cytochalasin B binding sites and the glucose transporter in human erythrocyte ghosts., *J. Biol. Chem. 252*, 5456–5463.

114. Sigma-Aldritch. (2006-2007) Biochemicals, Reagents & Kits LIfe Science Catalog.

115. Brockmann, K., Wang, D., Korenke, C. G., von Moers, A., Ho, Y. Y., Pascual, J. M., Kuang, K., Yang, H., Ma, L., Kranz-Eble, P., Fischbarg, J., Hanefeld, F., and De Vivo, D. C. (2001) Autosomal dominant glut-1 deficiency syndrome and familial epilepsy, *Ann Neurol 50*, 476-485.

116. Garcia, J. C., Strube, M., Leingang, K., Keller, K., and Mueckler, M. M. (1992) Amino acid substitutions at tryptophan 388 and tryptophan 412 of the HepG2 (Glut1) glucose transporter inhibit transport activity and targeting to the plasma membrane in Xenopus oocytes, *J Biol Chem 267*, 7770-7776.

117. Inukai, K., Asano, T., Katagiri, H., Anai, M., Funaki, M., Ishihara, H., Tsukuda, K., Kikuchi, M., Yazaki, Y., and Oka, Y. (1994) Replacement of both tryptophan

residues at 388 and 412 completely abolished cytochalasin B photolabelling of the GLUT1 glucose transporter, *Biochem J 302*, 355-361.

118. Joost, H. G., and Steinfelder, H. J. (1987) Forskolin inhibits insulin-stimulated glucose transport in rat adipose cells by a direct interaction with the glucose transporter, *Mol. Pharmacol. 31*, 279-283.

119. Insel, P. A., and Ostrom, R. S. (2003) Forskolin as a tool for examining adenylyl cyclase expression, regulation, and G protein signaling, *Cell Mol Neurobiol 23*, 305-314.

120. Tang, W. J., and Hurley, J. H. (1998) Catalytic mechanism and regulation of mammalian adenylyl cyclases, *Mol Pharmacol 54*, 231-240.

121. Shanahan, M. F., Morris, D. P., and Edwards, B. M. (1987) [3H]-forskolin. Direct photoaffinity labeling of the erythrocyte D-glucose transporter, *J. Biol. Chem. 262*, 5978-5984.

122. Katagiri, H., Asano, T., Ishihara, H., Lin, J. L., Inukai, K., Shanahan, M. F., Tsukuda, K., Kikuchi, M., Yazaki, Y., and Oka, Y. (1993) Role of tryptophan-388 of GLUT1 glucose transporter in glucose-transport activity and photoaffinity-labelling with forskolin, *Biochemical Journal*.

123. Merriam-Webster Inc. Medical dictionary, Merriam-Webster, [Bethesda, MD].

124. Lefevre, P. G. (1959) Molecular structural factors in competitive inhibition of sugar transport, *Science 130*, 104-105.

125. LeFevre, P. G. (1961) Sugar transport in the red blood cell: structure activity relationships in substrates and antagonists., *Pharmacol. Rev. 13, 39–70.*

126. Carruthers, A. (1986) ATP regulation of the human red cell sugar transporter, *J. Biol. Chem. 261*, 11028-11037.

127. Hebert, D. N., and Carruthers, A. (1986) Direct evidence for ATP modulation of sugar transport in human erythrocyte ghosts, *J. Biol. Chem. 261*, 10093-10099.

128. Carruthers, A., Helgerson, A. L., Hebert, D. N., Tefft, R. E., Jr., Naderi, S., and Melchior, D. L. (1989) Effects of calcium, ATP, and lipids on human erythrocyte sugar transport, *Ann N Y Acad Sci 568*, 52-67.

129. Helgerson, A. L., Hebert, D. N., Naderi, S., and Carruthers, A. (1989) Characterization of two independent modes of action of ATP on human erythrocyte sugar transport, *Biochemistry 28*, 6410-6417.

130. Cloherty, E. K., Hamill, S., Levine, K., and Carruthers, A. (2001) Sugar Transporter Regulation by ATP and quaternary structure, *Blood Clls, Molecules and Disease 27*, 102-107.

131. Leitch, J. M., and Carruthers, A. (2007) ATP-dependent sugar transport complexity in human erythrocytes, *Am J Physiol Cell Physiol 292*, C974-986.

132. Blodgett, D. M., De Zutter, J. K., Levine, K. B., Karim, P., and Carruthers, A. (2007) Structural basis of GLUT1 inhibition by cytoplasmic ATP, *J Gen Physiol 130*, 157-168.

133. Zoccoli, M. A., Baldwin, S. A., and Lienhard, G. E. (1978) The monosaccharide transport system of the human erythrocyte. Solubilization and characterization on the basis of cytochalasin B binding., *J. Biol. Chem. 253*, 6923-6930.

134. Takata, K., Kasahara, T., Kasahara, M., Ezaki, O., and Hirano, H. (1990) Erythrocyte/HepG2-type glucose transporter is concentrated in cells of blood-tissue barriers, *Biochemical & Biophysical Research Communications 173*, 67-73.

135. Diamond, D., and Carruthers, A. (1993) Metabolic control of sugar transport by derepression of cell surface glucose transporters: an insulin-independent, recruitment-independent mechanism of regulation, *J. Biol. Chem. 268*, 6437-6444.

136. Carruthers, A., and Helgerson, A. L. (1989) The human erythrocyte sugar transporter is also a nucleotide binding protein, *Biochemistry 28*, 8337-8346.

137. Heard, K. S., Diguette, M., Heard, A. C., and Carruthers, A. (1998) Membrane-bound glyceraldehyde-3-phosphate dehydrogenase and multiphasic erythrocyte sugar transport, *Exp Physiol 83*, 195-201.

138. Mueckler, M., and Makepeace, C. (1997) Identification of an amino acid residue that lies between the exofacial vestibule and exofacial substrate-binding site of the Glut1 sugar permeation pathway, *J Biol Chem 272*, 30141-30146.

139. Yi, C. K., Charalambous, B. M., Emery, V. C., and Baldwin, S. A. (1992) Characterization of functional human erythrocyte-type glucose transporter (GLUT1) expressed in insect cells using a recombinant baculovirus, *Biochem J*, 643-646.

140. Kasahara, T., and Kasahara, M. (1996) Expression of the rat GLUT1 glucose transporter in the yeast Saccharomyces cerevisiae, *Biochem J 315 (Pt 1)*, 177-182.

141. Wieczorke, R., Krampe, S., Weierstall, T., Freidel, K., Hollenberg, C. P., and Boles, E. (1999) Concurrent knock-out of at least 20 transporter genes is required to block uptake of hexoses in Saccharomyces cerevisiae, *FEBS Lett 464*, 123-128.

142. Reifenberger, E., Freidel, K., and Ciriacy, M. (1995) Identification of novel HXT genes in Saccharomyces cerevisiae reveals the impact of individual hexose transporters on glycolytic flux, *Mol Microbiol 16*, 157-167.

143. Heinisch, J. J., Muller, S., Schluter, E., Jacoby, J., and Rodicio, R. (1998) Investigation of two yeast genes encoding putative isoenzymes of phosphoglycerate mutase, *Yeast 14*, 203-213.

144. Johnston, M. (1999) Feasting, fasting and fermenting. Glucose sensing in yeast and other cells, *Trends Genet 15*, 29-33.

145. Day, R. E., Higgins, V. J., Rogers, P. J., and Dawes, I. W. (2002) Characterization of the putative maltose transporters encoded by YDL247w and YJR160c, *Yeast 19*, 1015-1027.

146. Mumberg, D., Muller, R., and Funk, M. (1995) Yeast vectors for the controlled expression of heterologous proteins in different genetic backgrounds, *Gene 156*, 119-122.

147. Schandel, K. A., and Jenness, D. D. (1994) Direct evidence for ligand-induced internalization of the yeast alpha-factor pheromone receptor, *Mol Cell Biol 14*, 7245-7255.

148. Laemmli, U. K. (1970) Cleavage of structural proteins during the assembly of the head of bacteriophage T4, *Nature 227*, 680-685.

149. Legesse-Miller, A., Sagiv, Y., Glozman, R., and Elazar, Z. (2000) Aut7p, a soluble autophagic factor, participates in multiple membrane trafficking processes, *J Biol Chem 275*, 32966-32973.

150. Yun, C. W., Ferea, T., Rashford, J., Ardon, O., Brown, P. O., Botstein, D., Kaplan, J., and Philpott, C. C. (2000) Desferrioxamine-mediated iron uptake in Saccharomyces cerevisiae. Evidence for two pathways of iron uptake, *J Biol Chem 275*, 10709-10715.

151. Cirillo, V. P. (1968) Relationship between sugar structure and competition for the sugar transport system in Bakers' yeast., *J. Bacteriol. 95*, 603-611.

152. Carruthers, A. (1986) Anomalous asymmetric kinetics of human red cell hexose transfer: role of cytosolic adenosine 5'-triphosphate, *Biochemistry 25*, 3592-3602.

153. Holman, G. D., Busza, A. L., Pierce, E. J., and Rees, W. D. (1981) Evidence for negative cooperativity in human erythrocyte sugar transport, *Biochim Biophys Acta 649*, 503-514.

154. Baker, G. F., and Widdas, W. F. (1988) Parameters for 3-O-methyl glucose transport in human erythrocytes and fit of asymmetric carrier kinetics, *J Physiol (Lond) 395*, 57-76.

155. Blodgett, D. M., and Carruthers, A. (2004) Conventional transport assays underestimate sugar transport rates in human red cells, *Blood Cells Mol Dis 32*, 401-407.

156. Basketter, D. A., and Widdas, W. F. (1978) Asymmetry of the hexose transfer system in human erythrocytes. Comparison of the effects of cytochalasin B, phloretin and maltose as competitive inhibitors, *J Physiol (Lond) 278*, 389-401.

157. Miller, D. M. (1968) The kinetics of selective biological transport. IV. Assessment of three carrier systems using the erythrocyte-monosaccharide transport data, *Biophys. J. 8*, 1339-1352.

158. Sultzman, L. A., and Carruthers, A. (1999) Stop-flow analysis of cooperative interactions between GLUT1 sugar import and export sites, *Biochemistry 38*, 6640-6650.

159. Eilam, Y., and Stein, W. D. (1972) A simple resolution of the kinetic anomaly in the exchange of different sugars across the membrane of the human red blood cell, *Biochim. Biophys. Acta 266*, 161-173.

160. Naftalin, R. J. (1998) Evidence from temperature studies that the human erythrocyte hexose transporter has a transient memory of its dissociated ligands, *Exp Physiol 83*, 253-258.

161. Ozcan, S., Dover, J., Rosenwald, A. G., Wolfl, S., and Johnston, M. (1996) Two glucose transporters in Saccharomyces cerevisiae are glucose sensors that generate a signal for induction of gene expression, *Proc Natl Acad Sci U S A 93*, 12428-12432.

162. Ozcan, S., Dover, J., and Johnston, M. (1998) Glucose sensing and signaling by two glucose receptors in the yeast Saccharomyces cerevisiae, *Embo J 17*, 2566-2573.

163. Kasahara, T., and Kasahara, M. (1998) Tryptophan 388 in putative transmembrane segment 10 of the rat glucose transporter Glut1 is essential for glucose transport, *J Biol Chem 273*, 29113-29117.

164. Kasahara, T., and Kasahara, M. (1997) Characterization of rat Glut4 glucose transporter expressed in the yeast Saccharomyces cerevisiae: comparison with Glut1 glucose transporter, *Biochim Biophys Acta 1324*, 111-119.

165. Wieczorke, R., Dlugai, S., Krampe, S., and Boles, E. (2003) Characterisation of mammalian GLUT glucose transporters in a heterologous yeast expression system, *Cell Physiol Biochem 13*, 123-134.

166. Naftalin, R. J., Smith, P. M., and Roselaar, S. E. (1985) Evidence for non–uniform distribution of D–glucose within human red cells during net exit and counterflow., *Biochim. Biophys. Acta 820*, 235–249.

167. Naftalin, R. J. (1997) Evidence from studies of temperature-dependent changes of D-glucose, D- mannose and L-sorbose permeability that different states of activation of the human erythrocyte hexose transporter exist for good and bad substrates, *Biochim Biophys Acta 1328*, 13-29.

168. Simons, T. J. B. (1983) Characterization of sugar transport in the pigeon red blood cell, *J. Physiol. 338*, 477-500.

169. Cheung, J. Y., Regen, D. M., Schworer, M. E., Whitfield, C. F., and Morgan, H. E. (1977) Anaerobic stimulation of sugar transport in avian erythrocytes, *Biochim. Biophys. Acta 470*, 212-229.

170. Regen, D. M., and Morgan, H. E. (1964) Studies of the glucose-transport system in the rabbit erythrocyte, *Biochim. Biophys Acta 79*, 151-166.

171. Naftalin, R. J., and Rist, R. J. (1991) 3-O-methyl-D-glucose transport in rat red cells: effects of heavy water, *Biochim Biophys Acta 1064*, 37-48.

172. Abumrad, N. A., Briscoe, P., Beth, A. H., and Whitesell, R. R. (1988) Temperature dependence of glucose transport in erythrocytes from normal and alloxan-diabetic rats, *Biochim Biophys Acta 938*, 222-230.

173. Helgerson, A. L., and Carruthers, A. (1989) Analysis of protein-mediated 3-O-methylglucose transport in rat erythrocytes: rejection of the alternating conformation carrier model for sugar transport, *Biochemistry 28*, 4580-4594.

174. Due, A. D., Cook, J. A., Fletcher, S. J., Qu, Z. C., Powers, A. C., and May, J. M. (1995) A "cysteineless" GLUT1 glucose transporter has normal function when expressed in Xenopus oocytes, *Biochem Biophys Res Commun 208*, 590-596.

175. Taylor, L. P., and Holman, G. D. (1981) Symmetrical kinetic parameters for 3-O-methyl-D-glucose transport in adipocytes in the presence and in the absence of insulin, *Biochim. Biophys. Acta 642*, 325-335.

176. Baker, P. F., and Carruthers, A. (1981) 3-O-methylglucose transport in internally dialysed giant axons of Loligo, *J. Physiol. (Lond.) 316*, 503-525.

177. Carruthers, A. (1983) Sugar transport in giant barnacle muscle fibres, *J. Physiol. (Lond.) 336*, 377-396.

178. Kasahara, M., and Hinkle, P. C. (1977) Reconstitution and purification of the D-glucose transporter from human erythrocytes., *J. Biol. Chem. 253*, 7384-7390.

179. Takata, K., Hirano, H., and Kasahara, M. (1997) Transport of glucose across the blood-tissue barriers, *Int Rev Cytol 172*, 1-53.
180. Bloch, R. (1973) Inhibition of sugar transport in the human erythrocyte by cytochalasin B, *Biochemistry 12*, 4799-4801.
181. Appleman, J. R., and Lienhard, G. E. (1985) Rapid kinetics of the glucose transporter from human erythrocytes. Detection and measurement of a half-turnover of the purified transporter, *J Biol Chem 260*, 4575-4578.
182. Lavis, V. R., Lee, D. P., and Shenolikar, S. (1987) Evidence that forskolin binds to the glucose transporter of human erythrocytes., *J. Biol. Chem. 262*, 14571-14575.
183. Gorga, F. R., and Lienhard, G. E. (1982) Changes in the intrinsic fluorescence of the human erythrocyte monosaccharide transporter upon ligand binding, *Biochemistry 21*, 1905-1908.
184. Carruthers, A. (1989) Hexose transport across human erythrocyte membranes, in *The Red Cell Membrane* (Raess, B. U., and G. Tunnicliff, G., Eds.), pp 249-279, Humana Press, Clifton, N.J.
185. Challiss, J. R., Taylor, L. P., and Holman, G. D. (1980) Sugar transport asymmetry in human erythrocytes--the effect of bulk haemoglobin removal and the addition of methylxanthines, *Biochim Biophys Acta 602*, 155-166.
186. Vera, J. C., Reyes, A. M., Velasquez, F. V., Rivas, C. I., Zhang, R. H., Strobel, P., Slebe, J. C., Nunez-Alarcon, J., and Golde, D. W. (2001) Direct inhibition of the hexose transporter GLUT1 by tyrosine kinase inhibitors, *Biochemistry 40*, 777-790.
187. Morris, D. I., Robbins, J. D., Ruoho, A. E., Sutkowski, E. M., and Seamon, K. B. (1991) Forskolin photoaffinity labels with specificity for adenylyl cyclase and the glucose transporter, *J Biol Chem 266*, 13377-13384.
188. Rampal, A. L., Pinkofsky, H. B., and Jung, C. Y. (1980) Structure of cytochalasins and cytochalasin B binding sites in human erythrocyte membranes, *Biochemistry 19*, 679-683.
189. Martin, G. E., Seamon, K. B., Brown, F. M., Shanahan, M. F., Roberts, P. E., and Henderson, P. J. (1994) Forskolin specifically inhibits the bacterial galactose-H+ transport protein, GalP, *J Biol Chem 269*, 24870-24877.
190. Hill, A. V. (1913) The Combinations of Haemoglobin with Oxygen and with Carbon Monoxide. I, *Biochem J 7*, 471-480.
191. Weiss, J. N. (1997) The Hill equation revisited: uses and misuses, *FASEB J 11*, 835-841.
192. Lemieux, M. J. (2007) Eukaryotic major facilitator superfamily transporter modeling based on the prokaryotic GlpT crystal structure, *Mol Membr Biol 24*, 333-341.
193. Pascual, J. M., Wang, D., Yang, R., Shi, L., Yang, H., and De Vivo, D. C. (2008) Structural Signatures and Membrane Helix 4 in GLUT1: INFERENCES FROM HUMAN BLOOD-BRAIN GLUCOSE TRANSPORT MUTANTS, *J Biol Chem 283*, 16732-16742.

194. Basketter, D. A., and Widdas, W. F. (1977) Competitive inhibition of hexose transfer in human erythrocytes by Cytochalasin B [proceedings], *J Physiol (Lond) 265*, 39P-40P.

195. Wang, D., Pascual, J. M., Yang, H., Engelstad, K., Jhung, S., Sun, R. P., and De Vivo, D. C. (2005) Glut-1 deficiency syndrome: clinical, genetic, and therapeutic aspects, *Ann Neurol 57*, 111-118.

196. Joost, H. G., and Thorens, B. (2001) The extended GLUT-family of sugar/polyol transport facilitators: nomenclature, sequence characteristics, and potential function of its novel members (review), *Mol Membr Biol 18*, 247-256.

197. Burant, C. F., Takeda, J., Brot, L. E., Bell, G. I., and Davidson, N. O. (1992) Fructose transporter in human spermatozoa and small intestine is GLUT5, *J Biol Chem 267*, 14523-14526.

198. Corpe, C. P., Bovelander, F. J., Munoz, C. M., Hoekstra, J. H., Simpson, I. A., Kwon, O., Levine, M., and Burant, C. F. (2002) Cloning and functional characterization of the mouse fructose transporter, GLUT5, *Biochim Biophys Acta 1576*, 191-197.

199. Darakhshan, F., Hajduch, E., Kristiansen, S., Richter, E. A., and Hundal, H. S. (1998) Biochemical and functional characterization of the GLUT5 fructose transporter in rat skeletal muscle, *Biochem J 336 (Pt 2)*, 361-366.

200. Inukai, K., Takata, K., Asano, T., Katagiri, H., Ishihara, H., Nakazaki, M., Fukushima, Y., Yazaki, Y., Kikuchi, M., and Oka, Y. (1997) Targeting of GLUT1-GLUT5 chimeric proteins in the polarized cell line Caco-2, *Mol Endocrinol 11*, 442-449.

201. Krupka, R. M., and Devés, R. (1981) An experimental test for cyclic versus linear transport models. The mechanism of glucose and choline transport in erythrocytes, *J. Biol. Chem. 256*, 5410-5416.

202. Robichaud, T. K., Henderson, P., and Carruthers, A. (2008) AFFINITY AND COOPERATIVITY DETERMINANTS AT THE GLUT1 ENDOFACIAL BINDING SITE, *Biochemistry (Submitted)*.

203. Murata, H., Hruz, P. W., and Mueckler, M. (2002) Indinavir inhibits the glucose transporter isoform Glut4 at physiologic concentrations, *AIDS 16*, 859-863.

204. Connolly, T. J., Carruthers, A., and Melchior, D. L. (1985) Effect of bilayer cholesterol content on reconstituted human erythrocyte sugar transporter activity, *J. Biol. Chem. 260*, 2617-2620.

205. Connolly, T. J., Carruthers, A., and Melchior, D. L. (1985) Effects of bilayer cholesterol on human erythrocyte hexose transport protein activity in synthetic lecithin bilayers, *Biochemistry 24*, 2865-2873.

206. Jigami, Y. (2008) Yeast glycobiology and its application, *Biosci Biotechnol Biochem 72*, 637-648.

207. Burant, C. F., and Bell, G. I. (1992) Mammalian facilitative glucose transporters: evidence for similar substrate recognition sites in functionally monomeric proteins, *Biochemistry 31*, 10414-10420.

208.   Blodgett, D. M., Graybill, C. and Carruthers, A. (2008) ANALYSIS OF GLUCOSE TRANSPORTER TOPOLOGY AND STRUCTURAL DYNAMICS, *Biochemistry SUBMITTED*.
209.   Popov, M., Tam, L. Y., Li, J., and Reithmeier, R. A. (1997) Mapping the ends of transmembrane segments in a polytopic membrane protein. Scanning N-glycosylation mutagenesis of extracytosolic loops in the anion exchanger, band 3, *J Biol Chem 272*, 18325-18332.
210.   Murata, H., Hruz, P. W., and Mueckler, M. (2000) The mechanism of insulin resistance caused by HIV protease inhibitor therapy, *J Biol Chem 275*, 20251-20254.
211.   Davidson, N. O., Hausman, A. M., Ifkovits, C. A., Buse, J. B., Gould, G. W., Burant, C. F., and Bell, G. I. (1992) Human intestinal glucose transporter expression and localization of GLUT5, *American Journal of Physiology*.